

**Design, Synthesis and Characterization of Heme-
proteins: Developing Potential Catalysts for
Bio-remediation**

Kinjalkumar K Shah

Thesis submitted to the Faculty of the
Virginia Polytechnic Institute and State University
in partial fulfillment of the requirements for the degree of

Master of Science
in
Biological Systems Engineering

Dr. Chenming (Mike) Zhang, Chair
Dr. Joel Gillespie, Co-Chair
Dr. David Bevan
Dr. John Cundiff

December 16th, 2004
Biological Systems Engineering Department of Virginia Tech
Blacksburg, Virginia

Keywords: Protein Design, Cytochrome b₅₆₂, Peroxidase Activity,
Hemeprotein, Solid Phase Peptide Synthesis, Four-helix Bundle Protein

Design, Synthesis and Characterization of Heme- proteins: Developing Potential Catalysts for Bio-remediation

Kinjalkumar K Shah

(ABSTRACT)

The next generation of toxic chemicals and hazardous wastes from sophisticated chemical industries will demand the environmental agencies to employ biological methods over the conventional physical and chemical remediation methods. Over the past decade, natural metallo-enzymes have been identified to degrade some of the major chemical contaminants through electron transfer pathways. However, these natural enzymes are less stable in organic solvents and they are not effective for the degradation of toxic compounds such as polychlorinated biphenyls or dioxins. This thesis explores the use of protein design approaches to produce chemically and molecularly modified enzymes, which are highly stable, possess little substrate specificity, and have higher activity than the natural enzymes. The experiments presented in this thesis make use of solid phase synthesis and site-directed mutagenesis for the synthesis and production of these enzymes and popular chromatographic techniques for their purification. The partial characterization of these proteins revealed the essential structural features of these proteins, and their catalytic activity was demonstrated by use of peroxidase assays.

ACKNOWLEDGEMENTS

I would like to express my sincere gratitude to Dr. Joel Gillespie for being my research advisor and for providing me the opportunity to conduct research in the field of my interest. His continual support and guidance throughout my research work in Virginia Bioinformatics Institute at Virginia Tech made this thesis a success. I thank Dr. Chenming (Mike) Zhang for being my academic advisor and mentor. His guidance and motivation is much appreciated. I also thank Dr. David Bevan and Dr. John Cundiff for their support and valuable suggestions. I appreciate their willingness to serve on my research committee.

I am really grateful to the entire Biological Systems Engineering department. Dr. John Perumpral and Dr. Saied Mostaghimi have been great educators and have been very supportive. I would also like to extend my sincere thanks to Deepa Balasubramaniam, Dewal Jani, and Rana Nagarkatti for their valuable suggestions and co-operation.

Finally, I would like to thank all of my friends and family. Their support and friendship have made all this worthwhile. My hard work and dedication is merely a reflection of my parent's underlying love for me. Without their endless cheer and blessings I wouldn't be where I am. My work here is dedicated to them.

Kinjalkumar Shah

December 2004

CONTENTS

LIST OF FIGURES	VIII
LIST OF TABLES	XII
1. INTRODUCTION.....	1
1.1 MOTIVATION	1
1.2 CONTRIBUTIONS	2
1.3 ORGANIZATION OF THESIS	3
2. BACKGROUND	5
2.1 THE CONCEPT OF BIOREMEDIATION.....	5
2.2 PROTEIN DESIGN.....	7
<i>2.2.1 Protein sequence modification</i>	<i>8</i>
<i>2.2.2 Altering the protein environment</i>	<i>12</i>
<i>2.2.3 Modification of the prosthetic group.....</i>	<i>13</i>
2.3 HEME PROTEINS	16
<i>2.3.1 Peroxidases.....</i>	<i>17</i>
<i>2.3.2 The prosthetic group in peroxidases</i>	<i>18</i>
<i>2.3.3 Peroxidase electron transfer and bioremediation.....</i>	<i>20</i>
2.4 SUMMARY	22

3. DESIGN AND CHEMICAL SYNTHESIS OF PEPTIDE BASED FOUR-HELIX BUNDLE HEME-PROTEINS.....	23
3.1 INTRODUCTION.....	23
3.1.1 Peptide based synthetic heme-protein models.....	23
3.1.2 Design strategy.....	25
3.1.3 Solid phase peptide synthesis.....	29
3.2 MATERIALS AND METHODS.....	32
3.2.1 Materials.....	32
3.2.2 Solid phase synthesis of peptides.....	32
3.2.3 Purification and assembly of the dimer/tetramer:.....	34
3.2.4 Mass spectrometry.....	35
3.3 RESULTS AND DISCUSSION.....	36
3.3.1 Solid phase synthesis of peptides.....	36
3.3.2 Purification of peptides.....	37
3.3.3 Explanation for the failure of SPPS.....	41
3.4 CONCLUSIONS.....	42
4. CLONING, EXPRESSION AND PURIFICATION OF <i>YERSINIA ENTEROCOLITICA</i> CYTOCHROME B₅₆₂ AND ITS MUTANTS.....	43
4.1 INTRODUCTION.....	43
4.2 MATERIALS AND METHODS.....	48
4.2.1 PCR amplification, cloning and expression of wild-type cytochrome b₅₆₂.....	49
4.2.2 Construction of C-terminal Trp mutant of cytochrome b₅₆₂: K103W.....	53
4.2.3 Construction of Trp point mutants within the gene of cytochrome b₅₆₂.....	54

4.2.4	<i>Deletion of heme axial ligand (M7A mutation) of cyt b₅₆₂</i>	57
4.2.5	<i>Protein over-expression and purification</i>	57
4.2.6	<i>Determination of protein concentration</i>	59
4.3	RESULTS AND DISCUSSION	60
4.3.1	<i>Cloning and expression of Y. enterocolitica cytochrome b₅₆₂</i>	60
4.3.2	<i>Site-directed mutagenesis of wild-type cyt b₅₆₂</i>	64
4.3.3	<i>Purification of the wild-type cytochrome b₅₆₂ and its mutants</i>	64
5.	BIOPHYSICAL CHARACTERIZATION OF WILD-TYPE YERSINIA	
	ENTEROCOLITICA CYTOCHROME B₅₆₂ AND ITS MUTANTS	72
5.1	INTRODUCTION	72
5.2	MATERIALS AND METHODS	72
5.2.1	<i>Absorbance measurements</i>	72
5.2.2	<i>Fluorometric measurements</i>	73
5.3	RESULTS AND DISCUSSION	75
5.3.1	<i>Spectroscopic properties of wild-type cytochrome b₅₆₂ and its mutants</i>	75
5.3.2	<i>Fluorescence properties of wild-type cytochrome b₅₆₂ and its mutants</i>	79
5.3.3	<i>Assay of peroxidase activity</i>	86
5.4	CONCLUSIONS	94
5.5	FUTURE WORK	94
	GLOSSARY OF ACRONYMS	96
	APPENDICES	99
	APPENDIX A	99

<i>Preparation of competent E. coli cells and transformation</i>	99
<i>Transformation of XL1-Blue supercompetent cells</i>	99
<i>Calculation of transformation efficiency</i>	100
APPENDIX B	101
APPENDIX C	102
<i>FPLC methods</i>	102
APPENDIX D	103
<i>Kaiser-ninhydrin test to assay for the presence of free amino group</i>	103
REFERENCES	104
VITAE	116

LIST OF FIGURES

Figure 2.1: Chemical structure of commonly occurring natural heme <i>b</i>	14
Figure 2.2: Chemical structures of heme <i>a</i> , heme <i>c</i> and heme <i>d</i>	15
Figure 2.3: Model of heme prosthetic group in peroxidases.....	19
Figure 2.4: A schematic diagram representing the peroxidase ping-pong.....	20
Figure 3.1: Proposed electron transfer path for the synthetic heme-binding four-helix bundle proteins.....	28
Figure 3.2: General approach to phase solid peptide synthesis.....	31
Figure 3.3: Reverse-phase HPLC purification of peptide A.....	38
Figure 3.4:UV/Vis absorbance spectra of fractions under peak eluted from the reverse-phase HPLC column.....	39
Figure 3.5:MALDI spectra for Fraction 39 from reverse-phase HPLC purification of peptide A.....	40
Figure 4.1: Sequence alignment of <i>E. coli</i> , <i>Y. enterocolitica</i> and <i>Y. pestis</i>	45
Figure 4.2: Overview of the QuickChange II site-directed mutagenesis method.....	56
Figure 4.3: Agarose gel analysis of PCR amplified gene of <i>Y. enterocolitica</i> Cyt <i>b</i> ₅₆₂	60
Figure 4.4: Transformation of pET26b(+) containing the cytochrome <i>b</i> ₅₆₂ gene into BL21(DE)3 strain of <i>E. coli</i>	61
Figure 4.5: SDS-PAGE showing the over-expressed bands at approximately	

12kDa size.....	62
Figure 4.6: Agarose gel (1%) analysis of the vector pET26b(+) cut with <i>Dra I</i>	63
Figure 4.7: Agarose gel (1%) analysis of the vector pET26b(+) digested with restriction enzymes <i>NcoI</i> and <i>EcoRI</i>	63
Figure 4.8: Ion-exchange separation of wild-type Cyt b ₅₆₂	65
Figure 4.9: SDS-PAGE gels showing the separation of the ion-exchange column fractions.....	66
Figure 4.10: Size-exclusion separation of wild-type cyt b ₅₆₂	67
Figure 4.11: SDS-PAGE gels showing the separation of the size-exclusion column fractions.....	67
Figure 4.12: Ion-exchange separation of M7A K95W Cyt b ₅₆₂	68
Figure 4.13: SDS-PAGE gels showing the separation of the size exclusion column fractions.....	69
Figure 4.14: MALDI spectra for the fraction 25 from the size exclusion column for the K95W mutant of cyt b ₅₆₂	70
Figure 5.1: UV/Vis absorption spectrum of oxidized (Fe ⁺³ in heme) and reduced (Fe ⁺² in heme) Cyt b ₅₆₂	75
Figure 5.2: UV/Vis absorption spectrum of oxidized and reduced forms of wild-type and M7A cyt b ₅₆₂	76
Figure 5.3: UV/Vis absorption spectrum of oxidized and reduced forms of K83W and M7A K83Wcyt b ₅₆₂	77
Figure 5.4: UV/Vis absorption spectrum of oxidized and reduced forms of K89W and M7A K89W cyt b ₅₆₂	78

Figure 5.5: UV/Vis absorption spectrum of oxidized and reduced forms of K95W and M7A K95W cyt b ₅₆₂	78
Figure 5.6: UV/Vis absorption spectrum of oxidized and reduced forms of K103W and M7A K103W cyt b ₅₆₂	79
Figure 5.7: Fluorescence spectra of oxidized WT cytochrome b ₅₆₂ and M7A with and without (w/o) H ₂ O ₂	81
Figure 5.8: Fluorescence spectra of reduced WT cytochrome b ₅₆₂ and M7A with and without H ₂ O ₂	81
Figure 5.9: Fluorescence spectra of oxidized forms of K83W and M7A/K83W cyt b ₅₆₂ with and without H ₂ O ₂	82
Figure 5.10: Fluorescence spectra of reduced forms of K83W and M7A/K83W cyt b ₅₆₂ with and without H ₂ O ₂	82
Figure 5.11: Fluorescence spectra of oxidized forms of K89W and M7A/K89W cyt b ₅₆₂ with and without H ₂ O ₂	83
Figure 5.12: Fluorescence spectra of reduced forms of K89W and M7A/K89W cyt b ₅₆₂ with and without H ₂ O ₂	83
Figure 5.13: Fluorescence spectra of oxidized forms of K95W and M7A/K95W cyt b ₅₆₂ with and without H ₂ O ₂	84
Figure 5.14: Fluorescence spectra of reduced forms of K95W and M7A/K95W cyt b ₅₆₂ with and without H ₂ O ₂	84
Figure 5.15: Fluorescence spectra of oxidized forms of K103W and M7A/K103W cyt b ₅₆₂ with and without H ₂ O ₂	85

Figure 5.16: Fluorescence spectra of reduced forms of K103W and M7A/K103W cyt b ₅₆₂ with and without H ₂ O ₂	85
Figure 5.17: Effect of pH on peroxidase activity of WT cyt b ₅₆₂	86
Figure 5.18: Effect of pH on peroxidase activity of HRP.....	87
Figure 5.19: Effect of pH on peroxidase activity of M7A Cyt b ₅₆₂	88
Figure 5.20: Effect of pH on peroxidase activity of M7A K83W Cyt b ₅₆₂	88
Figure 5.21: Effect of pH on peroxidase activity of M7A K89W Cyt b ₅₆₂	89
Figure 5.22: Effect of pH on peroxidase activity of M7A K95W Cyt b ₅₆₂	89
Figure 5.23: Effect of pH on peroxidase activity of M7A K103W Cyt b ₅₆₂	90
Figure 5.24: Effect of substrate (ABTS) concentration variation on peroxidase activity of M7A Cyt b ₅₆₂	91
Figure 5.25: Peroxidase activity of M7A cyt b ₅₆₂ at various concentrations of ABTS.....	92
Figure 5.25: Effect of [H ₂ O ₂] on the peroxidase activity of M7A Cyt b ₅₆₂	93
Figure 5.26: Dependence of the k _{obs} on [H ₂ O ₂] for M7A Cyt b ₅₆₂	93

LIST OF TABLES

Table 3.1: Distance of tryptophan from the plane of heme in the designed four-helix bundle proteins.....	29
Table 4.1: Concentrations of the purified proteins as determined by BCA assay.....	71

CHAPTER ONE

1. Introduction

1.1 Motivation

Bioremediation, defined as "the use of biological organisms to reduce or eliminate environmental hazards resulting from accumulations of toxic chemicals and other hazardous wastes" (Gibson et al., 1992) has been one of the five primary missions of the United States Department of Energy (DOE). Conventional physical or chemical methods or a combination have been applied for the remediation of soils, sediments, and groundwater contaminants. However, these methods have not yet been effective for all kinds of toxic chemicals and have been very expensive to apply. Hence, over the past decade, opportunities for applying bioremediation to a broad set of contaminants in a more cost effective manner have been identified. Natural enzymes have been demonstrated to degrade some of the major contaminants through redox chemistry involving electron transfer. In this context, the development of highly stable and non-specific enzymes for degradation of some toxic and recalcitrant chemical compounds (e.g. polychlorinated biphenyls (PCBs), dioxin, xenobiotics, etc.) has remained as an interesting area of research.

Early attempts have been made to develop small synthetic four-helix bundle proteins that bind heme or to modify the active site of the natural four-helix bundle proteins to achieve enhanced electron transfer efficiency and reduced substrate specificity for the catalysis of degradation of chemical contaminations. The present work is a continuation of such efforts. This thesis focuses on protein design and engineering approaches to develop chemically or molecularly modified enzymes that possess such catalytic activity and superior stability. Site-directed mutagenesis and *de novo* protein design concepts were explored in the current design approaches. With the availability of sophisticated computer modeling programs, it is now possible to design small peptides and estimate their properties before synthesizing them. Random mutation techniques are also becoming popular for creation of a library of different mutants of a protein and high-throughput screening may provide more accurate and faster way of assessing their properties. Although the current work uses much simpler methods for the design, synthesis, and characterization of the modified enzymes, the results obtained can be used to gain a useful insight into the concept of bioremediation.

1.2 Contributions

This thesis presents the use of molecularly and chemically modified heme-enzymes for bioremediation through the electron transfer pathways. Although not all aspects of biophysical characterizations of these proteins are explored, this thesis provides an adequate proof of some of the essential properties of these modified enzymes required for the purpose of bioremediation. The primary contribution of this research can be listed as follows:

1. The design of four-helix bundle proteins capable of binding the heme prosthetic group and catalyzing electron transfer reactions with enhanced rates with respect to natural enzymes for biodegradation of chemical contaminants. The designs were also tested for total chemical synthesis and assembly.
2. Cloning and expression of *Yersinia enterocolitica* cytochrome b₅₆₂ (cyt b₅₆₂) into *E. coli*. Cyt b₅₆₂ was modified by site-directed mutagenesis to generate four tryptophan mutants, with tryptophan being at different distances from the plane of heme in each of them to investigate how this distance affects the peroxidase properties in these proteins. Five more mutants were made, in which heme axial ligand (methionine7) was deleted in each of the wild-type cyt b₅₆₂ and four tryptophan mutants. These mutants allowed investigating how the presence of an open-coordination site enhances peroxidase properties in these proteins.
3. Development of purification protocols for wild-type *Yersinia enterocolitica* cytochrome b₅₆₂ and its mutants to obtain high purity enzymes.
4. Development of assays to characterize the basic peroxidase behavior of the wild-type and all molecularly modified enzymes.
5. Partial characterization of the structural properties of these enzymes.

1.3 Organization of thesis

Following the introductory chapter, Chapter 2 provides the necessary background information on the concept of bioremediation and presents the idea behind adapting various approaches for design of heme-proteins. The theory behind electron transfer in

these proteins and oxidation/reduction reactions they use to catalyze the degradation of chemical contaminants is elucidated. Chapter 3 elaborates the architecture of small peptides, their synthesis using solid phase Fmoc chemistry and the attempt to assemble them into four-helix bundle proteins. It also explains the rationale behind the failure of that project and talks about how it paved way to the molecular cloning of *Yersinia enterocolitica* cyt b₅₆₂. Chapter 4 discusses the cloning and expression of the *Yersinia enterocolitica* cytochrome b₅₆₂ protein and its various mutants designed to enhance the peroxidase activity of the proteins. Protocols established for purification of the wild-type enzyme and its mutants are explained in complete detail. Chapter 5 describes some of the techniques used for the characterization of the purified heme-proteins. It also provides information on the kinetics of the peroxidase activity assays performed on these proteins. Chapter 6 concludes the thesis with the summary of the research effort and suggestions for future work in the same direction.

CHAPTER TWO

2. Background

2.1 The concept of bioremediation

In the past century and particularly over the last few decades the amount and complexity of toxic waste effluents are increasing because of the rapid expansion of chemical industries. At the same time, fortunately, regulatory authorities have been paying more attention to problems of contamination of the environment. Industrial companies are therefore becoming increasingly aware of political, social, environmental, and regulatory pressures to prevent escape of toxic effluents into the environment. The occurrence of major incidents (such as *Exxon Valdez* oil spill, the Union Carbide Bhopal disaster; large-scale contamination of the Rhine River, and the progressive deterioration of the aquatic habitats and conifer forests in the Northwestern US, Canada, and parts of Europe, etc.) and the subsequent massive publicity due to the resulting environmental problems has highlighted the potential for imminent and long-term disasters in the public's conscience.

Even though policies and environmental efforts should continue applying pressure on industries to reduce toxic waste production, biotechnology offers attractive solutions to detoxify some complex industrial effluents. Natural bacterial populations already have

the ability to produce certain enzymes that metabolize industrial waste components that are toxic and difficult to degrade. It is now feasible to alter and manipulate the natural bacterial pathways and enzymes to enhance their ability to degrade pollutants. Since waste-management is a well-established industry, genetics, molecular biology and enzymology can add to the existing engineering expertise.

The technique of using biological organisms such as plants or microbes to clean up toxic contamination is called bioremediation. Bacteria generally break down the contaminants into harmless components such as carbon dioxide and water using naturally containing enzymes. However, the naturally existing enzymes are not necessarily effective at degrading some of the recalcitrant and highly toxic chemical wastes such as polychlorinated biphenyls (PCBs) and dioxin. One reason for this is the low level of these contaminants in soil or waste water effluents, making other sources of energy more attractive to bacteria. Hence, multidisciplinary approaches encompassing the techniques of molecular modeling, protein design, electrochemistry, electron paramagnetic resonance (EPR), X-ray crystallography and other spectroscopic techniques have been applied to design molecularly and chemically modified redox enzymes with enhanced activity and stability for bioremediation. Most of these redox enzymes are "metalloproteins", normal proteins that form complexes with transition metals, which typically act as the site of chemical catalysis. Hemoglobin, for example, which carries oxygen in the bloodstream, is an iron-containing metalloprotein. Other most common examples include myoglobin, chlorophyll, cytochromes, peroxidases, etc. The metal ions in metalloproteins are often critical to the protein's function, structure, or stability. These metalloproteins can help catalyze some of the most difficult biological reactions and fine-

tune the reactivity by using different metal ions, different redox states of the same metal ions, or different ligands or geometric arrangement of the same metal ions in the same redox state. Numerous studies have been published on the study of the native metalloproteins. However, little is known about how to design a metalloprotein with desired structure and activity and it remains one of the most popular areas of research. It is now broadly believed that the design and engineering of metalloproteins can provide great insights into the understanding of the fundamental principles in chemistry and biology and provide an economical alternative for biotechnological applications such as bioremediation.

The primary objective of the present work is to gain a fundamental understanding of the molecular and catalytic properties of the chemically and molecularly modified enzymes that are catalytically active and chemically stable. The study is also targeted to design and characterize redox enzymes possessing the electron transfer properties to achieve the goals of bioremediation. The foundation for this study is that stabilized and activated enzymes, which can function in harsh chemical conditions, are optimally suited for bioremediation in non-aqueous media where substrates of interest are more soluble and processed with greater efficiency.

2.2 Protein design

The field of protein design is emerging as a means to probe the intricacies of protein biochemistry, as well as a mechanism to create and integrate new catalytic functions in unique ways. From simple point mutations that heralded the early days of protein design to current functionally targeted *de novo* constructs, metalloprotein and

protein design has played a central role in enzymology, drug design, and biotechnology. The ability to design enzymes tailored to specific substrates and environments requires control in two areas: (i) development of an understanding of how protein sequence subtly regulates the catalytic site and protein structure and (ii) synthesis of novel prosthetic groups or cofactors in order to impart unique catalytic functions to proteins.

Understanding the role of the primary sequence in protein structure and function is one of the most intriguing questions in structural genomics. How do proteins fold into well defined three-dimensional structure? How do these structures relate to function? The answers to these questions lie at the heart of molecular and structural biology and biochemistry. Attempts have been made to address these questions through systematic characterization of the structures and properties of natural proteins and most recently, through design of novel proteins or protein engineering. Three approaches are popular in the field of protein design: (i) protein sequence modification, (ii) changing the protein environment and (iii) modification of the prosthetic group.

2.2.1 Protein sequence modification

In vitro site-directed mutagenesis (addition, deletion or substitution) is an invaluable technique, and it has allowed us to explore portions of the sequence of proteins, essential for their structure and function. However, in the early 1990s, a strong belief became prevalent that the ultimate test of our understanding of protein structure is to design sequences that fold into the structures that we specify. It has now been almost 16 years since the first serious attempts were made to design proteins from scratch. Since

then, *de novo* protein design has proven to be a powerful method for addressing questions in protein stability and folding.

In its most pristine form, *de novo* protein design refers to the design and construction of a protein intended to fold in a well-defined three-dimensional structure, with a sequence having little or no identity to that of any naturally existing protein (DeGrado et al., 1999). *De novo* design of proteins is a complementary approach to site-directed mutagenesis (Lloyd et al., 1998) and protein modification to understand how proteins fold into well-defined three-dimensional structures and how these structures relate to function. *De novo* design has proven an invaluable tool in understanding the mechanisms, dynamics, and thermodynamics governing protein structure and function. Understanding the relationship between structure and function has let us decipher the basic protein folding theories of secondary structure, protein stability, and conformational specificity (O'Neil et al., 1990; Hetch et al., 1990).

In *de novo* protein design, it is essential to compute a sequence that will adopt a given structure and often also a function. This remains a challenging job because even a short protein chain can have an astronomical number of potential sequences and also because a given sequence can adopt an astronomical number of conformations. The intellectual roots of this work go back to the early 1980s when protein engineers first thought about designing proteins. At that point, the prediction of a protein's three-dimensional structure from its sequence alone seemed a difficult proposition. However, the protein engineers proposed that the inverse problem - designing an amino acid sequence capable of assuming a desired three-dimensional structure - would be a more tractable problem, because one could "over-engineer" the system to favor the desired

folding pattern. Thus, the problem of de novo protein design reduced to two steps: selecting a desired tertiary structure and finding a sequence that would stabilize this fold.

Dahiyat and Mayo (1997), in an unprecedented work, distilled the rules, insights, and paradigms collected from two decades of experiments into a single computational algorithm that predicts an optimal sequence for a given fold. Further, when put to the test the algorithm actually predicted a sequence that folded into the desired three-dimensional structure. Dahiyat and Mayo's program divides the interactions that stabilize protein structures into three categories: interactions of side chains that are exposed to solvent, of side chains buried in the protein interior, and of parts of the protein that occupy more interfacial positions. Exposed residues contribute to stability, primarily through conformational preferences and weakly attractive, solvent-exposed polar interactions. The burial of hydrophobic residues in the well-packed interior of a protein provides an even more powerful driving force for folding. The side chains in the interior of a protein adopt unique conformations, the prediction of which is a huge combinatorial problem.

One important simplifying assumption arose from the early work of Jainin et al. (1978), who showed that each individual side chain can adopt a limited number of low-energy conformations (named rotamers), reducing the number of probable conformers available to a protein. Use of rotamer preferences greatly reduced the search spaces required. Although the side chains in natural proteins deviate from ideality (complicating the prediction of the structures of natural proteins), these deviations need not be considered in the designed sequences. Thus, various algorithms have been developed to examine all possible hydrophobic residues in all possible rotameric states, to find

combinations that efficiently fill the interior of a protein. A complementary approach uses genetic methods to exhaustively search for sequences capable of filling a protein core, and this work has been adapted for the *de novo* design of proteins. Interfacial residues are also quite important for protein stability. They are often amphiphilic (for example, Lys, Arg, and Tyr) and their apolar atoms can cap the hydrophobic core, while their polar groups engage in electrostatic and hydrogen-bonded interactions.

The use of solid phase peptide synthesis and genetic engineering methodology has allowed the design of proteins with novel functions. X-ray and NMR structures of *de novo* designed protein scaffolds, including helix-turn-helix (Fezoui et al., 1997), four- α -helix bundles (Schafmeister et al., 1993; Hill et al., 1998 and Skalicky et al., 1999) and mixed α/β architectures (Struthers, et al., 1996) are now available. These initial *de novo* protein design experiments have now progressed beyond the design of simple protein scaffolds to include the incorporation of metal and organic cofactor binding sites to enhance their catalytic, structural, regulatory, and electron transfer properties. Since the heme moiety was one of the earliest recognized inorganic biological cofactors, having been structurally elucidated by Hans Fischer, they turned out to be one of the initial *de novo* design metalloprotein targets. Heme-binding sites in proteins and peptides are attractive targets in protein engineering and design because the factors required for iron binding are relatively well understood, and iron metal binding frequently stabilizes folded peptides and proteins, thus facilitating the design.

2.2.2 Altering the protein environment

Perhaps the easiest approach to protein design is through modification of the structure and function of a naturally existing protein. An additional approach is to alter the solution environment of the protein. Change in solution conditions can affect for example, the pK_a of charged residues of proteins. The formation and breakage of salt bridges between pairs of charged residues are directly correlated with the pK_a values of the individual residues (Warshel et al., 1989) and can greatly affect protein stability. Recently, Kumar et al. (2000) have proposed that energy landscapes of individual proteins are dynamic, changing with the solvent environment, e.g., with pH, temperature, solvent conditions and the presence/absence of ligands and of cofactors. These extrinsic factors all alter the dynamic energy landscape, a reflection of the redistribution of protein conformer populations in response to environmental change. The specific three dimensional structure of a protein is the result of both intra-molecular interactions and from interactions between the polypeptide and its environment. Even slight changes in the environment can result in disruption of protein structure.

A study by Graupner et al. (1999) showed that the biophysical properties of enzymes change to a significant extent under conditions that modulate enzyme activities and stereoselectivities. They studied the intrinsic tryptophan fluorescence of the lipases from *Chromobacterium viscosum* (CVL), *Pseudomonas species* (PSL), and *Rhizopus oryzae* (ROL) in aqueous buffer, zwitterionic detergent micelles, and isopropanol-water mixtures. From the tryptophan lifetime distributions it was found that the conformation of CVL was not much affected by detergent or organic solvent (isopropanol). Accordingly,

CVL was enzymatically active in these systems and most active in the presence of isopropanol. In contrast, ROL and PSL showed high conformational mobility, depending on the solvent, because their lifetime distributions were very different in the presence and absence of detergent or isopropanol. Lipase aggregation was reversed by the addition of detergent or isopropanol, which competed for the hydrophobic surface domains of this protein. This dissociation contributed to the increase in lipase activity in the presence of a detergent or isopropanol.

A protein's surroundings in the cell can play an essential role in altering the final shape of the protein. An aqueous environment favors hydrophilic residues on the surface of the protein. A non-aqueous or non-polar environment favors hydrophobic residues on the surface of the protein. The temperature and pH level of the protein environment also affects protein shape. The final conformation determines the function and activity of the protein.

2.2.3 Modification of the prosthetic group

A third means of altering protein activity is to modify the nature of the prosthetic group, assuming one exists. In some cases, prosthetic group binding sites may be introduced into the “inert” proteins. Proteins that contain one or more hemes play an essential role in oxidative metabolism and electron transport systems, including microsomal and mitochondrial electron transport, removal of toxic peroxidases, and the oxygenation and hydroxylation of metabolically important organic molecules (Hatefi, Y., 1985). Heme proteins are ubiquitous in biological systems. Some of the heme proteins are also responsible for vital biological processes including steroid biosynthesis (Pikuleva

et al., 1999), aerobic respiration (Yoshikawa, S., 2002) and even programmed cell death (Narula et al., 1999).

Peroxidases, cytochromes, catalases and oxidases as well as mono- and dioxygenases are some examples of proteins incorporating the heme moiety. Regardless of their functions, the chromophore in each of these natural heme protein is a tetrapyrrole macrocycle, known as iron (II)-protoporphyrin IX, whose structure was synthetically demonstrated by Hans Fischer in 1929 (as shown in figure 2.1). The term “heme” specifically refers to the ferrous complex of protoporphyrin IX, with the ferric-hydroxy and ferric-chloride complexes referred to as hematin and hemin, respectively. Heme is commonly expected to be a planar molecule owing to its aromaticity.

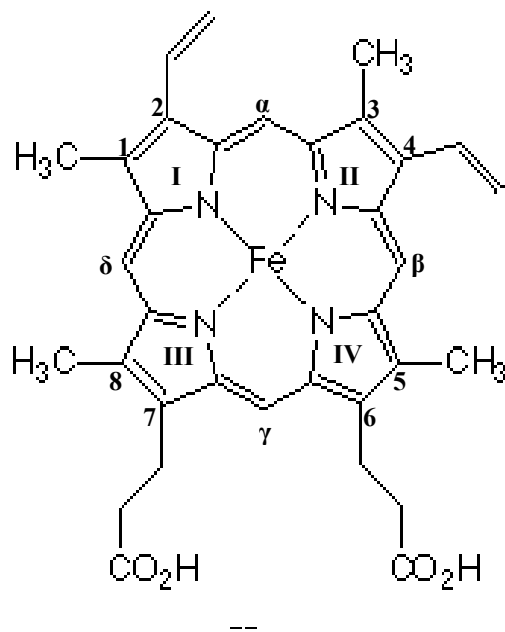


Figure 2.1: Chemical structure of commonly occurring natural heme *b*. It has methyl groups at positions 1, 3, 5 and 8, vinyl groups at positions 2 and 4, and propionates at positions 6 and 7 on the macrocycle. The carbon atoms of the methene bridges are labeled α , β , γ , and δ , with α carbon being located between side-chain positions 2 and 3.

There are three biologically important kinds of heme. The most common type of heme is called heme *b*; the others are heme *a*, and heme *c*. Heme *a* differs from heme *b* in

that a methyl side chain is oxidized into formyl group, and one of the vinyl side chains has been replaced by an isoprenoid chain. Like heme *b*, heme *a* is not covalently bound to the apoprotein in which it is found. An example of a heme containing protein that has heme *a* is cytochrome *c* oxidase. Heme *b* is the most abundant heme, both hemoglobin and myoglobin are examples of proteins that contain heme *b* (Figure 2.1). Heme *c* differs from heme *b* in that the two vinyl side chains are covalently bound to the protein itself. Examples of proteins that contain a *c* type heme are cytochrome *c* and the *bc₁* complex. In heme *d*, the prosthetic group is a chlorine and it is found in cytochrome *cd₁* nitrile reductase. Figure 2.2 shows the structures of heme *a*, heme *c* and heme *d*.

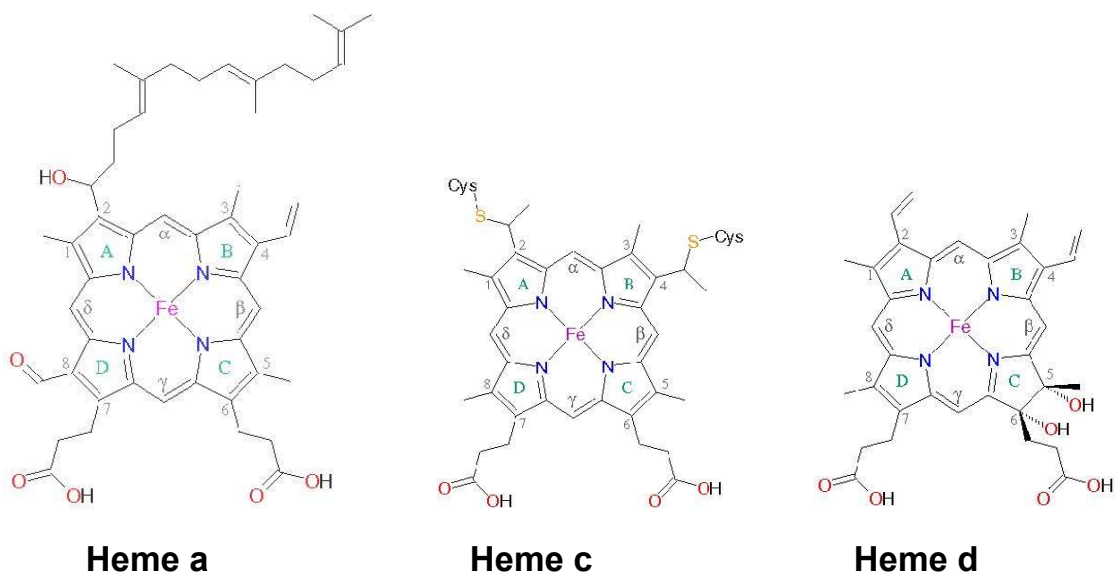


Figure 2.2: Chemical structures of heme *a*, heme *c* and heme *d*. The nomenclature is same as in Figure 2.1. The carbon atoms of the methene bridges are labeled α , β , γ , and δ , with α carbon being located between side-chain positions 2 and 3.

Protein scaffolds bind hemes via the combination of the axial coordination positions available on the iron metal center, hydrophobic interactions with the heme macrocycle, and polar interaction with the propionic acids (Hargrove et al., 1996).

The approach of modifying the prosthetic group in order to impart novel catalytic properties in heme proteins is particularly very interesting because there are a number of factors that can influence the function of heme-proteins, and it actually allows researchers to exercise tunability and control over protein activity. The metal center, pyrrole ring or reactive groups attached to the pyrrole rings can be changed to fine-tune the function of the protein via the chemical properties of the prosthetic group, until the desired activity is achieved. For example, reduction of one of the pyrrole units on the porphyrin ring leads to a class of porphyrin derivatives called chlorins. Chlorophylls (e.g. chlorophyll-a), found abundantly in green plants, belong to this category. They play very important roles in the conversion of solar radiation to biomass in the process of photosynthesis. Further reduction of chlorins gives another type of porphyrin derivative called bacteriochlorins, in which the reduced pyrrole units are diagonally opposite to each other. Bacteriochlorophylls (e.g. bacteriochlorophyll -a) are naturally occurring bacteriochlorins that are found in photosynthetic bacteria. Vitamin B₁₂ contains a porphyrin-like unit called a corrin, a reduced form of a corrole.

2.3 Heme proteins

Peroxidases and cytochromes are the two most widely studied heme-protein superfamilies promoting electron transfer reactions using a single prosthetic group (Sharp et al., 2003). Our interest in these two classes of proteins stems from their potential use for processing of renewable resources as well as for enzymatic transformations of polyaromatic hydrocarbons by oxidation.

2.3.1 Peroxidases

Peroxidases are found in many organisms including bacteria, fungi, plants, and animals (Welinder K. G., 1992). On the basis of sequence similarity, heme peroxidases can be categorized into two superfamilies: fungal, plant, and bacterial peroxidases form one superfamily and animal enzymes form another. On the basis of sequence comparison, fungal and plant peroxidases, which share similar overall protein folds and specific features such as catalytically essential histidine and arginine residues in their active sites, have been subdivided into three classes (Welinder K. G., 1985 and 1992). **Class I**, the intracellular enzymes, includes: yeast cytochrome *c* peroxidase (CCP), a soluble protein found in the mitochondrial electron transport chain; ascorbate peroxidase (APX) from plants, and bacterial catalase-peroxidases, exhibiting both peroxidase and catalase activities. **Class II** enzymes include the secretory fungal peroxidases: ligninases, or lignin peroxidases (LiPs), and manganese dependent peroxidases (MnPs), both from *Phanerochaete chrysosporium*, and *Coprinus cinereus* peroxidase, and *Arthromyces ramosus* peroxidase (ARP). These are monomeric glycoproteins involved in the degradation of lignin by wood rotting fungi. In MnP, Mn^{2+} serves as the reducing substrate. Lignin peroxidases catalyze one-electron oxidations of phenolic and non-phenolic compounds. Typical reactions catalyzed by lignin peroxidases are C α -C β cleavage, C- α oxidation, alkyl-aryl cleavage, aromatic ring cleavage, demethylation, hydroxylation, and free-radical polymerization (Reddy et al., 1994). Manganese peroxidases have lower redox potentials (up to 1.1 V) than LiP (LiP up to 1.5 V) and catalyze the Mn-mediated oxidation of lignin and phenolic compounds. The **Class III** enzymes consist of the secretory plant peroxidases such as those from horseradish (HRP),

barley or soybean, which have multiple tissue specific functions: e.g., removal of hydrogen peroxide from chloroplasts and cytosol; oxidation of toxic compounds; biosynthesis of the cell wall, etc. (Campa, A. 1991). Class III peroxidases are also monomeric glycoproteins.

On the basis of sequence similarity, a number of animal heme peroxidases can be categorized as members of a superfamily: myeloperoxidase (MPO); eosinophil peroxidase (EPO); lactoperoxidase (LPO); thyroid peroxidase (TPO); prostaglandin H synthase (PGHS); and peroxidasin (Kimuar et al., 1988 and Nelson et al., 1994). The structures of plant peroxidases and animal peroxidases are different. Plant peroxidases are bigger in size than the plant peroxidases and generally exist as dimers. For example, myeloperoxidase consists of two identical domains linked covalently by a single disulfide bridge.

2.3.2 The prosthetic group in peroxidases

Iron (Fe) is one of the most abundant transition metals making up the earth. Most of this iron is found in various ion oxides. Common oxidation states of iron include: the iron(II) state, Fe^{+2} or ferrous; the iron(III) state, Fe^{+3} or ferric (e.g., in rust); the iron (IV) state, Fe^{+4} or ferryl (e.g., in peroxidases). Iron is essential to all organisms, except for a few bacteria. Animals incorporate iron into the heme complex, an essential component of proteins involved in redox reactions, including respiration. Inorganic iron is also found in the iron-sulfur clusters of many enzymes, such as nitrogenase and hydrogenase.

In its inorganic compounds iron is commonly six-coordinate. However in peroxidases, for the native resting enzyme, the iron (III) is five-coordinate (possibly with

a weak H₂O ligand filling the sixth position); and the addition of common ligands such as cyanide or azide to the native enzyme results in six-coordinate iron (III) (Dunford, H.B., 1999). The coordination positions of the iron are numbered in Figure 2.1. In heme proteins, positions I to IV are occupied by the four pyrrole nitrogen atoms of the heme moiety. In peroxidases, position V is located on the proximal side of the heme and is commonly occupied by the imidazole side chain of the histidine residue. Position VI in the native resting enzyme is vacant and is located on the distal side of the heme (Figure 2.3). Most of the peroxidase reactions occur within the distal cavity. In peroxidases, the heme is attached to the apo-protein by a covalent bond, in which an amino acid side chain is attached to the fifth coordination position of the iron (III). This is dissimilar to some of the cytochromes, such as cytochrome *c*, where heme is covalently attached to the protein via two vinyl side chains.

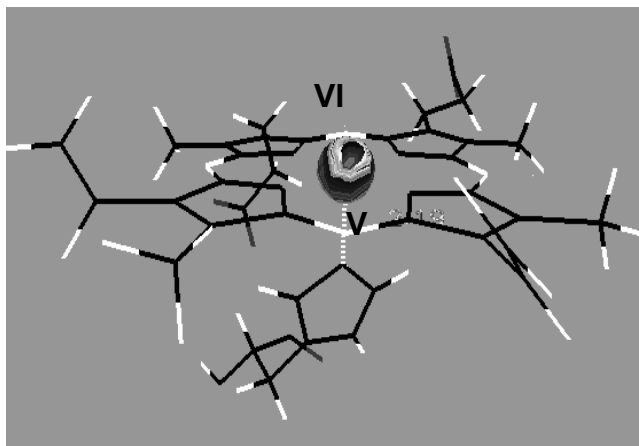


Figure 2.3: Model of heme prosthetic group in peroxidases. Iron of the heme is coordinated to the imidazole side chain of histidine on the proximal side, below the heme plane. The distal side, above the plane of heme is the active site of peroxidases.

2.3.3 Peroxidase electron transfer and bioremediation

Peroxidases use hydrogen peroxide (H_2O_2) as the electron acceptor to catalyze a number of oxidative reactions. Most heme peroxidases studied so far share much the same catalytic cycle that proceeds in three distinct and essentially irreversible steps and is often referred to as the “peroxidase ping-pong” mechanism (Dunford, H. B., 1991). The reaction scheme is shown below in figure 2.4.

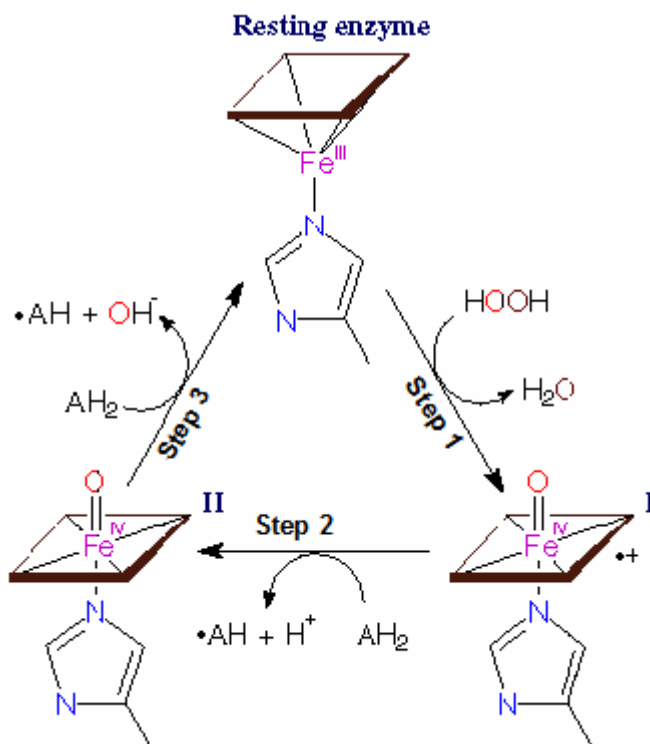


Figure 2.4: A schematic diagram representing the peroxidase ping-pong mechanism. In this mechanism, the enzyme first reacts with one equivalent of H_2O_2 to give compound I, a porphyrin π -cation radical containing Fe^{IV} . This is a two-electron oxidation/reduction reaction (step 1) where H_2O_2 is reduced to water and the enzyme is oxidized. One oxidizing equivalent resides on iron, giving the oxyferryl ($\text{Fe}^{\text{IV}}=\text{O}$) intermediate. Compound I then oxidizes an organic substrate to give a substrate radical ($\cdot\text{AH}$) product, which is often highly reactive, and water. Compound I undergoes a second one-electron oxidation reaction (step 2) yielding compound II, which contains an oxyferryl center coordinated to a normal (dianionic) porphyrin ligand. Finally, compound II is reduced back to the native ferric state with concomitant one-electron substrate oxidation (step 3).

The overall charge on the resting state and compound I is +1, while compound II is neutral. Some peroxidases (e.g., LiP) also catalyze the peroxidase-oxidase reaction, in which molecular oxygen in addition to H_2O_2 is an electron acceptor. In addition to the three steps mentioned above, this reaction system involves the incorporation of molecular oxygen in ferrous peroxidase forming compound III (inactive state of enzyme), which by reaction with free radicals becomes reduced to compound I and thus enters the classical cycle (Wariishi et al., 1990).

The peroxidase ping-pong provides an adequate description of the typical peroxidase reaction (Hiner et al., 2002). Numerous studies have reported that peroxidases (LiP, HRP, ARP etc.) use this electron transfer pathway (ping-pong mechanism) for the oxidation of substrates. For example, LiP first reduces H_2O_2 to H_2O to get oxidized from Fe^{+3} to $\text{Fe}^{+4}=\text{O}^\bullet$ (radical cation) and then transfers the heme-based free electrons to a surface exposed tryptophan which interacts with veratryl alcohol transfer these electrons to the organic substrates in the environment. Hence, redox enzymes like LiP are very useful in the bioremediation of recalcitrant compounds in aqueous, and potentially, in organic solvents because of their higher activity and stability where performance of other naturally occurring enzymes is quite limited (Hernandez et al., 2001). Considerable interest exists in developing novel strategies using chemically or molecularly modified enzymes with enhanced activity and thermodynamic stability for remediation of chemical contaminants (Huffman et al., 1998 and Privett et al., 2002). Another important consideration is substrate specificity, which depends on the nature of the solvents. A little substrate specificity of LiP allows it to be effective over a wide range of organic compounds. Kramar et al., 1998 and Yadav et al., 1995 have demonstrated the role of LiP

and MnP from the white-rot fungi, *P. chrysosporium* in degradation of lower-chlorinated and higher-chlorinated polychlorinated biphenyl mixtures. LiP also catalyzes the degradation of lignin, the most abundant biomass on earth, via oxidative metabolism (Ohkuma et al., 2001 and Mester et al., 2001).

2.4 Summary

The current work uses the sequence modification (*de novo* design and site-directed mutagenesis) approach to protein design to achieve specific aims:

1. To design and produce artificial four-alpha helix bundle proteins as scaffolds for examining the effect of mutations in these proteins on their heme binding and redox properties. To investigate the effect of substitutions in the vicinity of the heme binding on the electron transfer properties of the proteins.
2. To characterize the electron transfer and peroxidase properties of all these modified enzymes using spectroscopy and enzymatic assays.

In Summary, the purpose of the project is to design, synthesize, and characterize artificial peroxidases to better understand the structure-function relationships that govern oxidation/reduction potentials in this class of proteins and to develop potential catalysts for bioremediation and other industrial processes.

CHAPTER THREE

3. Design and chemical synthesis of peptide based four-helix bundle heme-proteins

3.1 Introduction

3.1.1 Peptide based synthetic heme-protein models

Metalloproteins are involved in some of the most fundamental biological processes including respiration, metabolism, nitrogen fixation, photo synthesis, and signal transduction. The role of metal ions in metalloproteins is both functional and structural, as the interactions between proteins and metal ions have been found to be critical to their catalytic function as well as their structural stability. One third of all proteins are metalloproteins, using metallic ions such as iron, copper, zinc, nickel, molybdenum, and vanadium. Some examples include hemoglobin, myoglobin, superoxide dismutase, nitrogenase, urease, chlorophyll, cytochromes and peroxidases. Heme-protein family is an example of metalloprotein containing a single prosthetic group promoting a variety of functions, such as dioxygen storage and transport, electron transfer and hydrogen peroxide disproportionation.

Here we seek to design and produce heme binding peptides to understand various factors that specify a singular global fold that suitably orients amino acid ligands for heme ligation. The design strategy can also be used to modulate the properties of the

bound heme via environmental factors such as solvent accessibility and alterations in the local dielectric constant that must be encoded in the primary structure. Perhaps the simplest protein designs incorporate α -helices since all the interactions within the protein are local and because of that the rules of *de novo* helix design are well established (Ho et al., 1987 and DeGrado et al. (1999)). That is one of the reasons why protein designers have utilized helical scaffolds extensively for *de novo* heme protein design. This design is divided into two groups based on the status of the hydrophobic core in the absence of heme: heme-peptide systems and heme-protein systems. Heme-peptide systems are smaller, mostly unfolded in the apo-state, and metal ligation induces the formation of secondary structure. In contrast, heme-proteins possess stably folded hydrophobic cores prior to heme incorporation. It is observed in naturally occurring heme proteins that the incorporation of heme in the apoprotein generally causes structural reorganization, since the metal ligation and hydrophobic interaction of the heme with the protein are closely related to protein folding, same applies to both these systems (Englander et al., 1998 and Dumont et al., 1994).

Heme-peptide systems are more complex than typical small molecule bioinorganic porphyrin model compounds, and yet are apparently not as puzzling as even the smallest natural heme proteins. Designed heme proteins potentially offer more diversity in peptide scaffold compared to designed heme peptide systems because of the presence of stably folded hydrophobic cores. As the field of protein design advances, the number and variety of global protein folds available for heme-protein design will expand. However, in practice, the majority of designed heme proteins are based on four- α -helix bundles similar to those originally described by Ho and DeGrado (1987). This similarity

offers comparison of their properties, and the development of novel scaffolds is still an exciting and demanding area of research.

The concepts of coordination chemistry based self-assembly of heme into designed protein scaffolds started developing in 1994. In a collaborative work, the laboratories of DeGrado and Dutton at University of Pennsylvania provided two related architectures for *de novo* heme protein design based on Ho and DeGrado's α_2 peptide. Choma et al. (1994), used a series of helix-loop-helix peptides containing one histidine residue dimerized via N-terminal cysteine residues to form monomeric four- α -helix bundles with a single bis-histidine heme binding site. All of these designs, including α_2 (S-S), which contained no potentially ligating histidine residues, bound heme tightly enough to elute with the four- α -helix bundles in size exclusion chromatography. The inclusion of histidine residues and introduction of a hydrophobic cavity enhanced the heme affinity with spectroscopic and electrochemical properties typical of bis-histidine ligated *b*-type cytochromes.

3.1.2 Design strategy

To design the four-helix heme-binding synthetic protein, LiP was chosen as the model protein, since LiP is able to oxidize a wide range of aromatic compounds with redox potentials higher than 1.4 V and has a very little substrate specificity. In LiP, Trp171 is an important residue in the electron transfer pathway. Trp171 is β -hydroxylated and solvent-exposed. Electrons are tunneled in LiP from the heme prosthetic group to this tryptophan residue and it acts as active site. By serving as an endogenous donor of electrons it rapidly reduces compound I to compound II and a tryptophan radical cation is generated. This radical cation then transfers the electrons to environment for oxidation of

surrounding chemical substrates. To mimic LiP activity, a four-helix bundle *maquette* was chosen as a structural scaffold on which the heme binding site and catalytic tryptophan were to be incorporated. A *maquette* is a peptide based synthetic analog of heme-proteins which is designed at the molecular level and has the flexibility of natural proteins and possesses same mechanical and physical properties but it is very simple in sequence. It is important to note that, to be useful, the model must contain a single heme binding site and the heme needs to be penta-coordinate (therefore having one open coordination site). This open coordination site is needed for binding of hydrogen peroxide to the metal center, with the resultant oxidation of the metal from Fe^{+3} to Fe^{+4} . During the oxidation of the ion metal center, a free radical is generated. This free radical is resided on the porphyrin ring. The model must also contain a single solvent exposed tryptophan residue that can act as the acceptor for the radical electron, to become a π -cation radical. This residue serves as the “active site” of the protein, though there is little substrate specificity and any substrate that comes in close proximity will likely be oxidized.

To use a four-helix bundle as model, the peptides were designed using a heptad repeat similar to that present in leucine zipper proteins (Landschulz et al., 1988). Leucine zippers are DNA binding motifs formed from two alpha-helices which interwine for about eight turns into a coiled coil and then bifurcate to form Y shaped structures. Leucines occurring in heptad repeats end up in same sides of the helices. The interior (buried) residues are largely hydrophobic (leucine and phenylalanine) while the solvent exposed (surface) residues are largely polar or charged (lysine, aspartic acid, glutamate, serine, and tyrosine). In addition, the method of assembly of the bundle, as a dimer of

dimers was needed to ensure the overall stability of the structure. To increase the chances of success, a known peptide sequence, a modified version of Dutton's design - the I₆F₁₃M₃₁ peptide (Huang et al., 2003) was used, where a disulfide bridge holds the dimers together. Since a single heme binding site with a penta-coordinate heme and a single tryptophan was desired, some degree of control over the assembly process at the dimer level was exercised. The five peptides are designed as follows:

Peptide A:

NH₃⁺ - CGGGE-IWKLH-EEFLK-KFEEL-LKLF E-ERLKK-LG-COOH

Peptide B:

NH₃⁺ - CGGGE-IKKLH-WEFLK-KFEEL-LKLF E-ERLKK-LG-COOH

Peptide C:

NH₃⁺ - CGGGE-IKKLH-EEFLW-KFEEL-LKLF E-ERLKK-LG-COOH

Peptide D:

NH₃⁺ - CGGGE-IKKLH-EEFLK-KFEWL-LKLF E-ERLKK-LG-COOH

Peptide E:

NH₃⁺ - CGGGE-IKKLI-EEFLK-KFEEL-LKLF E-ERLKK-LG-COOH

Note here that histidine and tryptophan are at different distances from each other, with the least distance between them in peptide A and most distance in peptide D and that peptide E has no tryptophan and no histidine. The desired final assembled four-helix bundle proteins are: A/E3, B/E3, C/E3 and D/E3. This configuration leaves only one peptide chain in the tetramer with histidine – a single axial ligand for the heme prosthetic group. These four-helix bundle proteins should follow the same electron transfer path as the naturally existing peroxidases to catalyze redox reactions using H₂O₂ as the electron

acceptor. A proposed electron transfer path for these synthetic heme-binding four-helix bundles with peroxidase activity is shown in figure 3.1.

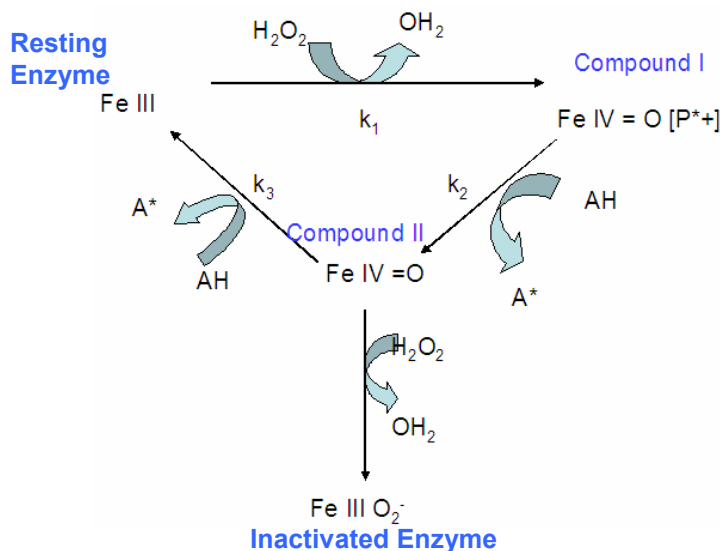


Figure 3.1: Proposed electron transfer path for the synthetic heme-binding four-helix bundle proteins. The enzyme first reacts with one equivalent of H_2O_2 to generate compound I, which is a porphyrin π -cation radical containing Fe^{IV} . The heme (iron protoporphyrin IX) in compound I then transfers these electrons to the tryptophan on the surface of the protein and generates a tryptophan radical cation, which serves as an active site to transfer the electrons to molecules in the environment and hence to hydrolyze chemical substrates. Compound I is oxidized to compound II in this process, which contains an oxyferryl centre coordinated to a normal (dianionic) porphyrin ligand. Finally, compound II, is reduced back to the native ferric state with concomitant one-electron substrate oxidation. The compound II can reduce one more molecule of H_2O_2 to and go to inactive state.

The rate of electron transfer is directly related to the distance between the heme and tryptophan. The closer the tryptophan to the surface of heme, the faster is the rate. To demonstrate this distance dependence, four different peptide assemblies were designed with tryptophan at different distances from the histidine, the heme binding site. It is proposed that for the B/E3 four-helix bundle assembly, where the tryptophan is closest to the surface of heme, the rate of electron transfer would be the highest while for the assembly D/E3 the electron transfer rate would be slowest. Table 3.1 shows the

distance of tryptophan from the plane of heme in these proteins. These distances were measured by creating their models in the molecular visualization program, VMD version 1.8.1.

Table 3.1: Distance of tryptophan from the plane of heme in the designed four-helix bundle proteins.

Peptide assembly	Distance of tryptophan from the plane of heme (Å)
A/E3	4.26
B/E3	6.73
C/E3	8.59
D/E3	13.89

3.1.3 Solid phase peptide synthesis

Since R. B. Merrifield's report (Merrifield, 1963) on the solid phase chemical synthesis of peptides and small proteins, solid-phase peptide synthesis (SPPS) has become a widely utilized technique for the production of peptides and small proteins. The synthetic peptides generated using SPPS are used extensively as antigens for the *in vivo* generation of selective antibody. In the current work, SPPS has been used to generate helical peptides containing 32 amino acid residues. These peptides self-assemble into four-helix bundle proteins and bind heme using a histidine axial ligation.

The basic idea of the solid-phase approach involves covalent attachment (anchoring) of the growing peptide chain to an insoluble polymeric support (resin), so that unreacted soluble reagents can be removed simply by filtration and washing without losses to the growing peptide chain. Subsequently, the insoluble peptide-resin is extended by addition of α -amino and side-chain protected amino acid residues in a series of addition reactions, which must be performed with high yields and fidelities. Excess soluble reagents are used to drive sequential coupling and deprotection reactions to

completion. The repetitive nature of the coupling and deprotection steps has led the major portion of the SPPS method to automation.

The general scheme of SPPS using Fmoc chemistry is illustrated in Figure 3.2. The acid-labile Boc group or base-labile Fmoc-group is used for *N*- α -protection of amino acids. Fmoc-group protected amino acids are most popular in SPPS since a mild base treatment using piperidine can be used for the Fmoc-group deprotection at every stage and stringent treatment using TFA is only required for the final cleavage and deprotection of the peptidyl resin. An *N*- α -derivatized amino acid is attached to an insoluble (solid) support via a flexible linker. The *N*- α -blocking group is then removed (deprotected) and the amino acid-linker-support is thoroughly washed with solvent. The next amino acid (which is also *N*- α -protected) is then coupled to the amino acid-linker-support directly in the presence of activators. The coupling may also be carried out using peptides instead of single amino acids, the method referred to as fragment condensation (Simmernan et al., 1982). After this reaction is complete, the *N*- α -dipeptide (or oligopeptide)-linker-support is washed with the solvent. The deprotection/coupling cycle is repeated until the desired sequence of amino acids is generated. The peptide-linker-support is cleaved to obtain the peptide as a free acid or amide, depending on the chemical nature of the linker. The cleavage reagent also removes the amino acid side chain protecting groups, which are stable to the deprotection reagent. These steps may be carried out as either a batch process, where the support is filtered between each step, or as a continuous flow process, where the support is always solvated during reagent exchange and the release of the protecting groups is monitored spectrometrically.

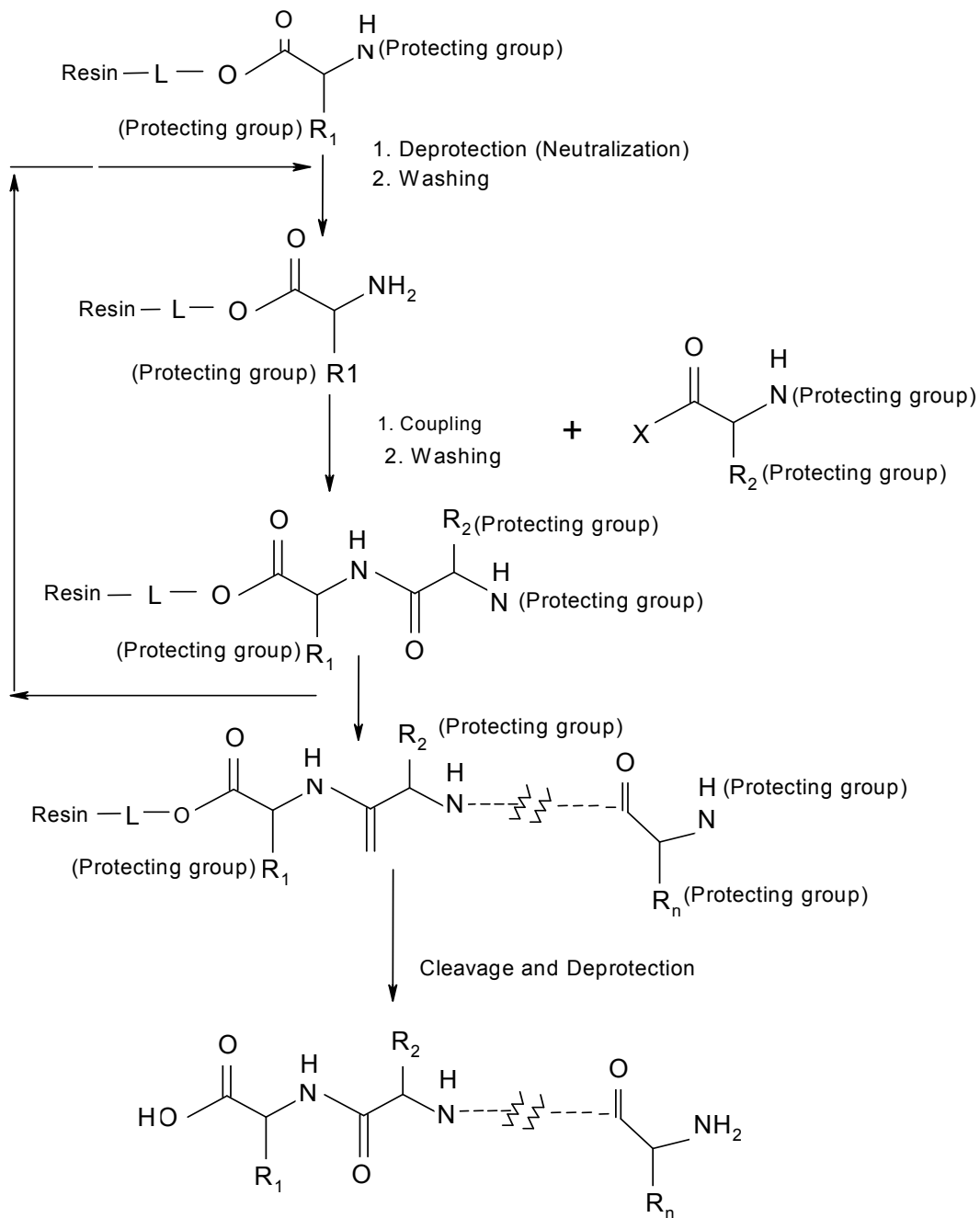


Figure 3.2: General approach to phase solid peptide synthesis using Fmoc chemistry. Peptides are synthesized from C-terminus to N-terminus by stepwise addition of α -amino and side chain protected amino acid residues to an insoluble polymeric support (resins). Final cleavage of the peptidyl resin and side chain deprotection is achieved using TFA.

3.2 Materials and Methods

3.2.1 Materials

All 9-fluorenylmethoxycarbonyl (Fmoc) protected amino acids, N- α -Fmoc protected Gly-Wang resins (100-200 mesh) and coupling reagents: N-hydroxybenzotriazole (HOBt), 2-(1H-benzotriazole-1-yl)-1,1,3,3-tetramethyluronium hexafluorophosphate (HBTU), and benzotriazole-1-oxo-tris-pyrrolidino-phosphonium hexafluorophosphate (PyBOP) were purchased from Novabiochem (EMD Biosciences, La Jolla, CA). Solvents: N,N-dimethylformamide (DMF) and dichloromethane (DCM), ethylene carbonate, piperidine, *N,N*-Diisopropylethylamine (DIPEA), trifluoroacetic acid (TFA), thioanisole, triisopropylsilane, pyridine, ethanol, phenol, methanol and ninhydrin reagent were from Sigma-Aldrich Co. (St Louis, MO). Triton X-100 was from TekNova Inc., Hollister, CA. Eanedithiol and 1-methyl-2-pyrrolidone (NMP) were purchased from Fluka. Potassium cyanide and ethyl ether were obtained from Fisher Chemicals (Fisher Scientific, Fairlawn, NJ).

3.2.2 Solid phase synthesis of peptides

Peptides A-E were synthesized manually in a batch-process at 0.25 mmol scale using a glass-funnel with glass frits to hold the resin, nitrogen gas to agitate the resin, and a vacuum line to drain the solvents and reagents in a flat-bottom flask. Water connections were made with the funnel to maintain the reactions at 55 °C with a recirculating water bath. The side chain protecting groups used were as follows: histidine (trityl); lysine (Boc); glutamic acid (OtBu); arginine (Pmc); cysteine (trityl); and tryptophan (Boc). As a free acid was desired in the final peptide, a *p*-alkoxybenzyl alcohol resin (Wang resin)

were chosen. To prevent the racemization of the first C-terminal amino acid during its coupling to the Wang resin, the resins were purchased with the L-Gly amino acid pre-coupled to it. *N*- α -Fmoc-Gly-Wang resins (0.25 mmol) were first swelled and washed thoroughly in magic mixture (1:1:1, DCM:DMF:NMP, 1% Triton X-100 and 2 M ethylene carbonate). The resins were then washed twice with DMF, DCM and again with DMF, each for 2 minutes and resuspended in magic mixture. To start the synthesis, the first resin-bound amino acid, Fmoc-Gly was deprotected using piperidine. Two resin volumes of freshly prepared 20% piperidine in DMF were recirculated through the resins two times for 6 minutes each. The reaction mixture was drained and the resins were washed thrice for 2 minutes each with excess magic mixture. At this point, the Kaiser ninhydrin test (see Appendix D) was performed to assay for the presence of free amino group. Upon a positive signal from the Kaiser ninhydrin test, 0.5 mmol of next amino acid to be coupled, 0.5 mmol each of the coupling reagents, HOBt, HBTU and PyBOP were added along with 1 mmol of activating reagent, DIPEA with an excess of magic mixture. The reaction mixture was agitated for 1 hour at 55 °C to couple the amino acid. A second ninhydrin test was used to assay for the presence of free amino group. The reaction was stopped if the ninhydrin test solution remained pale yellow, which indicated a complete coupling (no free amino group), otherwise the reaction was repeated. Some amino acids (cysteine, histidine, arginine, and proline) were routinely double-coupled.

The final peptide product was released from the resin in its fully deprotected form by treatment with TFA. Some scavengers (i.e., molecules that react preferentially with free radical and other reactive species released during the cleavage reaction) like thioanisole, ethanedithiol and triisopropylsilane were added to avoid undesirable

modification of the peptide during the cleavage process. At the end of the synthesis, the resins were washed three times each with DMF, DCM and methanol and allowed to dry. To cleave the peptide from the resin and deprotect the side chains, 3-4 resin volumes of freshly prepared ice-cold cleavage mixture (3% triisopropylsilane, 3% thioanisole, 5% ethanedithiol, 5% H₂O, 84% TFA) was added, and the mixture was incubated for 2 hours with agitation for 2 minutes of every 15 minutes to prevent the TFA from evaporating. The reaction mixture from resins was collected by draining it into a 30-ml glass centrifuge tube and the resins were washed again for 2 minutes with 5 resin volumes of undiluted TFA. The washing solution was collected from the resin by draining it into another 30-ml glass centrifuge tube. The peptide was precipitated immediately by adding 5 volumes of diethyl ether to the collected reaction mixture. The supernatant was decanted and precipitates were washed twice with three volumes of diethyl ether. The peptides were dried in atmosphere to remove diethyl ether and redissolved in water and stored at -20 °C.

3.2.3 Purification and assembly of the dimer/tetramer:

The finally cleaved crude peptides were purified from the scavengers and other impurities using high-pressure reversed-phase liquid chromatography. High-performance liquid chromatography was accomplished with a Waters 600 series HPLC equipped with a Waters 486 tunable absorbance detector (Waters, Milford, MA). Peptides were injected onto an Alltech Hi-prep C₁₈ reversed-phase column (Alltech Associates, Inc., Deerfield, IL) and were eluted at a flow rate of 10 ml/min using a linear gradient of aqueous acetonitrile (ACN) containing 0.1% formic acid. Fractions under the peak were collected

and UV-Vis absorbance spectra was measured on a Beckman DU 800 spectrophotometer (Beckman Coulter, Inc., CA) to check for the presence of trp and to estimate the concentration using the theoretical extinction coefficient values of the peptides.

Initial attempts were made to assemble the purified peptides A and E into a dimer via the disulfide bridge. Equimolar concentrations of peptides A and E were mixed together in the presence of 6 M urea and 1 mM DTT and then dialyzed against a 6 M urea buffer without DTT to facilitate the formation of disulfide bond by the cysteins in each peptide to compose a peptide A + peptide E dimer. An attempt was made to purify the (A+E) dimer from the other possible configurations [i.e., (A+A) and (E+E)] based on their pI using chromatofocusing. This also should also allow for the separation of small truncated sequences from full sequence peptides. The Mono P chromatofocusing column (Amersham Pharmacia Biotech, UK) is able to resolve samples by 0.02 pI units. Since the pI of the dimer (A+E) is 9.54, which is approximately 0.2 units less than that of (E+E) and 1.7 units more than (A+A), this difference should make the separation feasible. The column was charged using 75mM Tris-HAc buffer (pH 9.3) containing 6 M Urea. The peptide mixture was loaded in two 500 µl injections and the column was developed at 0.5 ml/min using 10% polybuffer, pH 6.0 (Amersham Pharmacia Biotech, UK) containing 6 M Urea. The fractions were scanned in the UV/Vis spectral range on Beckman DU 800 spectrophotometer to check for the presence of tryptophan.

3.2.4 Mass spectrometry

To determine whether the solid phase synthesis method has yielded the full sequences for all the peptides, the peptide samples were analyzed for exact molecular

weight using matrix-assisted laser desorption/ionization mass spectrometry (MALDI). Samples were prepared using the dried droplet method (Karas et al., 1988) on an 8 X 12 multi-well gold-plated sample plate. Alpha-cyano-4-hydroxy transcinnamic acid (Bruker, Billerica, MA) was used as the matrix and prepared as a saturated solution consisting of 40% - HPLC-grade acetonitrile; 60% - 1% trifluoroacetic acid in 18 M Ω water. One μ l of sample was deposited on the sample plate, immediately followed by 1.0 μ l of matrix solution and allowed to air evaporate and crystallize.

The MALDI mass spectra were produced using delayed ion extraction linear TOF-MS (Waters M@LDI-HT , Milford, MA) at an ion source bias potential of 15 kV, a 1400 V applied pulse voltage and a 500 ns pulsed ion extraction delay time. The laser fluence was adjusted to just above the threshold for ionization. Ion signals were detected using a dual microchannel plate detector having an applied voltage of 1900 V with a time resolution of 1 ns/data point. The externally calibrated mass spectra were smoothed, baseline subtracted and centroided to produce the mass-to-charge value of the ion signals. The mass spectral analysis was performed by the Core Laboratory Facility of Virginia Bioinformatics Institute at Virginia Tech.

3.3 Results and Discussion

3.3.1 Solid phase synthesis of peptides

Peptides were synthesized manually, because custom peptide synthesis was prohibitively expensive and lacked flexibility. In each of the solid-phase synthesis schemes, peptides were synthesized from the carboxyl terminus to the amino terminus. The carboxyl group of the carboxy-terminal amino acid of the desired peptide was

attached covalently to the solid support- Wang resin and the rest of the chain was synthesized by stepwise addition. A stable Fmoc- protecting group protected the reactive functional group of amino acids and prevented formation of complicated secondary chains. However, once the chain started to get longer (longer than 12-14 amino acids) the coupling reactions became more and more difficult presumably due to the formation of beta-sheet like secondary structures from hydrogen bonding either with neighboring peptide chains or with itself causing the alpha amino reaction site to be inaccessible. Residues cysteine, histidine, and arginine were difficult to couple and required longer reaction times or the reactions were repeated.

3.3.2 Purification of peptides

The synthesized peptides were cleaved from the resins using the TFA cleavage mixture. White flocculent precipitates appeared upon addition of diethyl ether to the cleavage mixture, and they were readily dissolved in water after evaporation of the ether. Crude peptides dissolved in water were injected onto the C₁₈ reverse-phase prep-scale column. The reversed-phase HPLC purification of the peptides yielded well isolated peaks and the UV-Vis absorbance spectra were recorded for the fractions under the peak. The spectra showed maxima at 280 nm corresponding to the presence of trp in the peptides A, B, C, and D. Figure 3.3 shows the HPLC chromatogram and Figure 3.4 shows the UV-Vis spectra for peptide A.

The peptides adsorbed to the reverse phase HPLC column in the aqueous mobile phase (Buffer A: 99.9 % H₂O+ 0.1% Formic Acid) and were eluted from the column with high organic (Buffer B: 90% Acrylonitrile + 10% buffer A) mobile phase. A linear

gradient of the organic solvent was used and the peptides were separated based on their hydrophobicity.

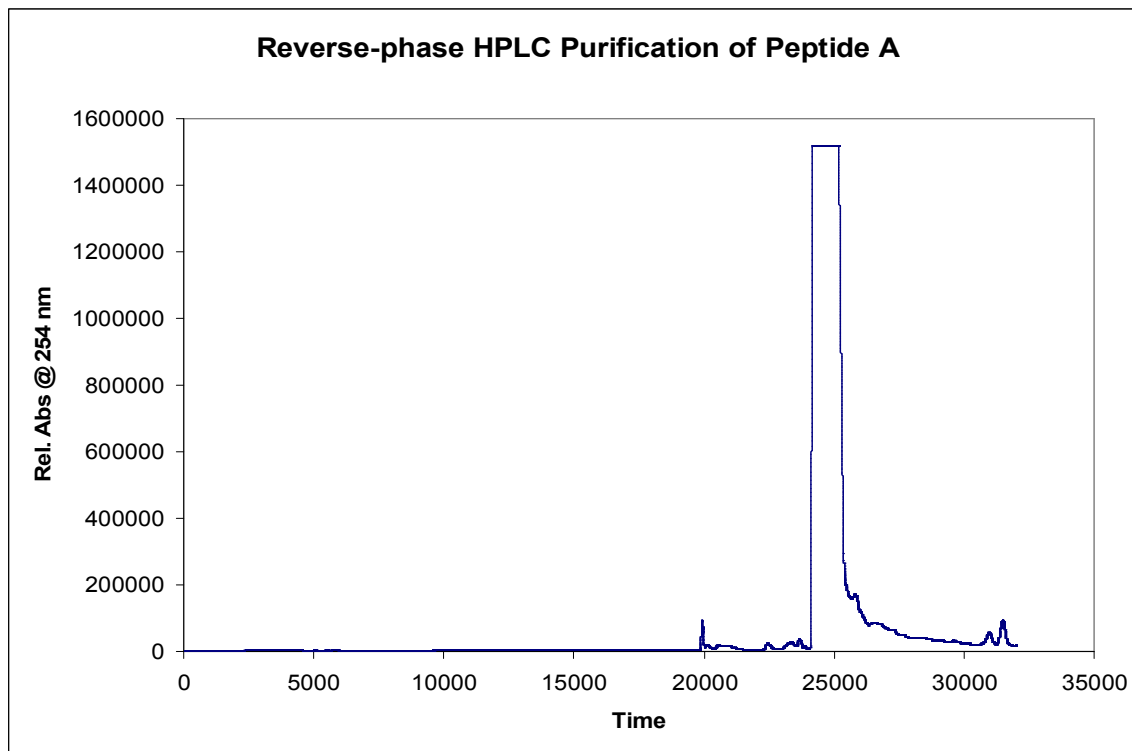


Figure 3.3: Reverse-phase HPLC purification of peptide A. The peptide was purified from crude mixture using a linear gradient of ACN with 0.1% formic acid and water as the aqueous mobile-phase component on Alltech Hi-prep C18 reversed-phase column with a flow-rate of 10 ml/min at room temperature.

Presumably, the complete peptide chains were larger than the truncated sequences and likely had more hydrophobic moieties to interact with the column and eluted later. The majority of peptides eluted by the time the gradient reached 35% buffer B. Although a prep scale C₁₈ column was used, the eluted peaks were sharp. All the four peptides purified showed very similar peaks at 35% buffer B concentration. All the three fractions under the peak showed absorbance corresponding to the presence of tryptophan in the peptide A. The UV-Vis spectra were similar for the fractions under the peak for all the other peptides as well, except peptide E, which did not contain any tryptophan.

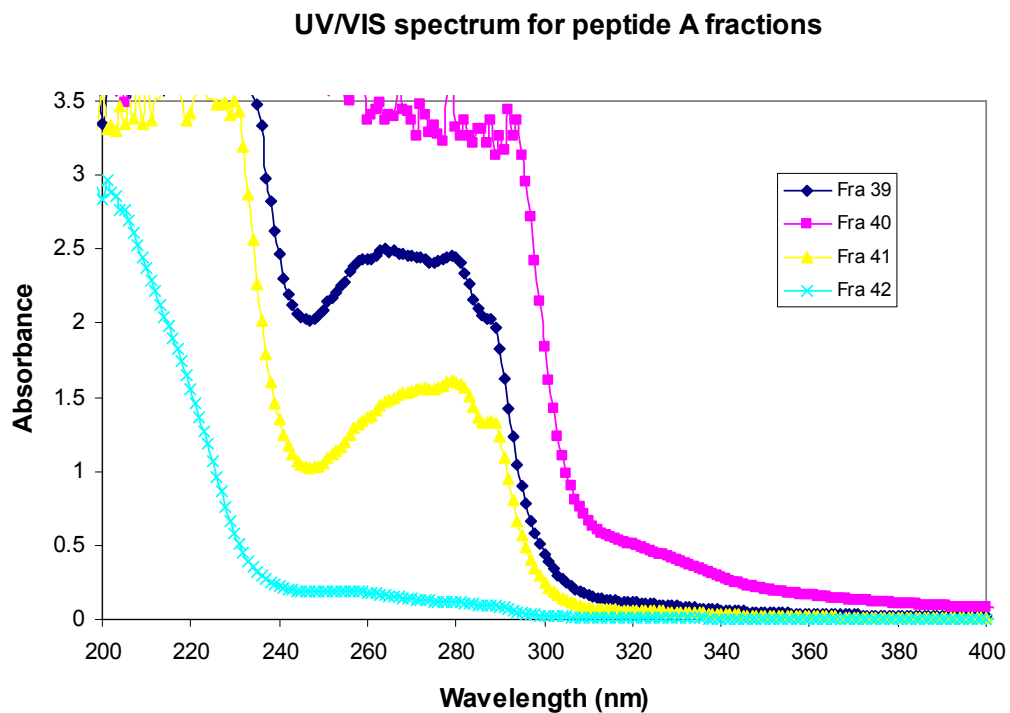


Figure 3.4: UV/Vis absorbance spectra of fractions under peak eluted from the reverse-phase HPLC column. The spectra showed a absorbance readings corresponding to the presence of tryptophan.

Since the tryptophan is just six amino acids from the N-terminus in the full length sequence, it was very likely that the full sequence of the peptide was present. However, the results of the MALDI spectra were discouraging, since it did not show a predominant peak corresponding to the exact mass of the full peptide sequence. In addition, the spectrum was cluttered with poorly resolved mass peaks indicating the presence of numerous small truncated sequences eluted under the same peak in HPLC. Figure 3.5 shows the MALDI mass spectral analysis of the fraction 39 from peptide A purification.

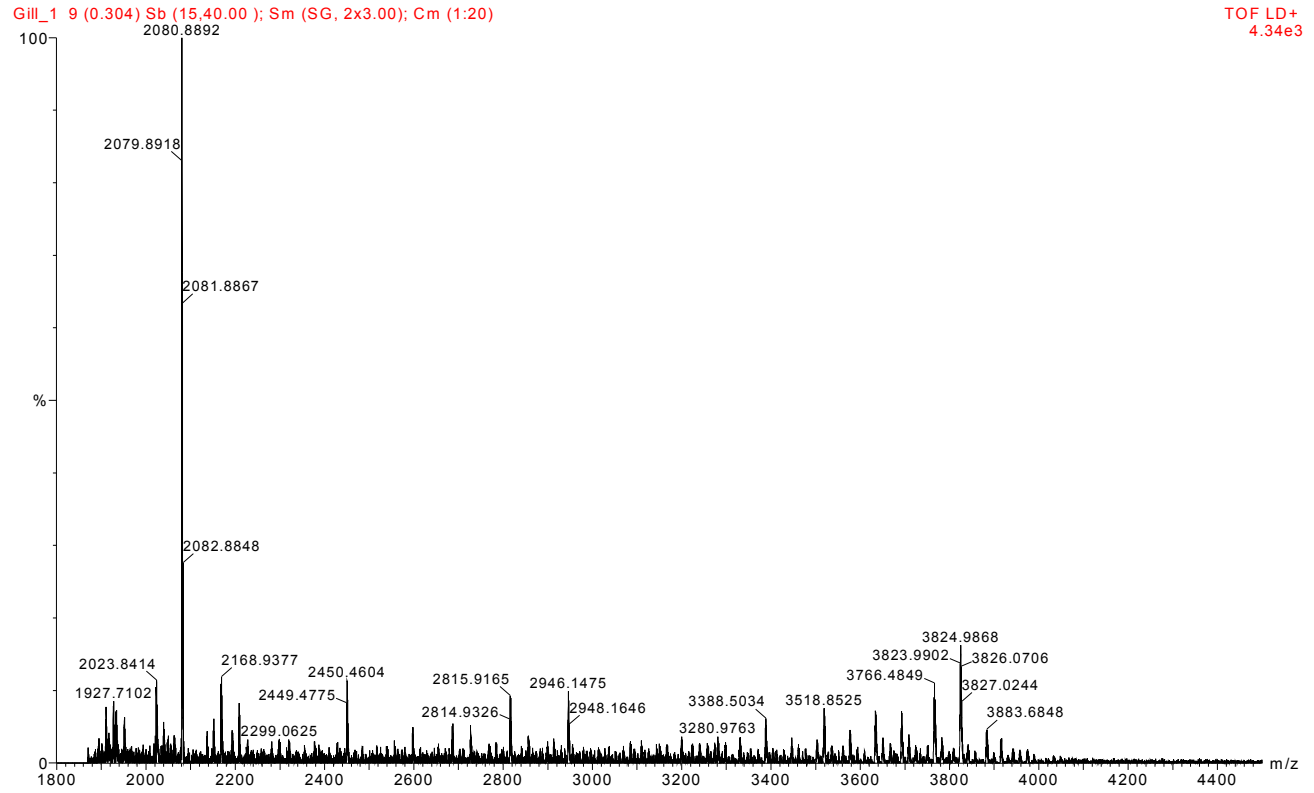


Figure 3.5: MALDI spectra for Fraction 39 from reverse-phase HPLC purification of peptide A. The expected mass of the full sequence peptide is 3850 Da.

The MALDI spectra for purified fractions of all other peptides were also cluttered with the presence of peaks for the truncated versions of the peptides. These products were identified as deletions due to an overall mass corresponding to an N-1, N-2 etc., where N is the mass of the full-length peptide. Depending upon the size of the deletion sequence and its chemical properties (e.g., relative hydrophobicity, HPLC retention time), separation of the full-length product from the crude mixture can prove to be difficult; hence the presence of truncated and full sequence fragments in the same peak can be explained.

For all of the peptides, the cysteine residue was at the N-terminus of the full sequence. For the formation of the dimers; the cysteine from one peptide chain should form a disulfide bond with the cysteine from other chain. Since the yield of the full-length peptides was relatively small, it drastically reduced the chances of dimer formation in the assembly experiments.

3.3.3 Explanation for the failure of SPPS

Although SPPS is highly efficient and can produce high quality peptides, the peptides synthesized in the current work contained some residues (histidine, arginine, phenylalanine and cysteine) which could have contributed to achieving less than quantitative yields of full-length product. This may arise from either hydrophobic interactions leading to aggregation or steric hindrance making extension of the growing peptide chain difficult. Potential problems during chain elongation leading to deletion sequences may include: (i) incomplete deprotection of the alpha amino Fmoc group; or (ii) incomplete activation or incomplete or low coupling efficiency of the incoming amino acid. Incomplete coupling would have reduced the overall yield of the final full-length product dramatically. For example, a 1% reduction in efficiency for each coupling step leads to a 24% loss of the total full-length product yield for a typical 30-mer. In addition, it is possible that the growing peptide chain could have a tendency for aggregation and form a beta-sheet like structure due to hydrogen bonding either with neighboring peptide chains, or with itself. Formation of such secondary structures would have caused the alpha amino reaction site to be inaccessible for further extension. Finally, although some scavengers (thioanisole, ethanedithiol etc.) were present in the cleavage

mixture, certain amino acids might have cyclized to form undesirable derivatives during the cleavage process (Chan et al., 2000) making the purification extremely difficult.

3.4 Conclusions

Five different 32-mer peptides were synthesized using SPPS via Fmoc chemistry and attempted to assemble them into four-helix bundle conformations. But since the yield of the full sequence from the synthesis was very low for all the peptides, the assembly experiments failed. The total cost of getting these peptides synthesized commercially was discouraging. Chemical synthesis of small peptides or proteins is typically much more difficult than genetic synthesis. Hence a four-helix bundle heme-protein, *Yersinia enterocolitica* cytochrome b₅₆₂, was chosen as a representative for the synthetic proteins and it was mutated to create exact models of the synthetic four-helix bundles described in this chapter.

CHAPTER FOUR

4. Cloning, expression and purification of *Yersinia enterocolitica* cytochrome b₅₆₂ and its mutants

4.1 Introduction

Heme-proteins serve diverse functions in biological systems such as electron transport, oxygen storage and delivery, and catalysis by effectively altering either the coordination of the heme iron or the orientation of amino-acid residues around the prosthetic group. The local protein environment surrounding the heme fine-tunes the heme-protein properties, such as the redox potential of the heme group. To modify the environment of the heme pocket, a rearrangement of the amino acid residues by mutagenic approach is a powerful method.

Soluble cytochrome b₅₆₂ from *Escherichia coli* is a well-studied heme-binding protein involved in electron-transport (Kamiya et al., 2001). The protein architecture consists of contains four antiparallel α -helices packed with a left-handed twist. Such a motif is known to occur in numerous proteins with varied amino acid sequences and functions (Weber et al., 1981). The four-helix structural arrangement is considered to possess extraordinary structural stability (Richmond et al., 1978 and Sheridan et al, 1982). The simplicity of the structure of cytochrome b₅₆₂ makes it a particularly amenable

model for the study of protein folding and structural dynamics. It has been established that cytochrome b_{562} binds non-covalently to iron-protoporphyrin IX as prosthetic group. In this respect, cytochrome b_{562} resembles hemoglobin and myoglobin. The amino acid sequence of *E. coli* cytochrome b_{562} was initially published by Igataki and Hager (1966), and later corrected by Lederer et al. (1981). It is a 106 amino acid protein with a molecular weight of approximately 12 kDa. Wild type cytochrome b_{562} does not contain any cysteine or tryptophan residues. The two axial heme ligands are Met7 on the first helix and His102 on the fourth helix (Itagaki et al., 1966 and Mathews et al., 1979).

Cytochrome b_{562} is an ideal model heme protein for studying the change in structural and functional properties by protein engineering because of its simple structure, single heme binding site, and ease of expression in *E. coli* (Barker et al, 1996 and Springs et al., 2000). However, to date the same protein from the organism, *Yersinia enterocolitica* has not been studied or characterized. We found a considerable amount of identity and similarity in the sequences of cytochrome b_{562} from *Y. enterocolitica* and *E. coli* using sequence alignment. Hence, we were able to correlate the structure of the two proteins. *Y. enterocolitica* cytochrome b_{562} is also a four-helix bundle heme-protein of about 12 kDa molecular weight containing 106 amino acids. Figure 4.1 shows an amino acid sequence alignment of cytochrome b_{562} in *E. coli*, *Y. pestis* and *Y. enterocolitica*. From the alignment it can be seen that there is 53% identity and 78% similarity of the *Y. Enterocolitica* with the *E. coli* cytochrome b_{562} amino acid sequence. Such high identity allowed us to correlate the structures of *E. coli* and *Y. enterocolitica* cytochrome b_{562} proteins with relative confidence.

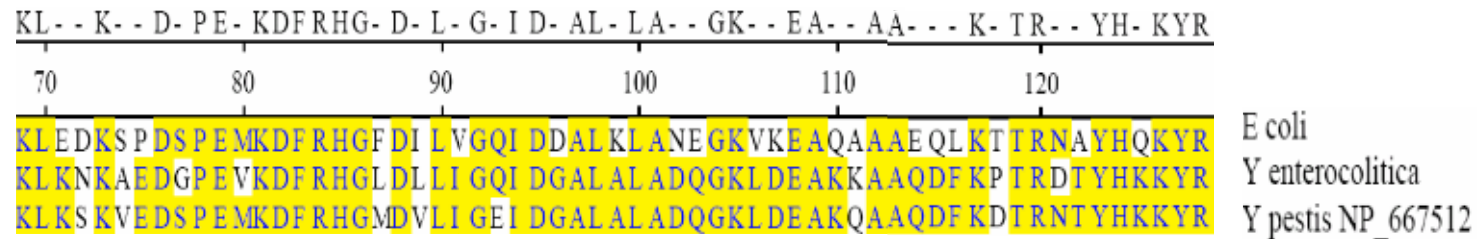
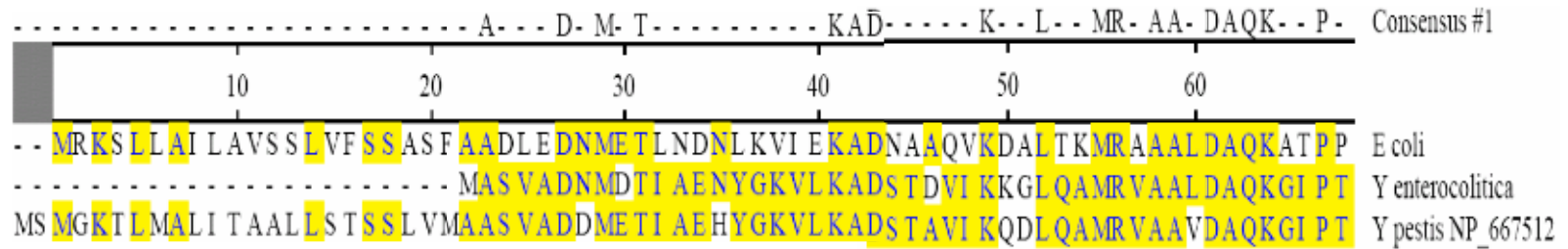


Figure 4.1: Sequence alignment of cytochrome b_{562} genes of *E. coli*, *Y. enterocolitica* and *Y. pestis*. The alignment was performed using the MegAlign module of DNA Star program on a personal computer. The shaded regions represent identity.

It is also obvious from the alignment that there is 84% identity and 96% similarity between the amino acid sequences of *Y. enterocolitica* and *Y. pestis*. Since *Y. pestis* was an organism of interest in the research group, it was thought that understanding the structure and functions of *Y. enterocolitica* cytochrome b₅₆₂ might provide some insight into the protein from *Y. pestis*.

Four single tryptophan substitution mutants were constructed in the gene of cytochrome b₅₆₂ to provide a unique site on the enzyme for electron transfer from the heme prosthetic group to the Trp residue and to the environment. These mutants allowed keeping alive the original idea of investigating the effect of having tryptophan at different distances from the plane of heme on the electron transfer properties of the enzyme. However since the heme is liganded by two stable axial ligands, it gives the organic substrates, such as H₂O₂, veratryl alcohol etc., little flexibility to diffuse in and bind heme and hence perform electron transfer. Hence the wild-type cytochrome b₅₆₂ and its tryptophan mutants were thought to likely have very little peroxidase activity. To generate four-helix bundles with peroxidase activity, one axial ligand, methionine7 was substituted with alanine so that the heme has one open coordination site. Later each of the tryptophan mutants was also incorporated into the M7A cytochrome b₅₆₂. The choice of methionine7 as a mutation site was based on following specific purposes:

1. To understand the effect of the heme axial ligand deletion on the structure and function of cytochrome b₅₆₂. According to a study by Hamada et al. (1995), the factors responsible for retaining the heme in the proteins are: (1) covalent bonding between the heme iron and axial ligand residues, (2) non-polar interactions between the heme and surrounding hydrophobic residues, and (3) polar interactions between

the heme propionates and surrounding hydrophilic residues (See, Figure 2.1). Since methionine⁷ is one of the axial ligands of heme, which contributes significantly to the overall structure of the protein, the substitution of methionine with alanine was predicted to affect the heme-binding capacity of the protein and in turn also affect the structural stability of the chain.

2. Since many of the various heme proteins with different functions carry the same prosthetic group, such as iron-protoporphyrin IX, function alteration between heme proteins by protein engineering becomes tricky. Cytochrome b_{562} would be a suitable candidate for this objective. As an example, in a complex functional process, the reaction of heme-proteins with peroxides often involves the formation of high-valent redox species containing ferryl heme $[\text{Fe}=\text{O}]^{4+}$ center (Dunford et al., 1991). The formation and stabilization of such ferryl heme species depend on the nature of the amino acid environment around the heme (Savenkova et al., 1998). Horseradish peroxidase (HRP), which is a naturally occurring peroxidase enzyme, has been shown to stabilize the high-valent intermediate and catalyze the oxidation of reducing substrates (such as ABTS, guaiacol etc.) by H_2O_2 at a very high rate (Gebicka, L., 1999). In recent years, the peroxidase reaction has been extensively studied. Several other heme-proteins and their mutants have been studied to understand specifically how the surrounding amino acids promote peroxidase-type activity in heme-proteins (Mazumdar et al., 2003). The hydrogen bonding between the distal histidine and arginine residues stabilizes the intermediate, which plays a key role on the catalytic activity of peroxidases like HRP (Poulos et al., 1980 and Tanaka et al., 1997).

Hemeproteins devoid of such suitable hydrogen bonding residues, e.g. cytochromes often show little or no peroxidase activity (Kamiya et. al., 2001).

Since the M7A mutants of cytochrome b_{562} can bind exogenous ligands to the heme iron, the enzymatic function may be similar to that of peroxidases. If this is true then the overall reaction cycle for holom7A cytochrome b_{562} catalyzed reactions proceeds in two clearly defined steps. First, the enzyme stores oxidizing equivalents derived from either molecular oxygen or hydroperoxides by cleaving the O-O bond and releasing a water molecule. Next, the enzyme utilizes these stored equivalents to oxidize other cellular components, either small organic molecules or another redox protein. The type of molecule oxidized by the heme enzyme determines its physiological and biochemical function. A generalized reaction scheme for heme enzymes is outlined below;



4.2 Materials and methods

Reagents were purchased from Sigma-Aldrich or Fisher Scientific unless otherwise indicated. Oligonucleotides were synthesized by Sigma Genosys (Malvern, PA). Restriction endonucleases and nucleotides were purchased from New England

Biolabs. Plasmids were obtained from Novagen (Madison, WI). The QuickChange® Point Mutation kit was from Stratagene (La Jolla, CA).

4.2.1 PCR amplification, cloning and expression of wild-type cytochrome b₅₆₂

The genomic DNA from *Yersinia enterocolitica* was obtained from ATCC. The genomic DNA was resuspended in 10mM Tris-Cl, pH 6.0 buffer to a final concentration of 200 ng/μl. A stock solution of 100 ng/μl was made from the main stock and it was digested with *HindIII* restriction endonucleases to make it linear. Note here that *HindIII* was used because *HindIII* restriction sites are not present in the gene of Cytb₅₆₂.

The following primers were used to carry out PCR primer extension:

N-terminal primer:

5' – ATA CCATGG CGA GTG TGG CTG ATA ACA TGG ACACT – 3'

C-terminal primer:

5' – GCG GAATTC TCA GCG GTA CTT TTT GTG – 3'

Polymerase chain reaction (PCR) was carried out in a total volume of 50 μl using 1 μl (approximately 100 ng) of the genomic DNA as template, 5 μl each of the primers (1μM stock solutions), 5 μl of dNTP mixture (2.5 mM for each dNTP), 5 μl of 10X thermopol buffer (10mM KCl, 20mM Tris-HCl pH 8.8, 10mM (NH₄)₂SO₄, 2mM MgSO₄ and 0.1% Triton X-100), 28 μl of dH₂O, and 1 μl of NEB Vent polymerase (approximately 1U, NEB # 254L from *T. litoralis* with 3' to 5' proofreading exonuclease activity). The extension reaction was carried out using an Eppendorf Mastercycler® (Eppendorf AG, Germany) with the following temperature program:

- a. Initial dissociation of template - 5 minutes at 94 °C
- b. Annealing of primers – 1 minute at 60 °C
- c. Primer extension – 1 minute at 72 °C
- d. Dissociation – 30 seconds at 95 °C
- e. Repeat steps b to d for a total of 30 cycles
- f. Final 10 minute extension at 72 °C

After a total of 30 cycles of amplification, the reaction mixture was transferred to a 1.5 ml eppendorf tube and precipitated with 1 ml of absolute ethanol for 1 hour. The pellet was washed with absolute ethanol and dried under vacuum. The dried pellet was resuspended in 20 µl 1X TE buffer. The yield and purity of the PCR product was checked by fractionating 2 µl of the DNA by electrophoresis in 2% agarose in 0.05 M Tris, 0.05 M acetate, and 0.01 M EDTA (TAE) buffer containing 0.5 mg/ml ethidium bromide (Sambrook et al., 1989). A 100bp ladder (NEB, Beverly, MA) was run along with the PCR product to estimate the size of the PCR product.

The PCR product was then digested to prepare sticky ends for ligation into a transformation vector, pET26b+ obtained from Novagen. A total of 8 µl (approximately 1 µg) was diluted into 1 µl of 10x NEB buffer 4 (20mM Tris-Acetate, 50mM Potassium acetate, 10mM magnesium acetate, 1mM DTT, pH 7.9 @ 25 °C) and 1 µl dH₂O. A total of 1 µl of *NcoI* (NEB # R0193S) was added to the reaction mixture and the digestion was allowed to proceed for 4 hours at 37 °C. The digestion reaction was brought to 200 µl with dH₂O, phenol-chloroform extracted, ethanol precipitated and finally resuspended into 10 µl of dH₂O. A total of 1 µl of 10x NEBuffer *EcoRI* (100 mM Tris-HCl, 50mM NaCl, 10mM MgCl₂, 0.025% Triton X-100, pH 7.5 @ 25 °C) and 1 µl of *EcoRI* was then

added to the mixture and again incubated at 37 °C for 4 hours. The double digested DNA was fractionated by electrophoresis on a 0.75% agarose gel. The DNA corresponding to the PCR product was extracted using the QIAquick® gel extraction kit (Qiagen, Valencia, CA) following the provided instructions.

The digested PCR product was ligated into the pET26b(+) vector, previously treated with *NcoI* and *EcoRI* using quick ligation kit (NEB # M2200S). Prior to ligation, the double digested plasmid was treated with calf intestine alkaline phosphatase, CIP (NEB # M0290S) to prevent recircularization and then purified by gel extraction. Ligation reaction was carried out using a 3:1 molar ratio of insert:vector. Quick ligase was used as suggested by New England Biolabs. The ligated plasmid DNA was directly transformed into *E. coli* strain BL21(DE)3. These cells had been made competent following the methods described by Sambrook et. al. (1989), using cold MgCl₂ and CaCl₂ (See Appendix A). Approximately 50 µl of competent cells were incubated with about 2 µl (approximately 20 ng) of ligation mix for 30 min on ice. The cells were then heat-shocked at 42 °C for 90 seconds and 500 µl of LB media was added to the transformation mix. The cells were allowed to recover at 37 °C for 60 minutes. A 200 µl aliquot of the cell culture was spread onto LB plates with the appropriate antibiotic (kanamycin in this case) and incubated overnight at 37 °C. A control transformation reaction was set up using the CIP treated plasmid but with no insert.

Well isolated transformants (colonies) were picked from the LB+kanamycin plates and used both to streak out colonies on a second LB+kanamycin plate and to inoculate several 3 ml LB+kanamycin broth cultures. Both cultures were incubated at 37 °C, the latter with constant aeration in a roller-drum. The broth cultures were used to

check for protein overexpression and were allowed to grow until the optical density was approximately 1.2 (measured at 600 nm wavelength in a spectrophotometer) and were then induced with 3 μ l of 1M IPTG (isopropyl β -D-thiogalactopyranosidase) each and allowed to grow for four more hours except for one culture, which was used as an uninduced control. At that point, 100 μ l of the broth was transferred to 1.5 ml Eppendorf centrifuge tubes and centrifuged at 5000 rpm for 15 minutes in an Eppendorf table-top centrifuge. The broth was decanted and the pellet were resuspended in 42 μ l of dH₂O and 6 μ l of 6X SDS sample buffer (350mM Tris-Cl, pH 6.8, 3% glycerol, 10% SDS, 0.3% DTT, and 10% bromophenol blue). The suspension was boiled for 10 minutes at 94 °C, re-centrifuged at 12000 rpm to pellet cell debris, and a 20 μ l aliquot was loaded onto a SDS-PAGE gel (15% acrylamide with 37.5:1 crosslinker ratio). The gel was run using the Laemmli method (1970) at 120 V for approximately 110 minutes. The gel was stained with Coomassie blue, washed and destained with acidic methanol (5% acetic acid, 16.5% methanol in water).

The LB+kanamycin plate was grown at 37 °C overnight and was used to prepare stock glycerols (50% glycerol, 50% LB+kanamycin broth, 500 μ l volume) of those colonies that were observed to express the cytochrome *b₅₆₂* gene when induced by IPTG and which showed an over-expressed band (positive clones) on the SDS-PAGE gel. Glycerol stocks were stored at -80 °C until needed.

To further test the clones, 3 ml LB+kanamycin broth starter cultures were prepared from the glycerol stocks and grown overnight. The plasmid containing the cytochrome *b₅₆₂* gene was extracted out of each of the bacterial cell pellet using QIAprep® Spin Miniprep Kit (Qiagen, Valencia, CA) following the provided

instructions. The purified plasmids were then sequenced to check for the presence of cytochrome b_{562} gene. The plasmids were also digested with *DraI* restriction endonuclease, which has a unique restriction site present in the cytochrome b_{562} gene but which is otherwise absent in the plasmid. After the digestion, the plasmids were fractionated by electrophoresis on 1% agarose. Hence, the presence of cut plasmid would suggest the presence of insert. Later, three of these plasmids were digested with same restriction enzymes used for cloning, i.e. *NcoI* and *EcoRI* to cut the insert out and were fractionated by electrophoresis on 1% agarose.

4.2.2 Construction of C-terminal Trp mutant of cytochrome b_{562} : K103W

Synthesis of K103W mutant of cytochrome b_{562} was carried out in the same manner as the wild-type using the polymerase chain reaction. The following primers were used to carry out PCR primer extension:

N-terminal primer (same as wild-type):

5' – ATA CCATGG CGA GTG TGG CTG ATA ACA TGG ACACT – 3'

C-terminal primer (contains the K103W mutation):

5' – TATT GAATTC TCA GCG GTA CTT CCA GTG ATA AGT ATC – 3'

The cloning of the K103W PCR product into the expression vector pET26b(+) and screening of the colonies was performed using the same protocol. The plasmid containing the K103W cytochrome b_{562} gene was extracted out of the BL21(DE)3 cells using QIAprep spin miniprep using the directions provided and it was also digested with the restriction endonucleases, *NcoI* and *EcoRI* to cut the insert out and fractionated by electrophoresis on 1% agarose.

4.2.3 Construction of Trp point mutants within the gene of cytochrome b₅₆₂

Three single tryptophan substitution mutants were constructed within the gene of cytochrome b₅₆₂ using the Stratagene Quickchange® II mutation kit (Stratagene, CA). These mutants were: K83W, K89W, and K95W. The rapid three-step procedure recommended by Stratagene was used to generate these mutants with high efficiency in single reactions. The miniprep purified double-stranded plasmid DNA (dsDNA) containing the wild-type cytochrome b₅₆₂ gene was used as a template for all site-directed mutagenesis. Two synthetic oligonucleotide primers, each complementary to opposite strands of the vector and both containing the desired mutation flanked by unmodified nucleotide sequence were used for each mutant strand synthesis reaction.

The synthesis reactions were set up as indicated below: 5 µl of 10X reaction buffer, 20 ng of dsDNA template, 125 ng of oligonucleotide primer # 1, 125 ng of oligonucleotide primer # 2, 1 µl of dNTP mix, ddH₂O to a final volume of 50 µl. Then, 1 µl of *PfuUltra* HF DNA polymerase (2.5 U/µl) was added to this reaction mixture and the extension reaction was carried out using an Eppendorf Mastercycler® (Eppendorf AG, Germany) with the following temperature program:

- a. Initial dissociation of template - 30 seconds at 95 °C
- b. Annealing of primers – 1 minute at 55 °C
- c. Primer extension – 6 minute at 68 °C
- d. Dissociation – 30 seconds at 95 °C
- e. Repeat steps b to d for a total of 12 cycles

The primer extension time was determined from the length of plasmid with insert (1 minute/kb of plasmid length required). Since pET26b(+) with insert was

approximately 5650 kb in length, the extension time was set to 6 minutes. Thermal cycling extension of the oligonucleotide primers generated mutated plasmids containing staggered nicks. After a total of 12 cycles of amplification, each product was treated with *Dpn* I. The *Dpn* I endonuclease (target sequence: 5' – Gm ATC – 3') is specific for methylated and hemimethylated DNA and was used to digest the parental DNA template and to select for the mutation-containing synthesized DNA (Nelson et al., 1992). One μ l of the *Dpn* I restriction enzyme (10 U/ μ l) was directly added to each amplification reaction and mixed gently and thoroughly by pipeting the solution up and down several times. The reaction mixtures were centrifuged in a microcentrifuge for 1 minute and each reaction was incubated immediately at 37 °C for 1 hour to digest the parental (i.e., the nonmutated) supercoiled dsDNA. The nicked vector DNAs containing the desired mutation were then transformed into XL1-Blue supercompetent cells supplied with the kit (Appendix A). Figure 4.2 shows an overview of the mutagenesis method.

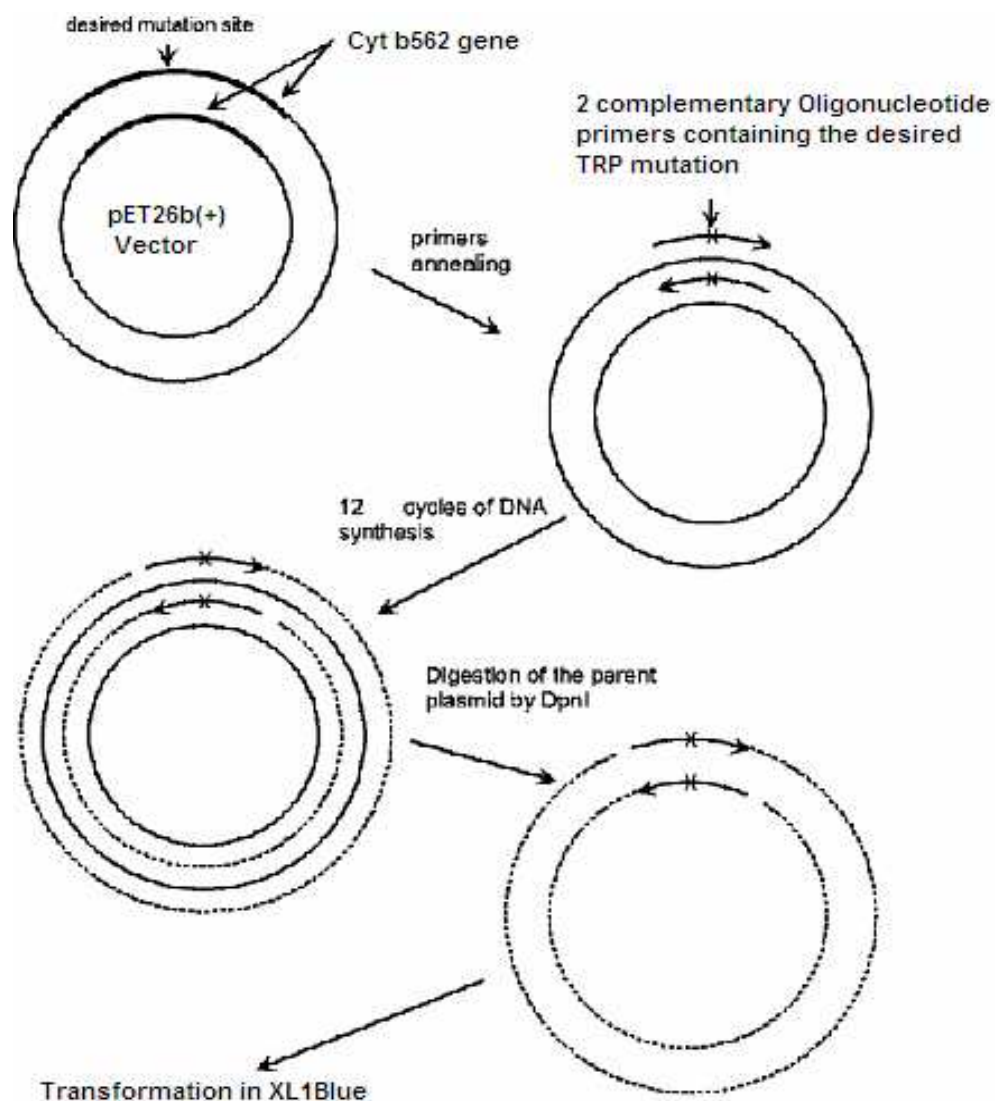


Figure 4.2: Overview of the QuickChange® II site-directed mutagenesis method. This method involves three simple steps: mutant strand synthesis, *Dpn I* digestion of parental DNA template and transformation of the resulting annealed double-stranded nicked DNA molecules. After transformation, the XL1 Blue *E. coli* cell repairs nicks in the plasmid.

Single colonies were picked up from each transformation to inoculate 3 ml starter cultures of LB+kanamycin and grown overnight. The plasmids containing the tryptophan substitution mutants in the cytochrome b_{562} gene were extracted out of the XL-1 Blue bacterial cell pellet using QIAprep® Spin Miniprep Kit (Qiagen, Valencia, CA) following the provided instructions. The purified plasmids were then sequenced to check

for the presence of the right mutations of cytochrome b_{562} gene. These plasmids were then transformed into the expression strain BL21(DE)3 for protein production.

4.2.4 Deletion of heme axial ligand (M7A mutation) of cyt b_{562}

To investigate the effect of the deletion of one of the heme axial ligands, methionine7 on heme binding and overall structural integrity, several new mutants were generated, in which methionine7 was replaced by Ala in each of the wild-type cytochrome b_{562} and its tryptophan substitution mutants. These mutations were also created using the Stratagene Quickchange® II site-directed mutation kit. The plasmid containing the wild-type Cyt b_{562} gene was used as template to generate the M7A single point mutant. The plasmids containing the tryptophan mutants were used as a template to incorporate one more single point mutation of M7A. All M7A mutant plasmids were then transformed into BL21(DE)3 for protein production. Glycerols stocks were prepared for all the tryptophan substitution and M7A mutants.

4.2.5 Protein over-expression and purification

BL21(DE)3 cells containing the pET26b(+) vector with the cytochrome b_{562} insert from glycerol stocks were used to inoculate a 100 ml LB+kanamycin starter cultures and grown overnight. One liter of LB+kanamycin was inoculated with this starter culture, was subdivided into two sterile 2 L Erlenmeyer flasks, and allowed to grow at 37 °C with constant shaking at 250 rpm in a New Brunswick I2400 shaking incubator (New Brunswick Scientific Co., Edison, NJ) until the optical density was approximately 1.2 (measured at 600 nm wavelength in a spectrophotometer). At that time, the cells were

induced to begin overexpression by the addition of IPTG (550 μ l of 1 M aqueous solution per flask). After induction cells were allowed to grow for four additional hours. The induced cells were then gently centrifuged at 5000 rpm for 15 minutes in a Sorvall RC5B centrifuge with a SLA-1500 rotor at 4 °C. The supernatant was decanted and the cell pellets were resuspended in 50mM sodium succinate, pH 4.5 buffer. The resuspended cells were completely disrupted by sonication with the Branson sonifier 450 (VWR Scientific Products, Sand Dimas, CA) with duty cycle set to 50 and output control set to 5 for five 4 minute cycles and incubation on ice in between each cycle. The ultrasonically disrupted cell suspension was centrifuged at 18000 rpm for 1 hour in the Sorvall RC5B centrifuge with a SS-34 rotor at 4 °C to obtain the crude cell-free extract. All subsequent steps of purification were performed at 4 °C, with the exception of the chromatographic steps. The supernatant then contained the overexpressed protein, cyt b₅₆₂ along with other cytoplasmic and periplasmic bacterial proteins and also some lipo-proteins and lipids. To remove these other proteins, lipo-proteins and lipids, which impart viscosity to the supernatant, it was passed through disposable poly-prep chromatography columns (Bio-Rad laboratories, Hercules, CA), packed with Q-sepharose anion-exchange beads. Since the pI of wild-type cyt b₅₆₂ is approximately 8.8, it is positively charged at pH 4.5, and so it passed through the Q sepharose column without binding. This procedure helped eliminate some of the proteins, lipo-proteins and lipids that bound to the Q sepharose column at this pH and facilitated loading of the subsequent chromatographic columns. The total cell lysate was then purified over HiPrepTM 16/10 SP sepharose fast-flow (Amersham Pharmacia Biotech, UK) cation-exchange column. The column was first equilibrated with five column volumes of 50mM sodium succinate, pH 4.5 buffer. Then

the total cell lysate was slowly loaded on the column using a superloop. After adsorption of the protein onto the column, the matrix was extensively washed with 4 column volumes of the equilibration buffer. The column was run at the flow rate of 5 ml/min on a Pharmacia bio-tech FPLC system. After thorough washing, the column was developed with a salt gradient from 0 to 1 M NaCl in the same buffer. A detailed description of the method used is attached in Appendix C. The 5 ml fractions were collected in 15 ml Falcon centrifuge tubes. Fractions from the eluted peak were run on 15% acrylamide SDS-PAGE gel. The fractions that were observed to contain the cytochrome b₅₆₂ protein band were combined and concentrated using a Centriplus 80 concentrator (Millipore, MA). A total volume of 60 ml of the combined fractions was concentrated to about 500 µl. The concentrated protein was further purified using a Superpose 6 HR 10/300 (Amersham Pharmacia Biotech, UK) gel filtration (size exclusion) column with a 50mM potassium phosphate buffer containing 150mM NaCl at pH 7.0. For each run of the size exclusion column, 200 µl of concentrated protein was loaded on the column and the elution of protein resulted in one major peak with cytochrome activity. The size exclusion column also provided an exchange of buffer.

4.2.6 Determination of protein concentration

The concentration of the purified protein in the fractions from the size exclusion column was determined by method described by Smith et al. (1985). Known concentrations of bovine serum albumin (BSA) were incubated in working reagent (50:1, BCATM reagent A: BCATM reagent B, PIERCE, IL) and absorbance at 562 nm was obtained to generate a standard curve. Experimental protein solutions (protein samples of

unknown concentrations) were treated with working reagent and absorbance at 562 nm was determined. The protein concentration was calculated based on the standard curve.

4.3 Results and Discussion

4.3.1 Cloning and expression of *Y. enterocolitica* cytochrome b₅₆₂

The *Yersinia enterocolitica* cytochrome b₅₆₂ gene amplified by PCR was 333 bases long (corresponding to the protein size of 106 amino acids flanked by the restriction site sequence and adaptor sequence). Figure 4.3 shows the 2% agarose gel used to fractionate the PCR product along with 100 bp ladder used for a size reference.

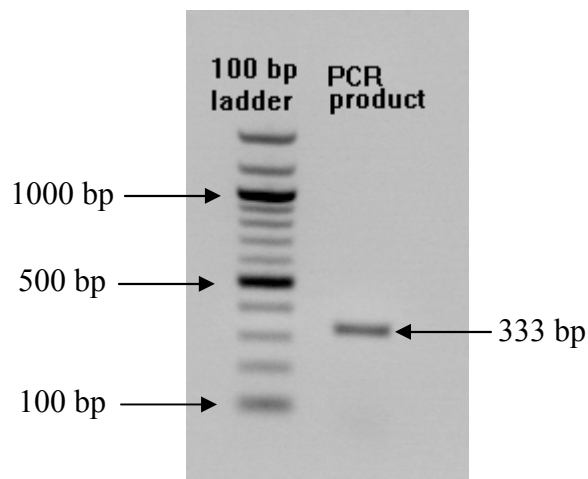


Figure 4.3: Agarose gel analysis of PCR amplified gene of *Y. enterocolitica* Cyt b₅₆₂

The PCR product was digested with restriction enzymes *NcoI* and *EcoRI* and cloned into the multiple cloning site of the pET26b(+) expression vector. The plasmid containing the insert was then transformed into the BL21(DE)3 strain of *E. coli*. The transformation efficiency was approximately 2.56×10^5 cfu/ μ g DNA (See Appendix A for

calculation). Figure 4.4 shows the comparison of the experimental transformation with the control transformation (CIP treated plasmid without insert).

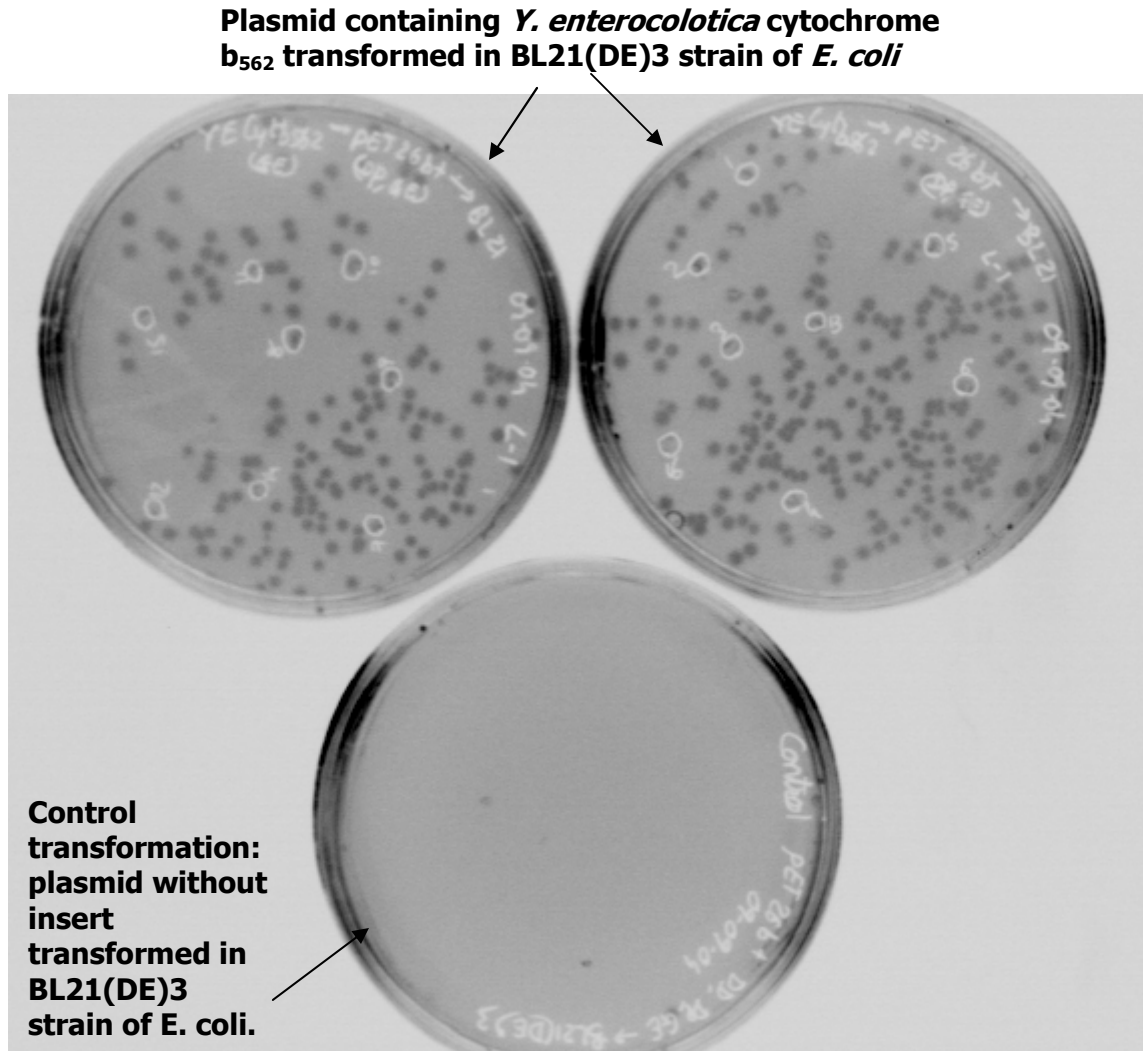


Figure 4.4: Transformation of pET26b(+) containing the cytochrome b_{562} gene into BL21(DE)3 strain of *E. coli*. Control transformation has CIP treated pET26b(+) but no insert. The image was enhanced with Scion Image and an invert picture is displayed here.

Six well isolated colonies were chosen from the transformants obtained and screened for protein over-expression on induction with IPTG. After 4 hours of induction the cultures showed a visible difference in color (red) as compared to the control

uninduced culture. Upon centrifugation, the cell pellets were red in color, which was an obvious indication of over-expression of the heme-containing protein. Figure 4.5 shows the 15% SDS-PAGE gel with overexpressed bands at about 12 kDa size, corresponding to the predicted size of cytochrome b_{562} .

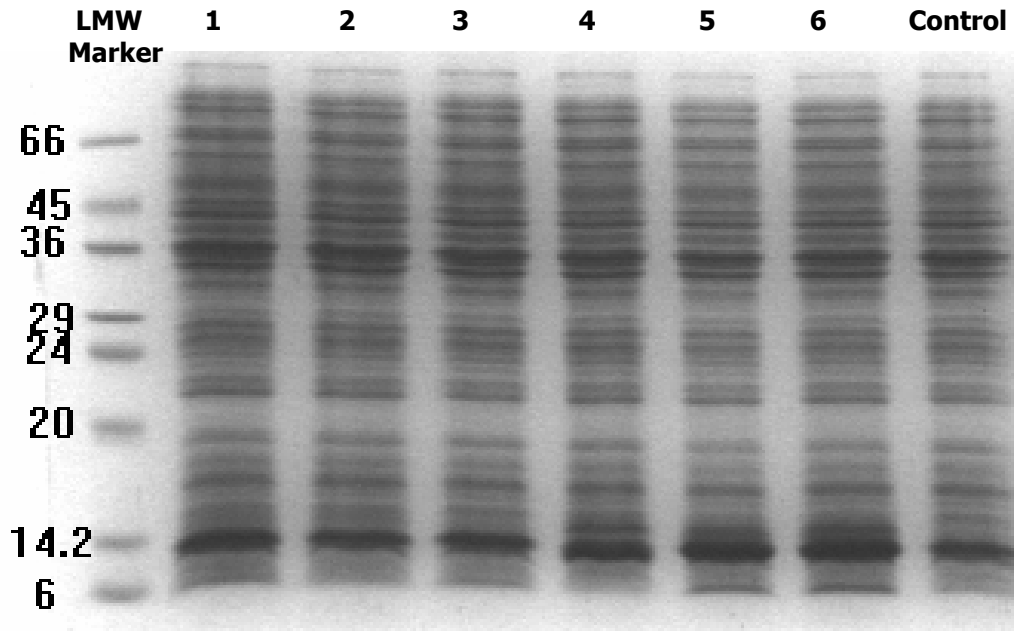


Figure 4.5: SDS-PAGE showing the over-expressed bands at approximately 12kDa size. Because of the presence of a leaky promoter, the control culture also showed a little expression of cytochrome b_{562} without induction with IPTG.

Plasmid DNA was extracted from each of the six colonies, and was tested for the presence of *Dra I* restriction site, which is present only in the cytochrome b_{562} gene and not in pET26b(+). Aliquots of these plasmids were also digested with the restriction endonucleases, *NcoI* and *EcoRI* and were visualized on a 1.5 % agarose gel. A band corresponding to the insert of about 320 bp was clearly seen. Figure 4.6 shows a picture of 1% agarose gel used to fractionate the plasmid cut with *Dra I* and Figure 4.7 shows the double digestion. The identity of the positive colonies was also confirmed by sequencing the minilysate plasmid DNA using the T7 oligonucleotide probes as sequencing primers.

The sequencing chromatogram for the wild-type cytochrome b_{562} is shown in Appendix B. All the mutants of cytochrome b_{562} were also confirmed with sequencing for quality control.

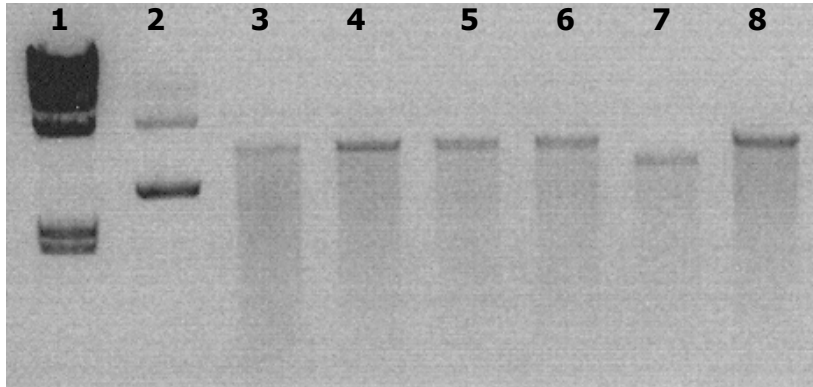


Figure 4.6: Agarose gel (1%) analysis of the vector pET26b(+) cut with *Dra I* to check for the presence of insert. Lane 1: λ DNA *HindIII* digest, Lane 2: uncut plasmid as control, Lane 3-8: Plasmids isolated from six different colonies and cut with *Dra I*. Since the *Dra I* site is present only in the gene of cytochrome b_{562} , this gel proves that it has been cloned into the vector.

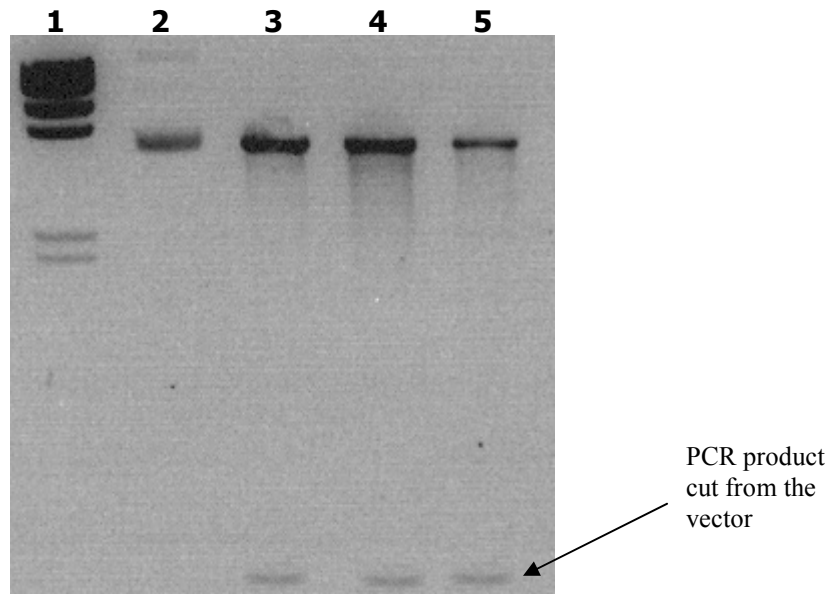


Figure 4.7: Agarose gel (1%) analysis of the vector pET26b(+) digested with restriction enzymes *NcoI* and *EcoRI*, used for cloning. Lane 1: λ DNA *HindIII* digest, Lane 2: uncut plasmid as control, Lane 3-6: Cut plasmid from three different colonies. A faint band corresponding to the PCR product of approximately 330 bp can also be seen.

4.3.2 Site-directed mutagenesis of wild-type cyt b₅₆₂

A total of four single tryptophan mutants (K83W, K89W, K95W, and K103W), one single methionine mutant (M7A) and four tryptophan and methionine double mutants (M7A/K83W, M7A/K89W, M7A/K95W, and M7A/K103W) were individually introduced into the gene of cytochrome b₅₆₂ using site-directed mutagenesis. Each of the single tryptophan and methionine mutant proteins was expressed in high yield as judged by SDS-PAGE gel electrophoresis while the yield of Met-Trp double mutants was drastically low. This lower yield was expected because of the removal of one of the axial heme ligands (methionine⁷) was expected to reduce the heme-binding capacity and overall structural stability of the protein.

4.3.3 Purification of the wild-type cytochrome b₅₆₂ and its mutants

Wild-type cytochrome b₅₆₂ was highly over-expressed constitutively from the pUC *lac* promoter in the BL21(DE)3 strain of *E. coli*. This crude cell lysate (from sonication) was applied over a Q sepharose column to remove the lipo-proteins and lipids that impart viscosity to the lysate. Each batch of the clarified lysate was adsorbed on the SP sepharose fast flow cation exchange column. Cytochrome b₅₆₂ was tightly bound to the column. After washing the column with 4-5 column volumes of the start buffer, the red pigmented protein was eluted from each column with 325 ml of the elution buffer (50 mM sodium succinate with 1 M NaCl, pH 4.5). Figure 4.8 is showing the chromatogram for the ion-exchange separation. A sharp peak is distinctly seen at approximately 23 minutes.

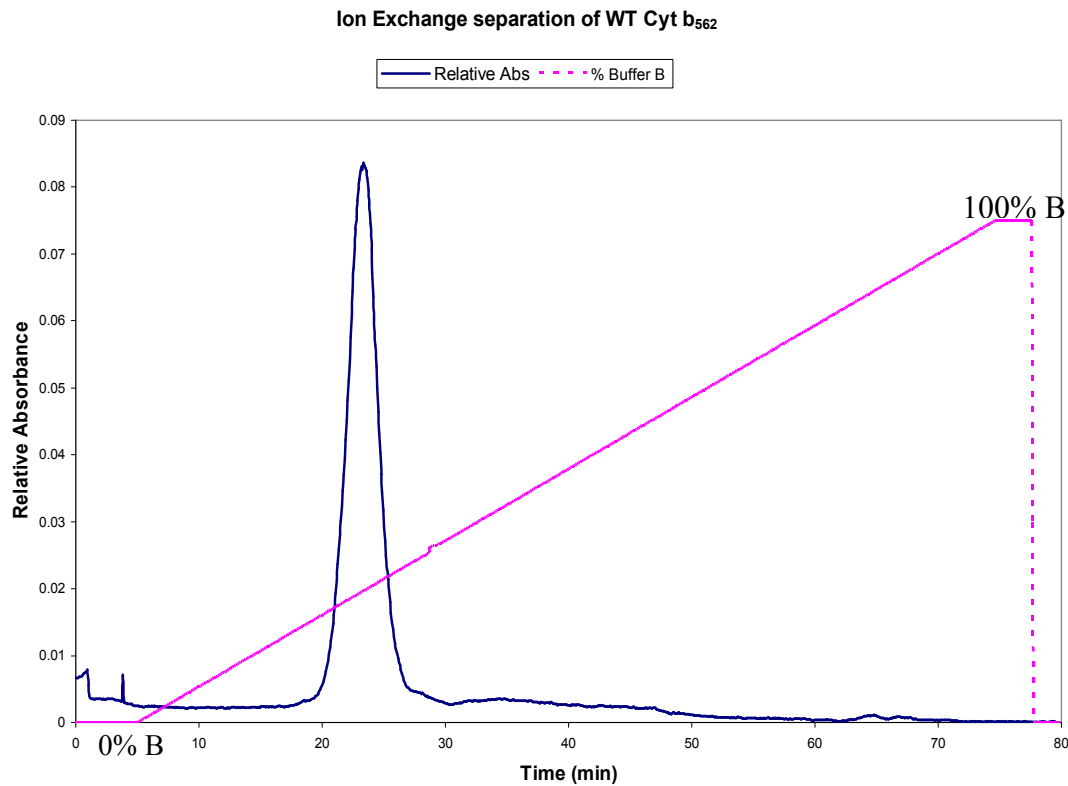


Figure 4.8: Ion-exchange separation of wild-type cytochrome b_{562} . The protein was eluted in one major peak, starting at approximately 24.5% buffer B (elution buffer) concentration. Absorbance was detected at 280 nm.

The fractions under the major peak were red in color indicating the presence of the holo-protein (heme bound to the protein). These fractions were run on 15% SDS-PAGE gel. Figure 4.9 shows a representative picture of the gels showing a clear separation of cytochrome b_{562} from other bacterial proteins. Since a total lysis of the bacterial cell pellets was performed, the crude cell lysate contained proteins from both the periplasm and cytoplasm. The proteins from the cytoplasm have the *pelB* leader sequence present, and hence they are slightly bigger than the native proteins.

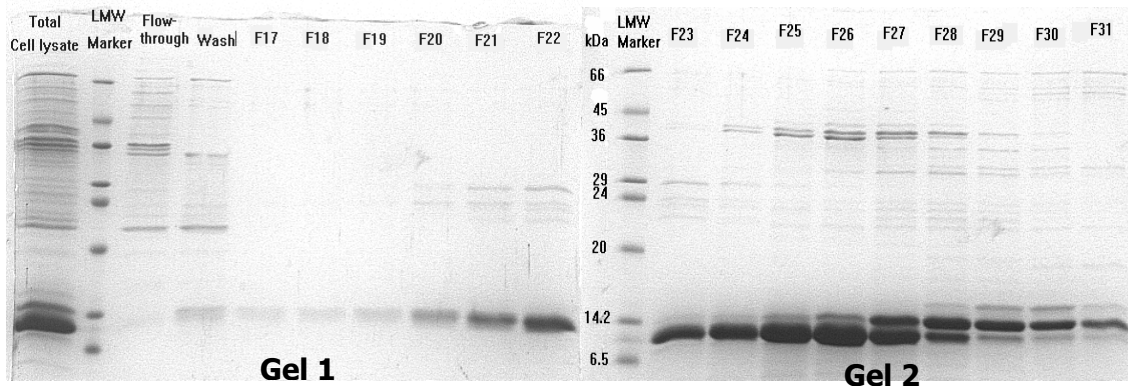


Figure 4.9: SDS-PAGE gels showing the separation of the ion-exchange column fractions eluted in a major peak as compared to the total cell lysate (lane 1 in Gel 1). Gel 2 shows that fractions eluted towards the end of the peak have at least two different forms of cytochrome b₅₆₂.

The presence of two separate bands in the later fractions under the peak can be possibly explained by this. Only the fractions having one distinct band (the smaller of the two) were combined and concentrated. The concentrated enzymes were then further purified using size exclusion column to eliminate of the proteins of bigger size. Figure 4.10 shows the chromatogram for size exclusion purification. The column also provided a buffer exchange, which is visible by the change of conductivity.

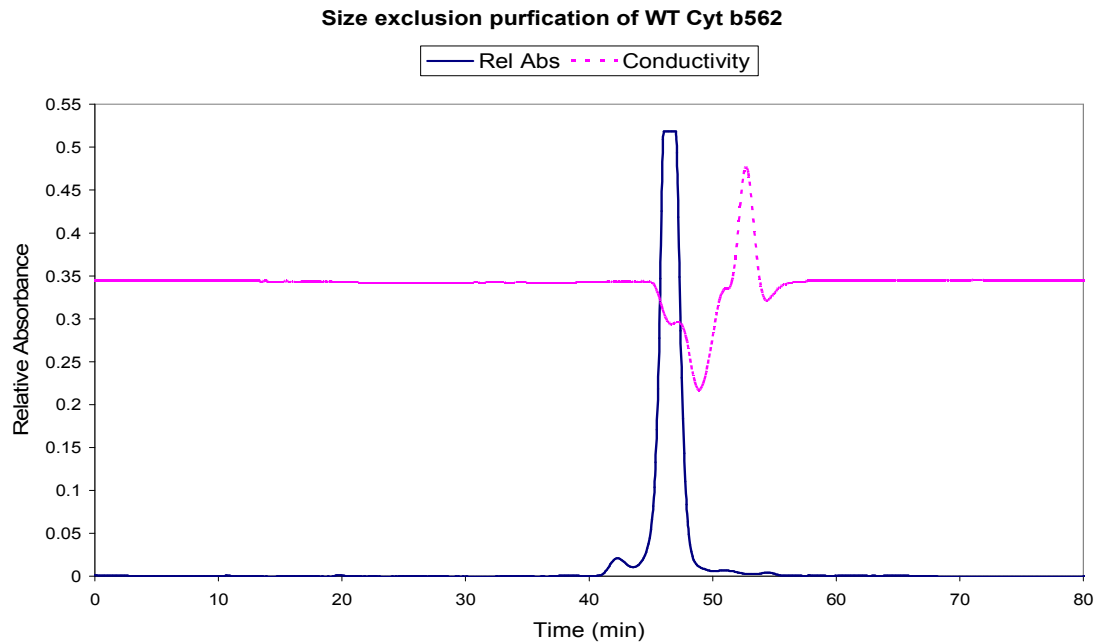


Figure 4.10: Size-exclusion separation of wild-type cyt b₅₆₂. The protein was eluted in one major peak. Absorbance was detected at 280 nm.

The fractions under the peak were run on SDS PAGE gel to verify identity of the proteins and to get an estimate of the purity. Figure 4.11 shows the picture of the gel. Fractions were collected at every two minutes.

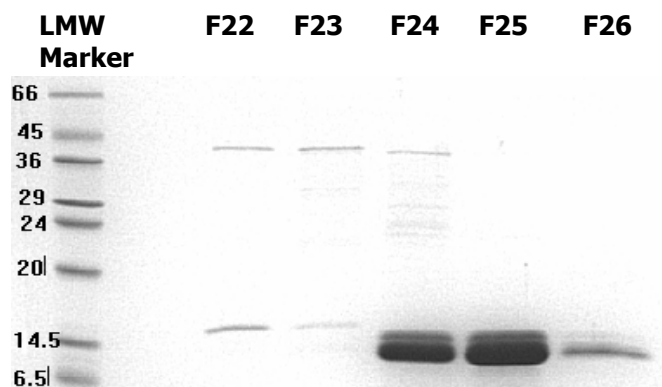


Figure 4.11: SDS-PAGE gels showing the separation of the size-exclusion column fractions eluted in a major peak. Fraction 25 was the purest.

All the mutants were purified using the same protocol and exhibited similar results except M7A/K95W and M7A/K103W. The ion-exchange chromatograph for each of these mutants showed two distinct peaks eluted off the SPFF column. The fractions under the second peak were colorless, but showed a large amount of protein on the SDS-PAGE gel, indicating that they were apo-proteins (did not bind heme). Figure 4.12 shows the chromatogram for the ion-exchange separation of M7A/K95W.

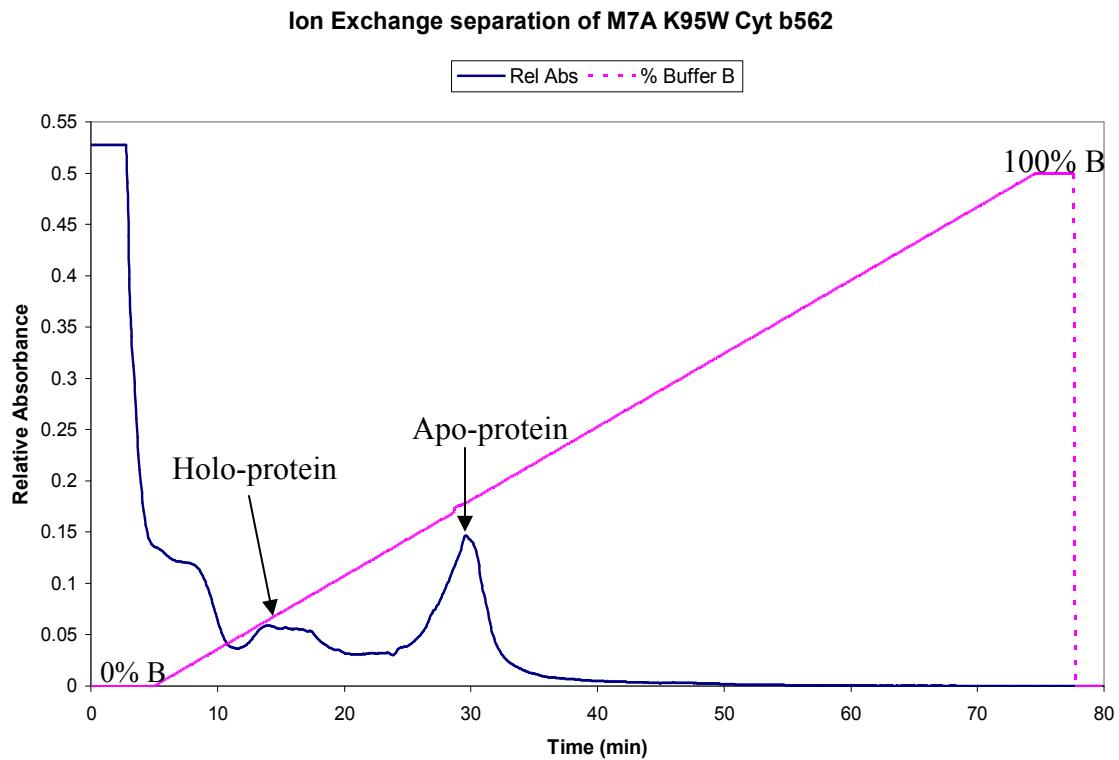


Figure 4.12: Ion-exchange separation of M7A/K95W cytochrome b_{562} . Two distinct peaks are seen. The first peak eluted at approximately 11% of buffer B and second peak eluted at 27% buffer B concentration. The apo-protein was eluted in the second peak. Absorbance was detected at 280 nm.

The fractions under the two peaks were combined separately, concentrated and further purified on the gel filtration column in separate batches. The size exclusion column fractions for the apo-protein showed fewer impurities compared to the holo-

proteins (Figure 4.13), and they did not have multiple forms of cytochrome b_{562} . A crude experiment was performed where we tried to add excess hemin to the protein solution of apo- form (100 μM hemin into 1 μM protein) and it was observed that heme was readily bound to the protein and retained there. The loss of heme may have affected the structure of the enzymes but this was not further investigated in the current work.

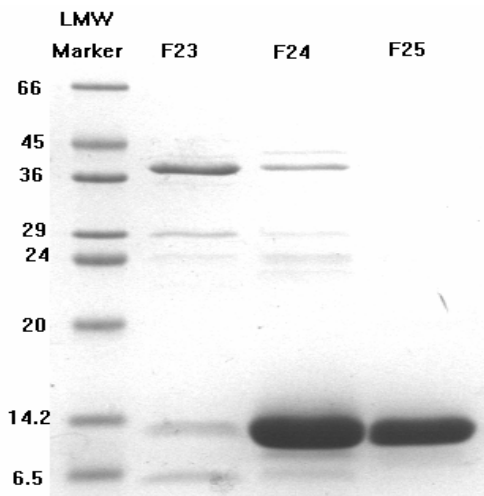


Figure 4.13: SDS-PAGE gels showing the separation of the size exclusion column fractions for the apo-protein eluted from the major peak at 46 minutes. Fraction 25 was the purest.

The BL21(DE)3 strain of *E. coli* was successfully used to devise a protocol for the purification of cytochrome b_{562} from *Y. enterocolitica*. The yield of the wild-type protein and all of its mutants was good and from all the chromatograms and SDS-PAGE gel analysis, it can be seen that it was purified to a reasonable extent (approximately 95% purity). The purified protein was subjected to mass spectroscopy and the analysis showed the purified protein was of the correct molecular weight and it was predominant in the

purest fraction. Figure 4.14 shows the picture of the MALDI spectrum for the K95W mutant of cytochrome b_{562} .

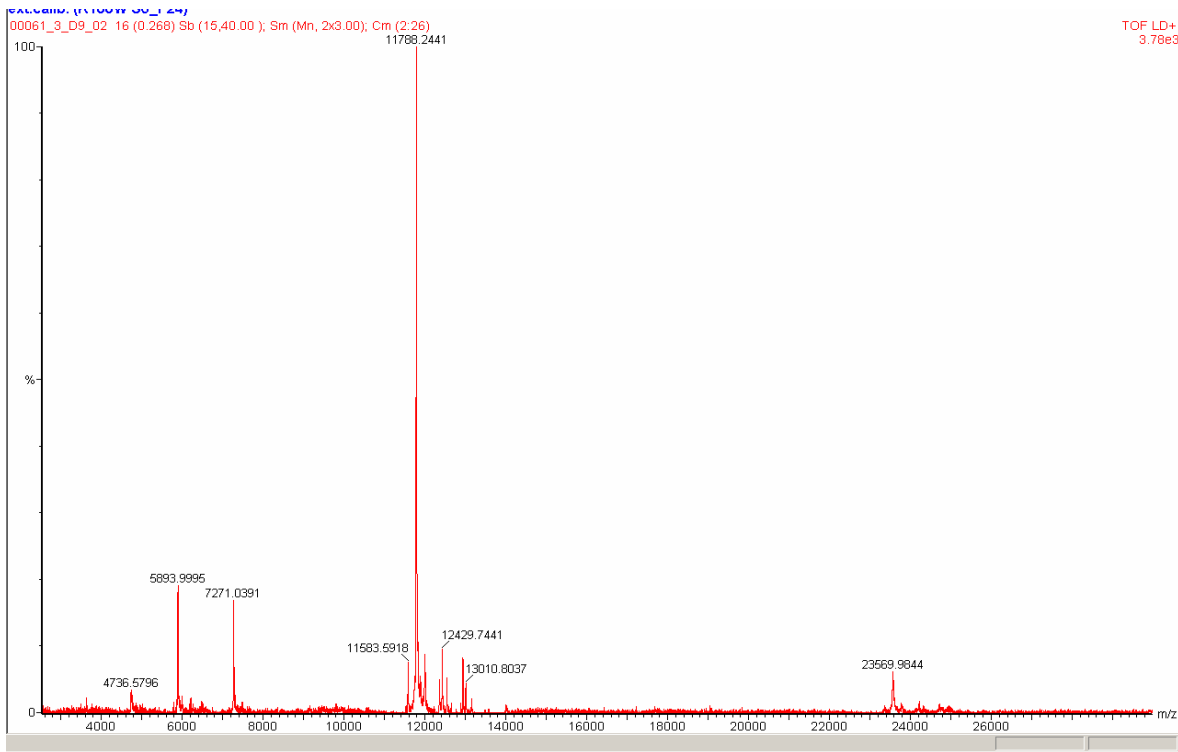


Figure 4.14: MALDI spectra for the fraction 25 from the size exclusion column for the K95W mutant of cytochrome b_{562} . The expected mass was 12168 Da.

The concentrations of the purified proteins were determined using the BCA assay. The data are tabulated in Table 4.1. It can be seen that the concentrations and yield of the Met-Trp double mutants were much lower than that of the wild-type and single mutants. This clearly implied that the heme axial ligand deletion affects the heme-binding ability of the enzyme and overall structure.

Table 4.1: Concentrations of the finally purified proteins as determined by BCA assay.

Sample ID	Actual concentration		Total volume (ml)	Total amount of protein (mg)
	mg/ml	μ M		
Wild-type cytochrome b_{562}	1.545	131.72	2.4	3.7080
K83W cytochrome b_{562}	3.342	283.49	0.8	2.6733
K89W cytochrome b_{562}	1.139	96.64	5.6	6.3793
K95W cytochrome b_{562}	1.246	105.73	5.6	6.9790
K103W cytochrome b_{562}	0.729	61.86	4	2.9167
M7A cytochrome b_{562}	1.198	102.69	1.6	1.917
M7A/K83W- cytochrome b_{562}	0.470	40.10	2.4	1.1278
M7A/K89W- cytochrome b_{562}	0.245	20.85	1.6	0.391
M7A/K95W-Holo protein	0.302	25.75	1.6	0.483
M7A/K95W-Apo protein	1.179	100.51	2.4	2.829
M7A/K103W-Holo protein	0.281	23.94	3.2	0.898
M7A/K103W-Apo protein	2.641	225.18	2.4	6.338

These proteins were used for characterization experiments and to evaluate their peroxidase activity. The procedures and results are reported in Chapter 5.

CHAPTER FIVE

5. Biophysical characterization of wild-type *Yersinia enterocolitica* cytochrome b₅₆₂ and its mutants

5.1 Introduction

In this chapter, a partial characterization of the purified wild-type cytochrome b₅₆₂ and its mutants is presented. The UV/Visible spectrum was obtained for all of these proteins, which allowed us to estimate the contributions of the amino acid residues and the heme prosthetic group to the absorbance. Fluorescence spectra were collected to examine the tryptophan residue in those mutants of cyt b₅₆₂ containing tryptophan substitutions and for which electron transfer from the heme to tryptophan may occur. Cyt b₅₆₂ is a small protein compared to the naturally existing peroxidases such as HRP and LiP. However several cytochromes are shown to possess the peroxidase-like activity. This chapter also investigates the peroxidase activity of these mutated proteins, including the pH dependence, and substrate (ABTS) and H₂O₂ concentration dependence.

5.2 Materials and methods

5.2.1 Absorbance measurements

Steady-state UV-visible absorption spectra of fully oxidized and reduced forms of wild-type *Y. enterocolitica* cyt b₅₆₂, the M7A mutant, tryptophan mutants and all M7A-

tryptophan double mutants were measured on a Beckman DU 800 spectrophotometer (Beckman Coulter, Fullerton, CA). The measurements were performed with a protein concentration of 10 μ M in a total volume of 300 μ l. Two samples were made for each protein in separate eppendorf tubes. One was oxidized with potassium ferricyanide (3 mM final concentration) and other was reduced with sodium dithionate (3 mM final concentration) and all samples were incubated for 10 minutes. All measurements were made in 50 mM potassium phosphate buffer (pH 7.0) and 150 mM NaCl at room temperature using quartz cell (Starna Cells, Atascadero, CA) with 10 mm path length.

5.2.2 Fluorometric measurements

Steady-state fluorescence spectra of fully oxidized and reduced forms of wild-type cytochrome b_{562} , the M7A mutant, tryptophan mutants and all M7A-tryptophan double mutants were measured on a Hitachi F-2000 spectrofluorometer (Hitachi High-Technologies Corporation, Japan). The fluorescence spectra were recorded at excitation wavelength (λ_{ex}) of 295 nm and emission wavelength (λ_{em}) of 300 nm for the same samples used to obtain UV/Vis spectra. All measurements were made in 50 mM Potassium phosphate buffer (pH 7.0) and 150 mM NaCl at room temperature using semi micro fluorometer cell (Starna Cells Inc., Atascadero, CA) with 10 mm path length.

5.2.3 Assay of peroxidase activity and steady-state kinetics of oxidation reaction

Peroxidase activity was evaluated by measuring the oxidation rate of 2,2'-azino-di-(3-ethyl-benzthiazoline-6-sulphonic acid) (ABTS, Sigma Co., St. Louis, MO) with hydrogen peroxide (H_2O_2 , 3%, CVS Pharmacy, USA). The product formation was

detected by the change in absorbance at 405 nm in a BioKinetic EL312 kinetic plate reader (Bio-Tek Instruments Inc., Winooski, VT). Absorbance measurements were made every 20 seconds for a total of 1500 seconds each time. The data were recorded using KCjunior for windows Data Reduction Software.

The pH dependence of the peroxidase activity was determined by setting up 150 μ l reactions (2 mM ABTS, 1 μ M protein, 20mM pH buffer, 1 mM H₂O₂) in a 96-well microplate (NalgeNunc International, Roskilde, Denmark) at room temperature within the pH range of 2 to 9.5 at every 0.5 pH. Phosphate buffers were used in the pH range of 2-3 and 6.5-7.5, citrate buffers were used in the pH range of 3.5-6, tris buffers were used in the range for pH 8-8.5, and ethanalamine buffers were used in the pH range of 9-10. The reactions were triggered by addition of 1mM H₂O₂ and the kinetic reads were recorded every 20 seconds for a total time of 1500 seconds using KCjunior. The H₂O₂ stock solution was freshly made each time. The extinction coefficient for ABTS oxidation product (the π -cation radical of ABTS) at 405 nm was 36.8 mM⁻¹ cm⁻¹ (Childs et. al., 1975). The optical path length was determined to be 5 mm (150 μ l/0.302 cm²).

For substrate concentration experiments, steady-state kinetics was measured with 1 μ M protein in 20 mM sodium citrate buffer (pH 5.0) at room temperature. The concentration of H₂O₂ was 1 mM and the concentration of substrate was varied (0.1-20 mM ABTS). For peroxide concentration variation experiments, steady-state kinetics was measured with 1 μ M protein in 20 mM sodium citrate buffer (pH 5.0) at room temperature. The concentration of H₂O₂ was varied from 0.25 to 5 mM at different concentrations of ABTS (0.02-2 mM).

5.3 Results and Discussion

5.3.1 Spectroscopic properties of wild-type cytochrome b_{562} and its mutants

The UV-visible absorption spectra of the fully oxidized and fully reduced forms of wild-type cytochrome b_{562} are shown in Figure 5.1. The spectra show intense absorption at around 417 nm (the "Soret" band), followed by several weaker absorptions at higher wavelengths, which are called Q Bands: α -band at around 562 nm and β -band at around 532 nm. These absorption bands are a typical characteristic of free base (Q-bands) and the corresponding highly conjugated iron-protoporphyrin IX (soret band).

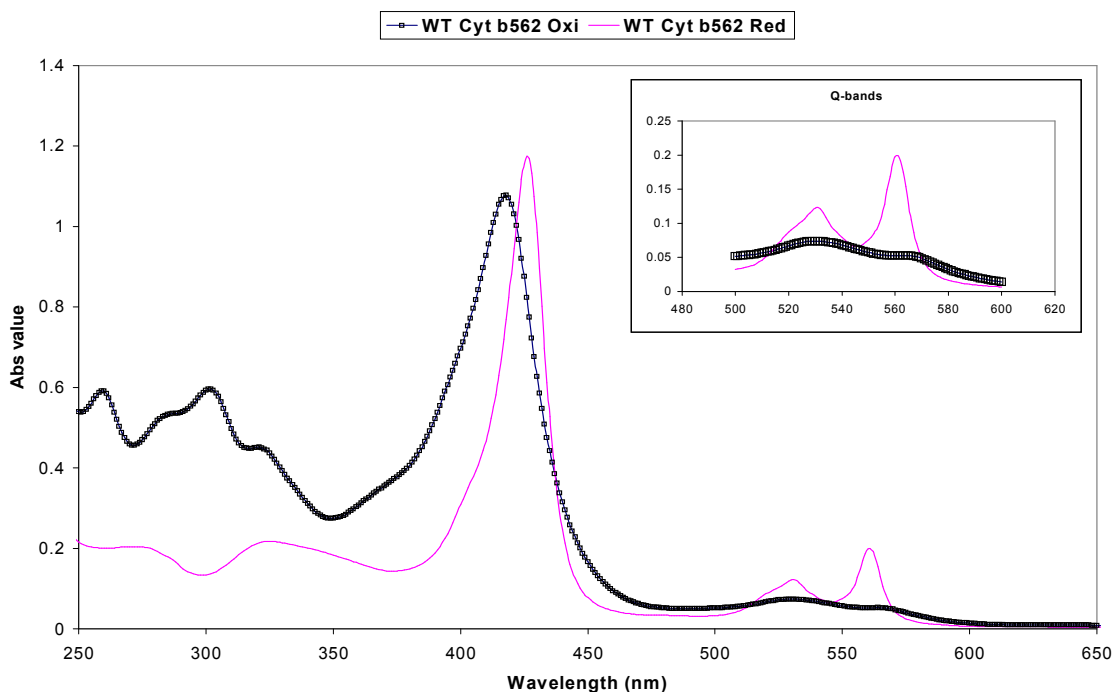


Figure 5.1: UV/Vis absorption spectrum of oxidized (Fe^{+3} in heme) and reduced (Fe^{+2} in heme) cyt b_{562} . The protein concentration is $10 \mu\text{M}$. The reduced form of cyt b_{562} shows the soret maximum at 427 nm while the oxidized form has soret maximum at 417 nm. The Q bands are shown in detail in the inset graph.

Figure 5.2 shows a comparison of the UV/Vis spectra of oxidized and reduced form of wild-type cyt b_{562} with the oxidized and reduced form of M7A mutant of Cyt

b₅₆₂. Because of the deletion of one axial ligand (M7A substitution mutation), the spectrum is typically that of high-spin ferric heme and is distinct from that of WT Cyt b₅₆₂.

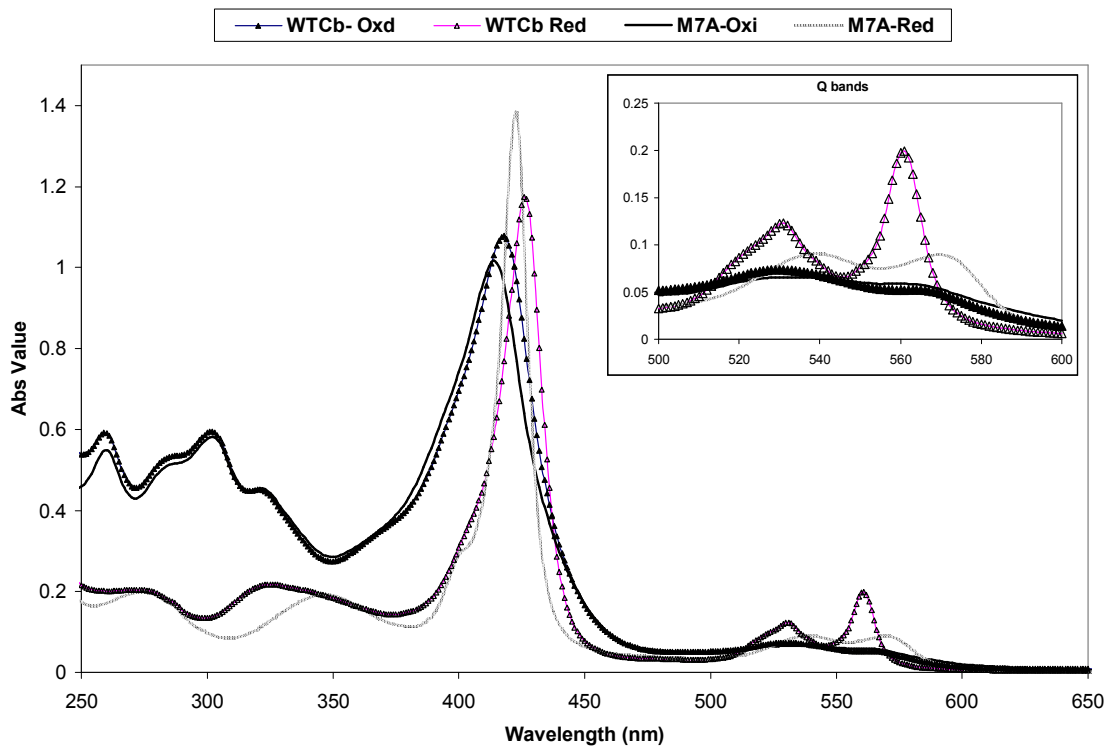


Figure 5.2: UV/Vis absorption spectrum of oxidized and reduced forms of wild-type and M7A cyt b₅₆₂. Oxidized M7A Cyt b₅₆₂ shows a sharp Soret band at 415 nm while the reduced form has the Soret band at 423 nm, which are different from that of wild-type.

Figures 5.3 to 5.6 show a comparison of the UV/Vis spectra for the tryptophan mutants K83W, K89W, K95W, and K103W, respectively, with their M7A double mutant analogues. It should be noticed that both the oxidized and reduced forms of the M7A/K95W and M7A/K103W mutants show much smaller peaks for the Soret and Q bands as compared to those of K95W and K103W mutants. This was likely due to the reduction in the thermodynamic stability of the protein, an issue which will be addressed in the future, along with the heme binding capacity of the proteins. Here we assume

complete heme loading. This is not observed with other mutants, which shows that tryptophan being at different distances is also contributing to the spectra and the overall structure of the protein.

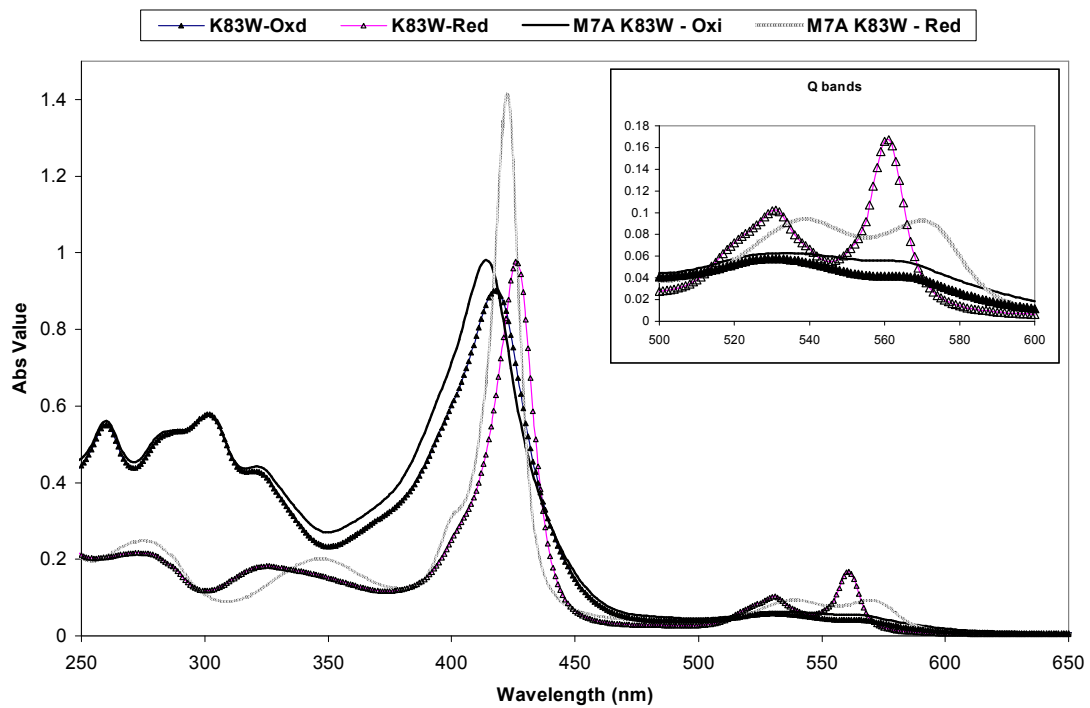


Figure 5.3: UV/Vis absorption spectrum of oxidized and reduced forms of K83W and M7A/K83W cytochrome b_{562} .

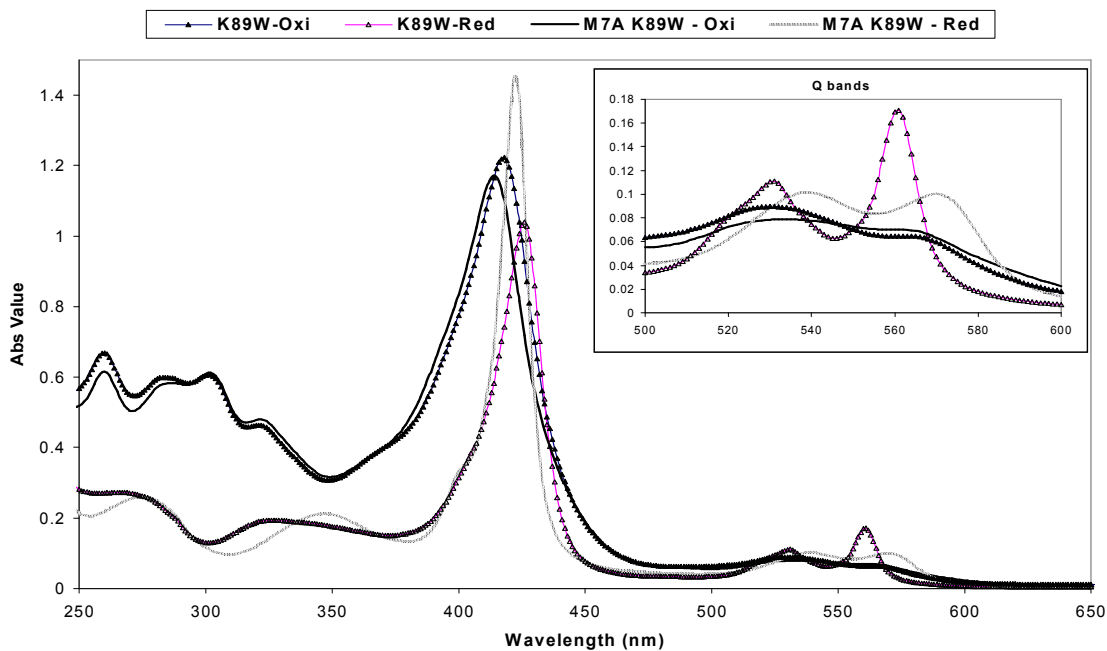


Figure 5.4: UV/Vis absorption spectrum of oxidized and reduced forms of K89W and M7A/K89W cytochrome b_{562} .

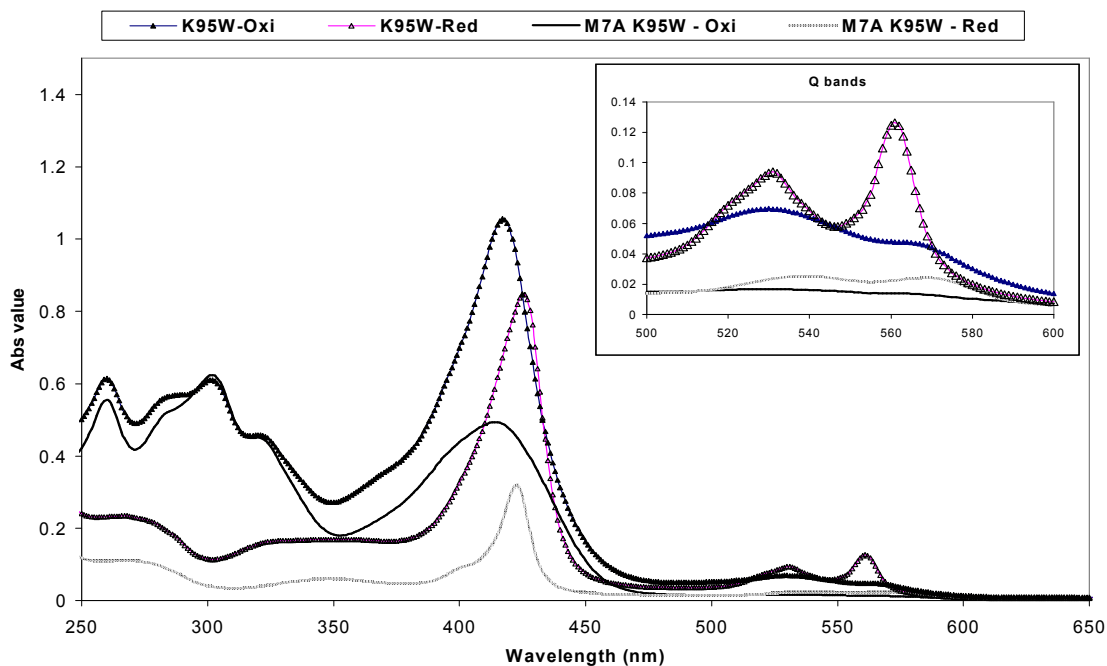


Figure 5.5: UV/Vis absorption spectrum of oxidized and reduced forms of K95W and M7A/K95W cytochrome b_{562} .

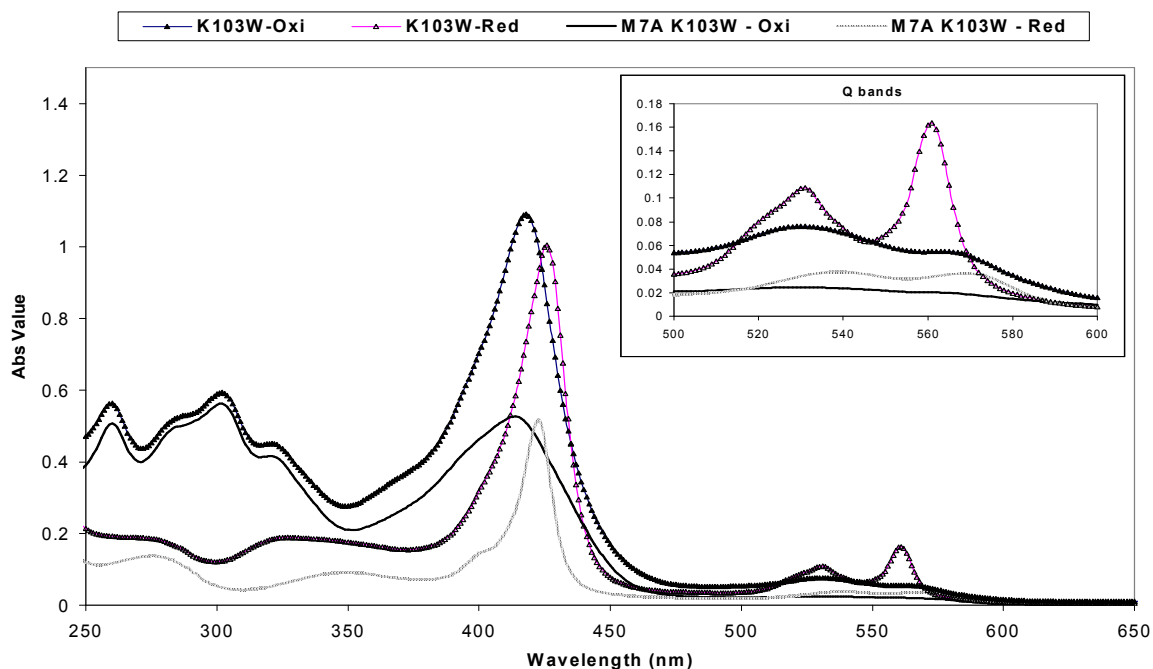


Figure 5.6: UV/Vis absorption spectrum of oxidized and reduced forms of K103W and M7A/K103W cytochrome b_{562} .

From the UV/Vis studies, it was observed that the spectrum of cytochrome b_{562} in the visible region is that expected for a typical b-type cytochrome, however, the spectrum in the UV region is not a characteristic one. The ultraviolet absorption spectra of all of the holo-proteins show only a shoulder rather than a peak in the 280 nm region. These results can be interpreted as the contribution of aromatic amino acids to the UV absorption spectrum of these proteins is minimal and is covered by the absorption of the heme group.

5.3.2 Fluorescence properties of wild-type cytochrome b_{562} and its mutants

All the oxidized and reduced forms of all proteins were also scanned on a fluorescence spectrophotometer, first without adding H_2O_2 and then after the addition of H_2O_2 under steady state conditions. Fluorescence spectroscopy serves to probe the

structure of rigid aromatic systems, including both the heme, which is nearly fluorescent and tryptophan, which may be fluorescent depending on the local environment. The spectrum for wild-type was different from those of the tryptophan mutants and the Met-Trp double mutants, which was expected, because the tryptophan contributes to the intrinsic fluorescence. Since the fluorescence of a folded protein is a mixture of fluorescence from individual aromatic residues, if excited at 295 nm, most of the emissions are due to excitation of tryptophan residues in the case of these proteins. However, the heme (iron-protoporphyrin prosthetic group) might also have contributed to the fluorescence. Figures 5.7 to 5.16 show the fluorescence spectra of oxidized and reduced forms of each of the proteins with and without the addition of H_2O_2 , each compared to their methionine analogues. The addition of H_2O_2 induces the peroxidase activity in these proteins (mainly in the M7A mutants, because the presence of an open coordination site readily starts the electron transfer reaction). Ideally, the electrons from the reduced H_2O_2 are transferred from the edge of heme to the tryptophan, yielding a tryptophan cation radical (compound I). It is expected that this radical will have different fluorescence properties than the native tryptophan. This can be observed clearly in the M7A mutants. For almost of all of the Met-Trp double mutants, the emission for the samples with H_2O_2 is more significant than those of tryptophan single mutants. However, since we are looking at steady state fluorescence emission, and the reaction has the mixture of native enzyme and its intermediates, compound I and compound II, the results are not absolutely quantitative. EPR spectroscopy will be employed to better understand this radical mechanism and to look at the free tryptophan radical cations and to quantify them.

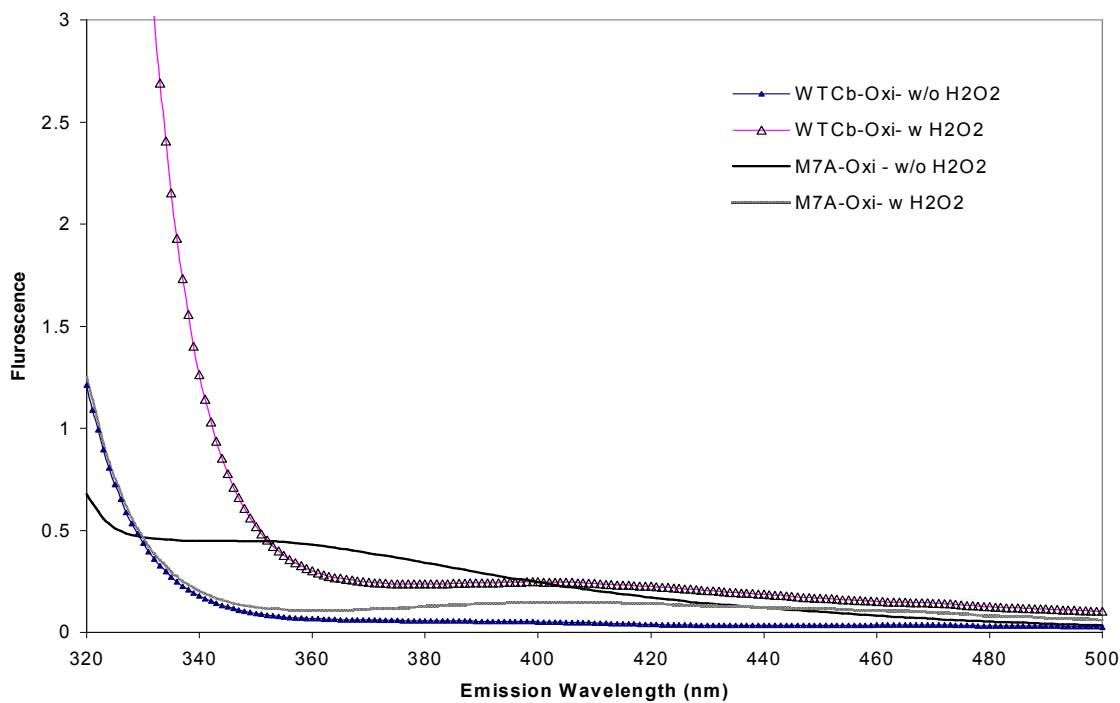


Figure 5.7: Fluorescence spectra of oxidized WT cytochrome b_{562} and M7A with and without (w/o) H_2O_2 .

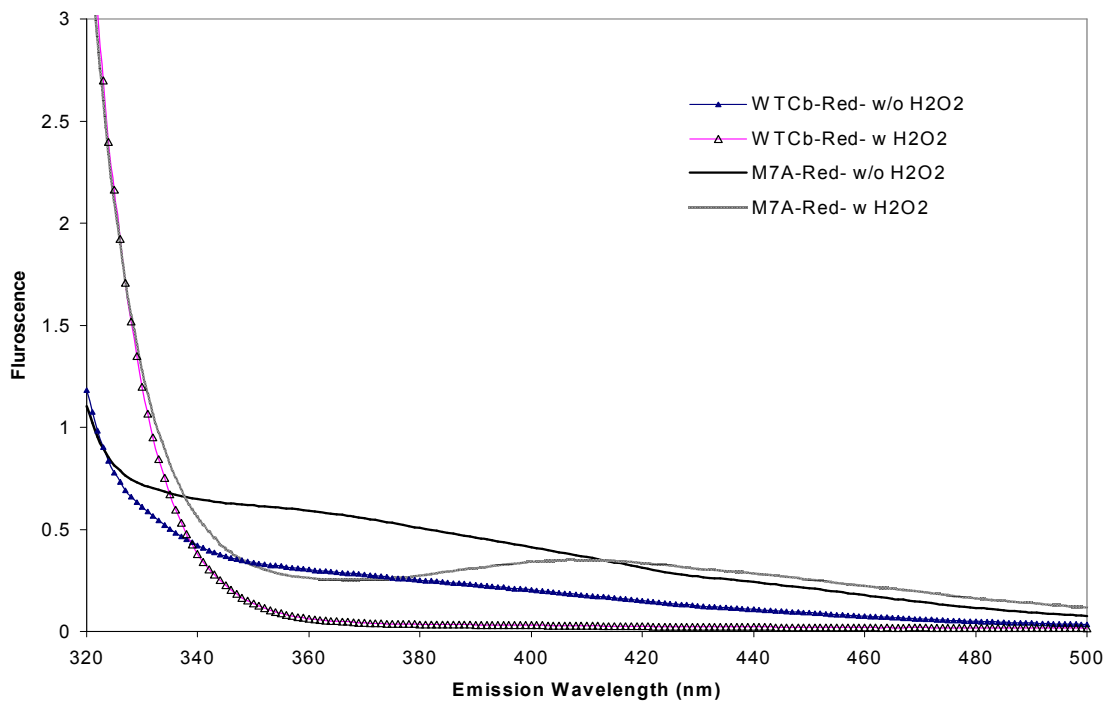


Figure 5.8: Fluorescence spectra of reduced WT cytochrome b_{562} and M7A with and without H_2O_2 .

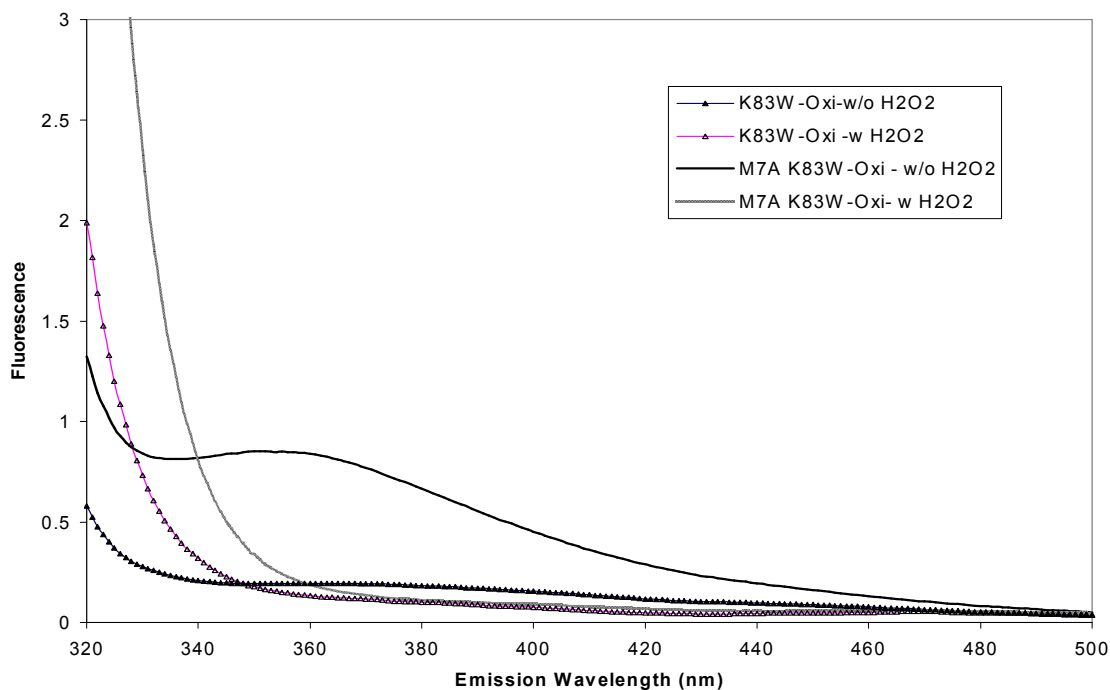


Figure 5.9: Fluorescence spectra of oxidized forms of K83W and M7A/K83W cyt b₅₆₂ with and without H₂O₂.

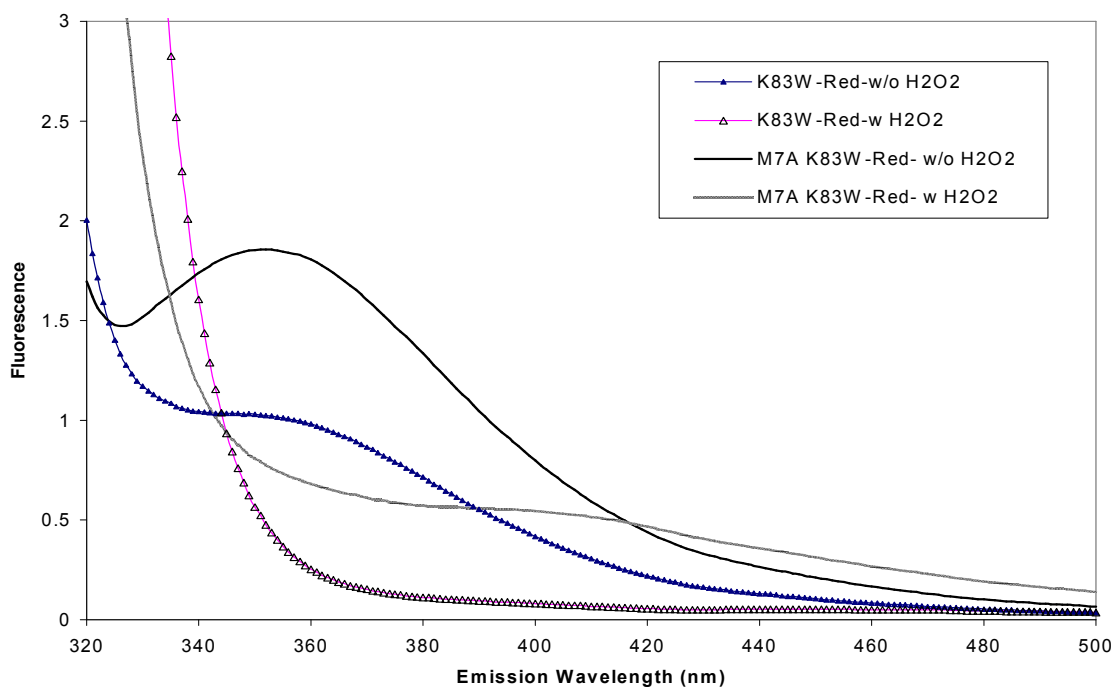


Figure 5.10: Fluorescence spectra of reduced forms of K83W and M7A/K83W cyt b₅₆₂ with and without H₂O₂.

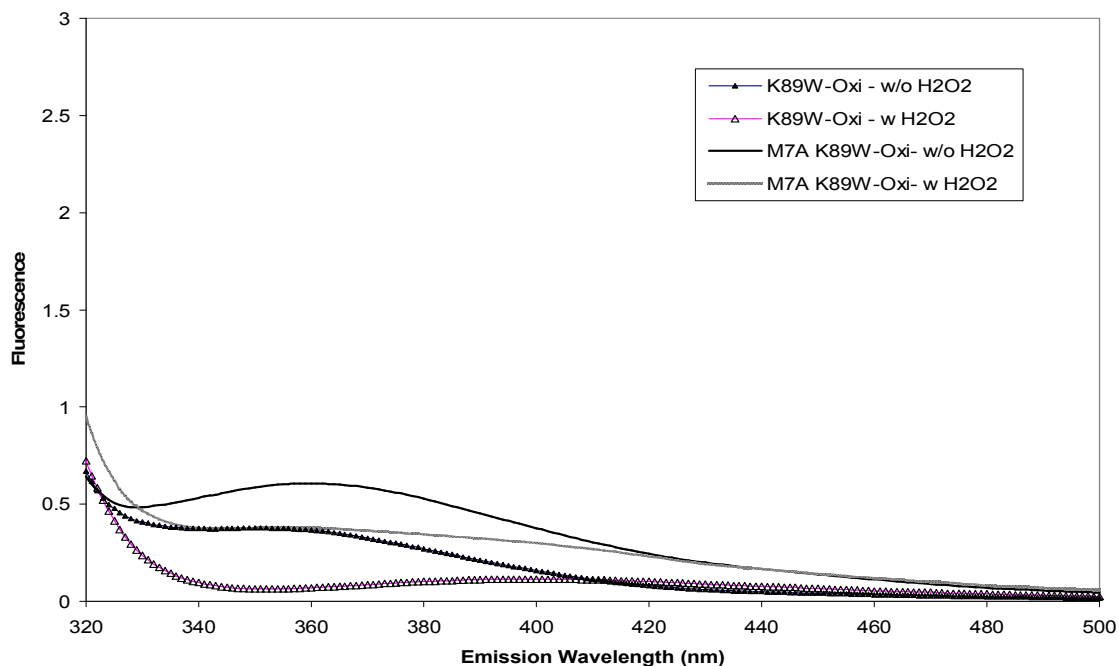


Figure 5.11: Fluorescence spectra of oxidized forms of K89W and M7A/K89W cyt b₅₆₂ with and without H₂O₂

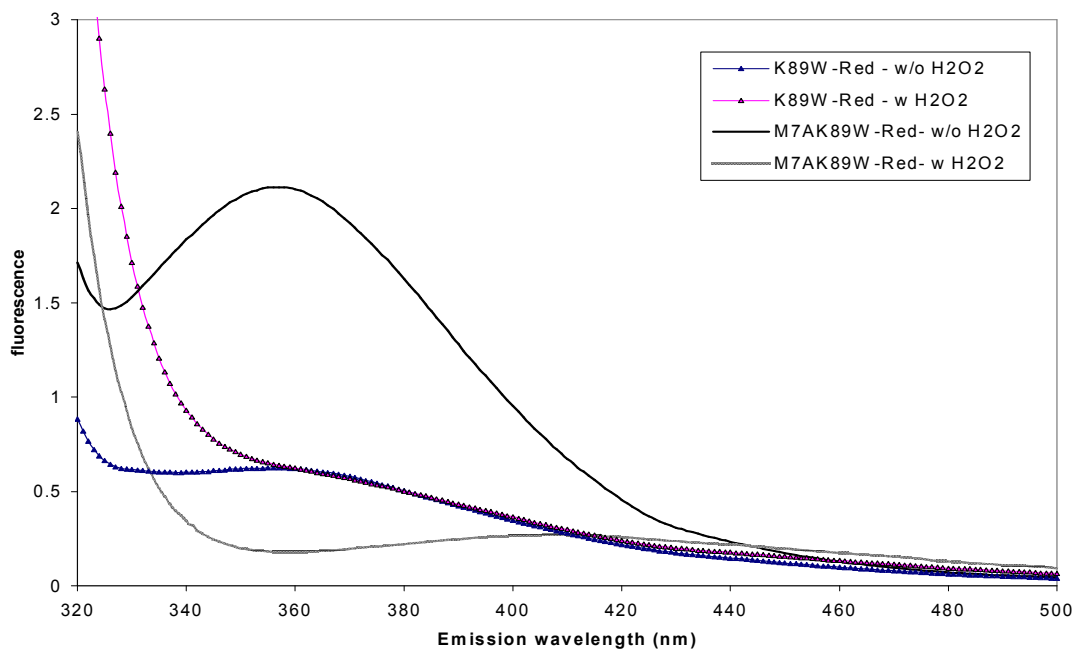


Figure 5.12: Fluorescence spectra of reduced forms of K89W and M7A/K89W cyt b₅₆₂ with and without H₂O₂.

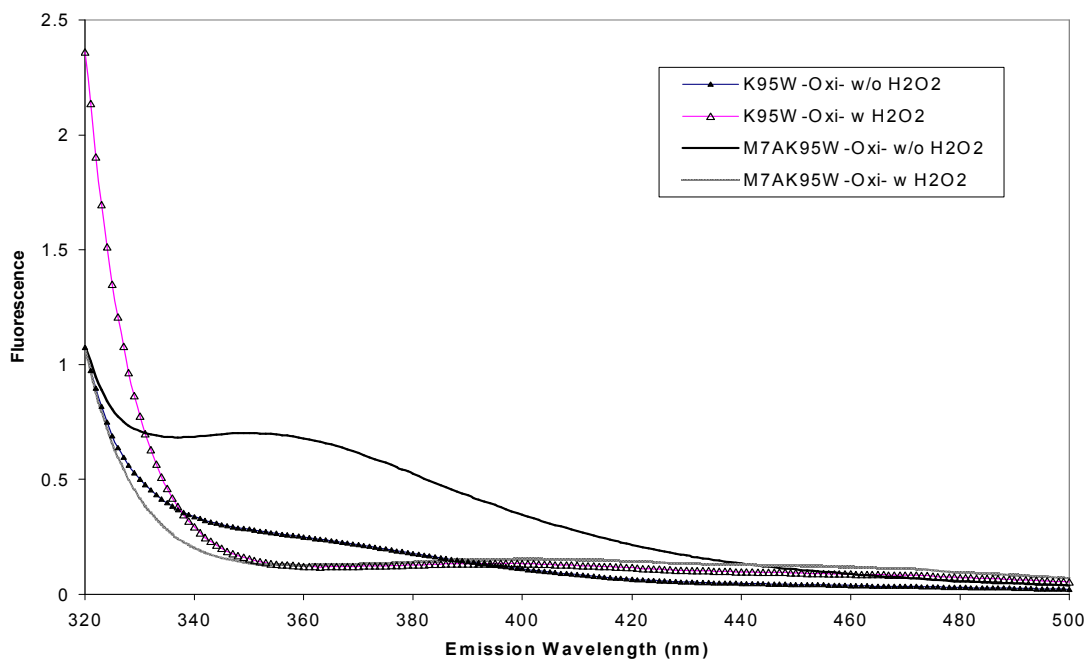


Figure 5.13: Fluorescence spectra of oxidized forms of K95W and M7A/K95W cyt b₅₆₂ with and without H₂O₂.

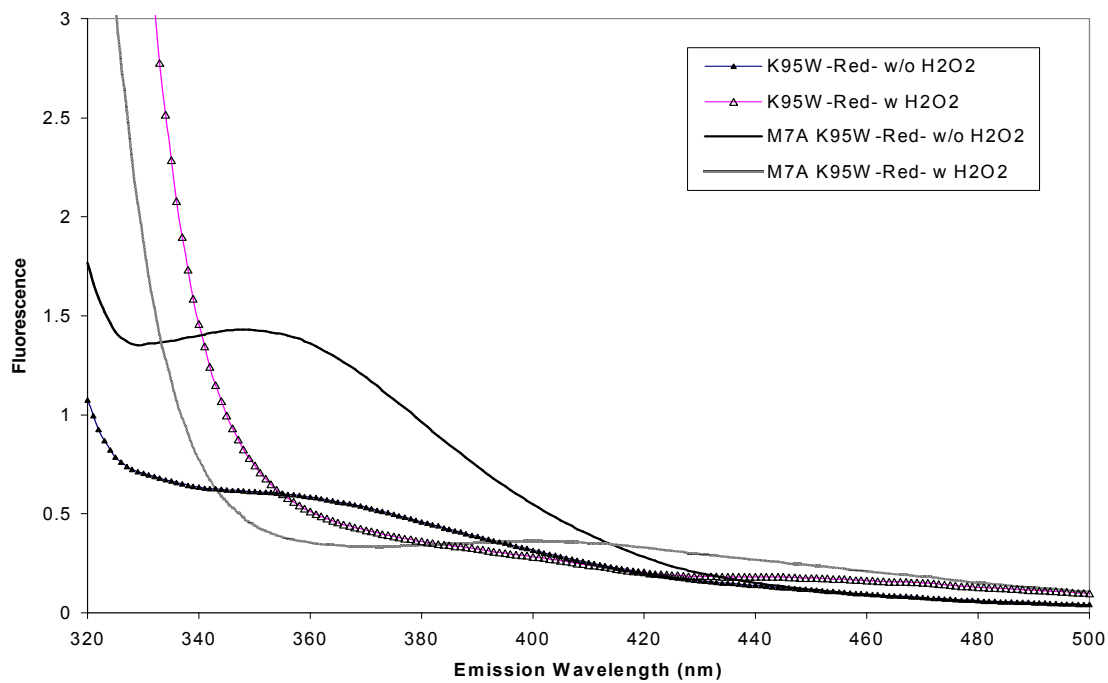


Figure 5.14: Fluorescence spectra of reduced forms of K95W and M7A/K95W cyt b₅₆₂ with and without H₂O₂.

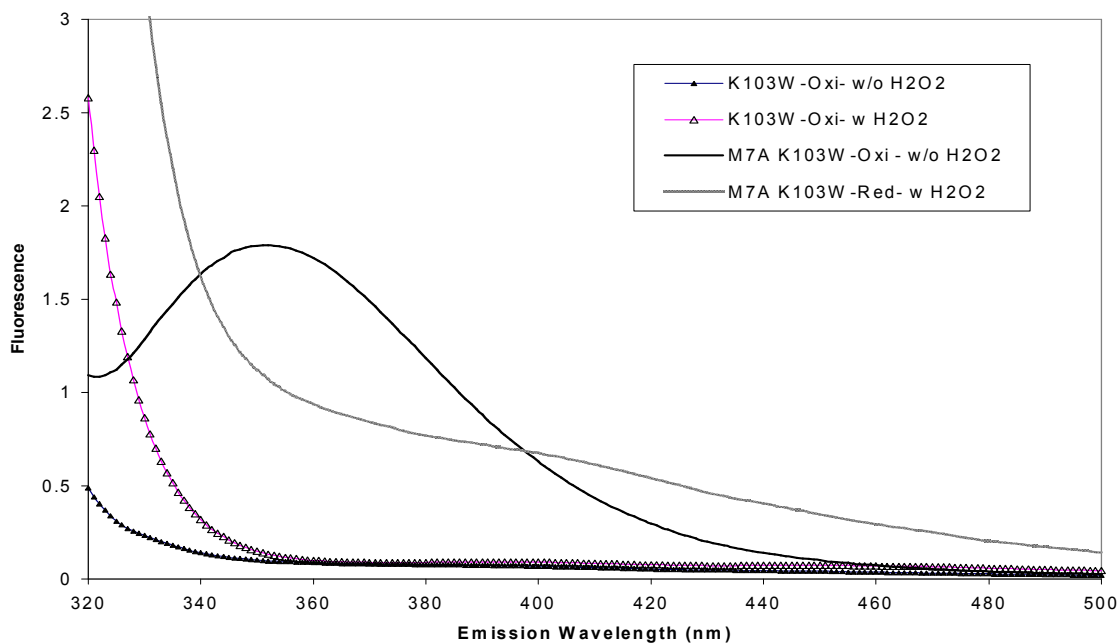


Figure 5.15: Fluorescence spectra of oxidized forms of K103W and M7A/K103W cyt b₅₆₂ with and without H₂O₂.

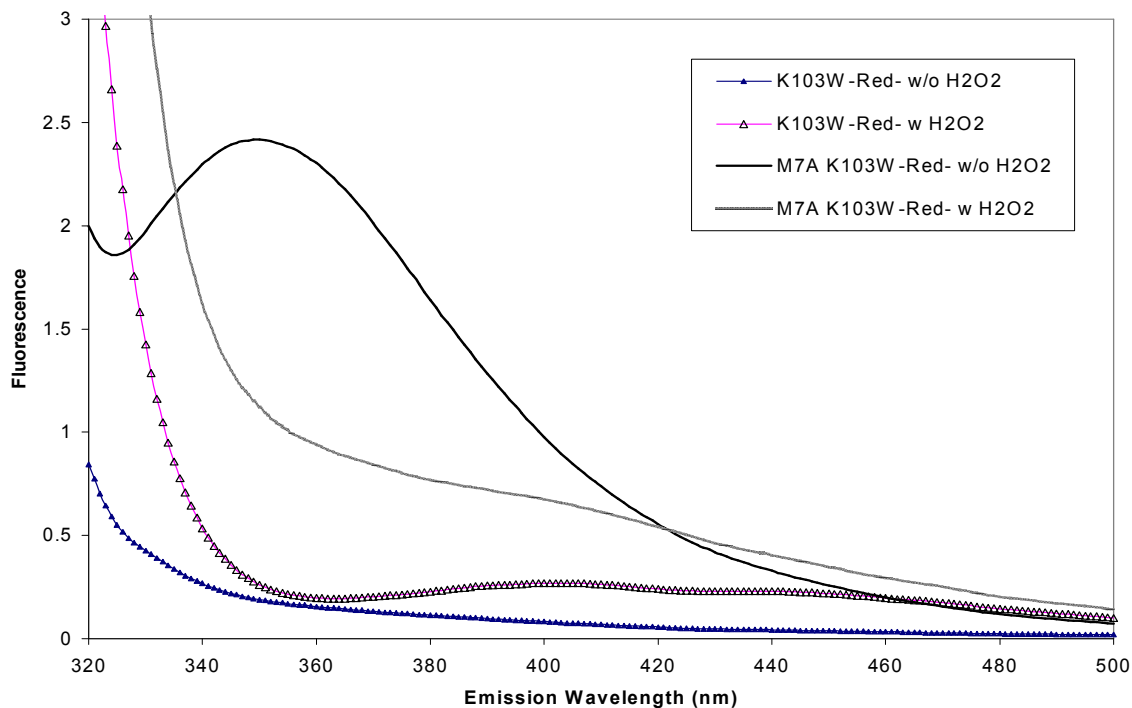


Figure 5.16: Fluorescence spectra of reduced forms of K103W and M7A/K103W cyt b₅₆₂ with and without H₂O₂.

5.3.3 Assay of peroxidase activity

Effect of pH

The effect of pH on the peroxidase activity of the WT cyt b_{562} and its mutants was assessed by performing the ABTS assay over sixteen different pHs, starting from pH 2 to pH 9.5 at every 0.5 pH interval. This study was a prerequisite to ultimately perform the kinetics of peroxidase inactivation (or oxidation of the substrate, ABTS in this case) at an optimum pH. It was observed that peroxidase activity of these enzymes depends strongly on pH. The steady-state rate increases with increasing pH up to pH 5 or pH 6, after which a decrease is seen. The wild-type cyt b_{562} and tryptophan mutants showed very little or no activity as expected and explained earlier in chapter 4. The M7A mutants showed distinct pH dependence. Figure 5.17 shows the pH dependence for WT cyt b_{562} .

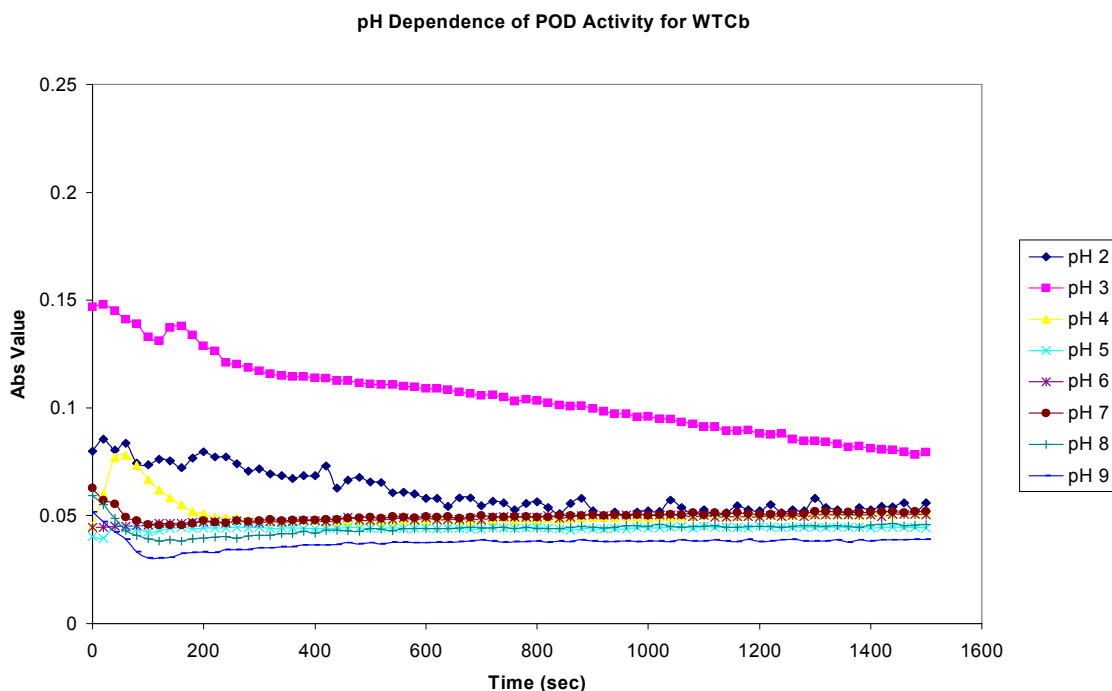


Figure 5.17: Effect of pH on peroxidase activity of WT cyt b_{562} . The data shown here are in the range of pH 2 to pH 9. It can be seen that the WT cyt b_{562} has no activity at any pH. Similar behavior was observed for all tryptophan single mutants also.

The activity of these mutants was compared to HRP over the similar pH range (Figure 5.18). The concentration of HRP used was 0.1 nM, all other conditions were the same. Since the M7A mutants of cyt b_{562} can bind exogenous ligands to the heme iron, they showed significant peroxidase activity (Figure 5.19 to 5.23). It has been reported in literature that LiP is most active at pH 3.0 while MnP and HRP display maximum activity at pH 4.5 (Hiner et al., 2002), which was observed our experiments. At very low pH (pH 2-3), all these enzymes are inactive and may be unfolded. At low pH, the substrate is auto-oxidized and shows color formation.

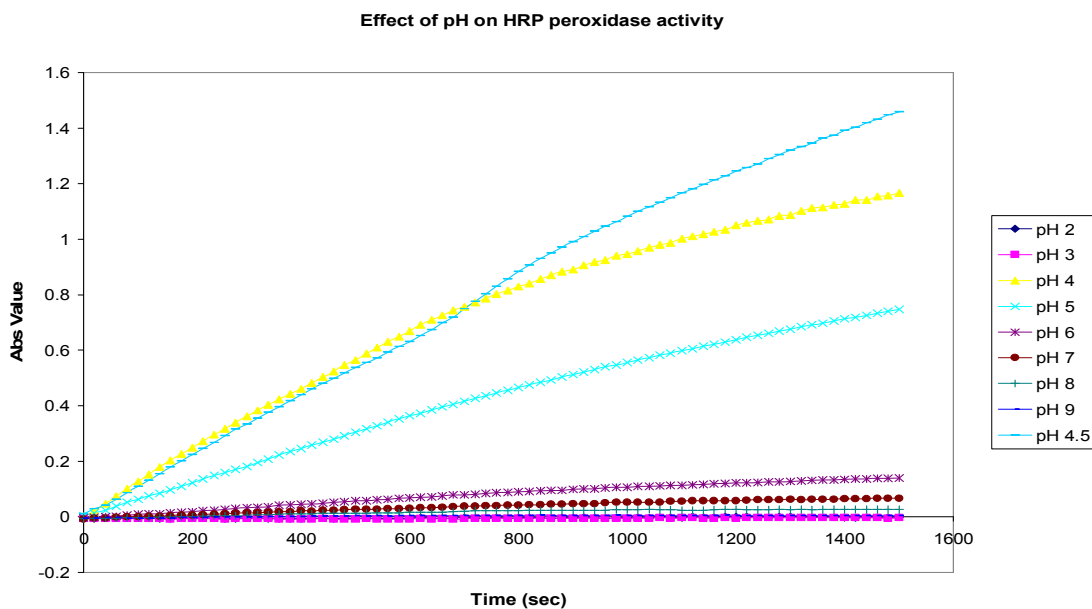


Figure 5.18: Effect of pH on peroxidase activity of HRP. The enzyme displays optimum activity at pH 4.5.

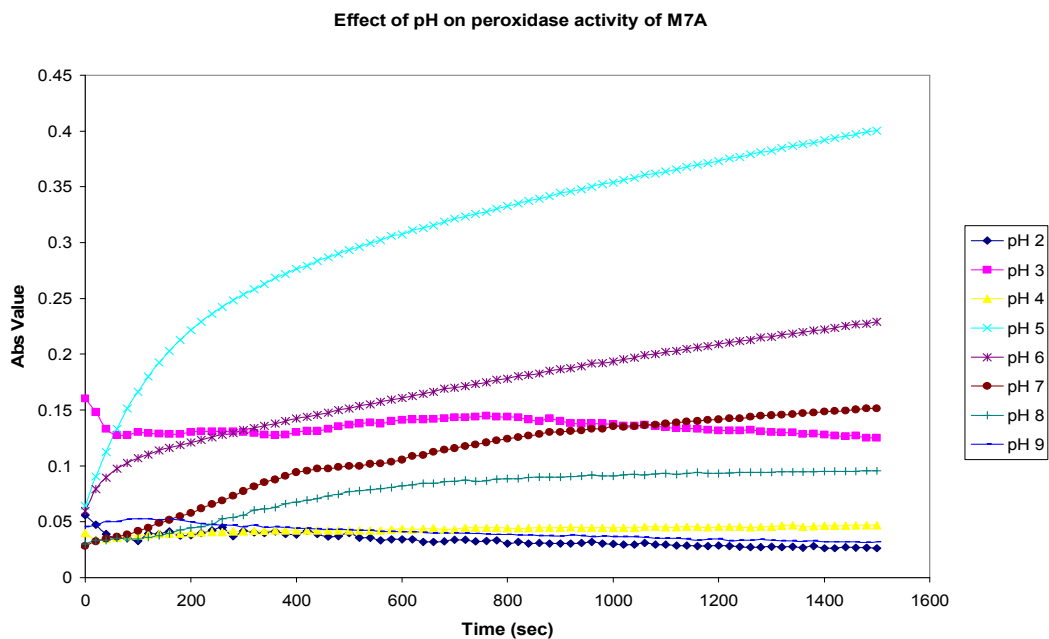


Figure 5.19: Effect of pH on peroxidase activity of M7A Cyt b_{562} . The enzyme displays optimum activity at pH 5.0.

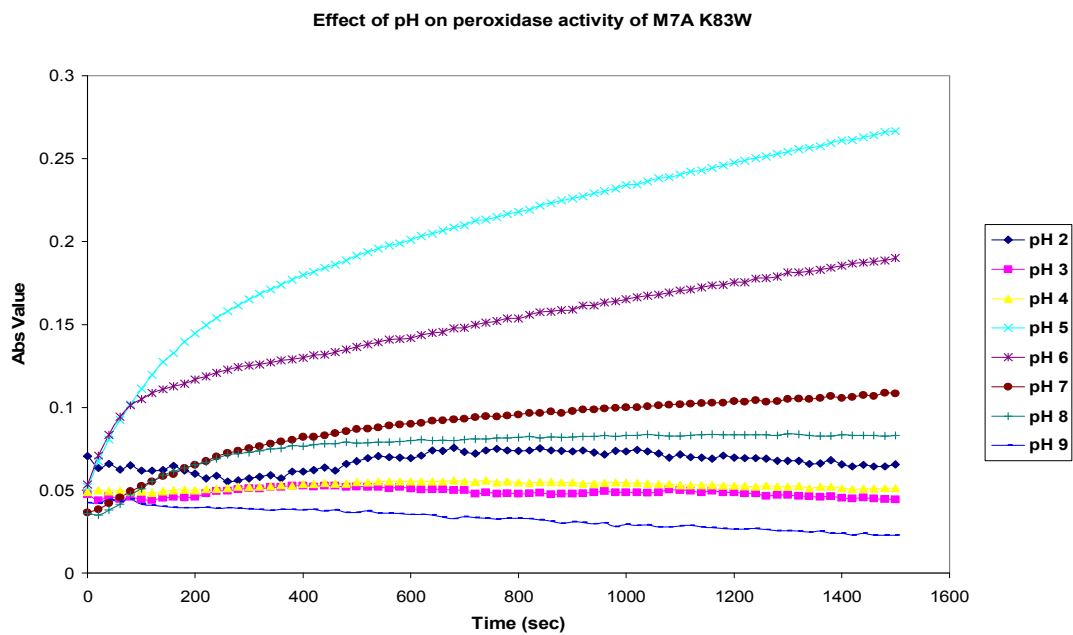


Figure 5.20: Effect of pH on peroxidase activity of M7AK83W Cyt b_{562} . The enzyme displays optimum activity at pH 5.0.

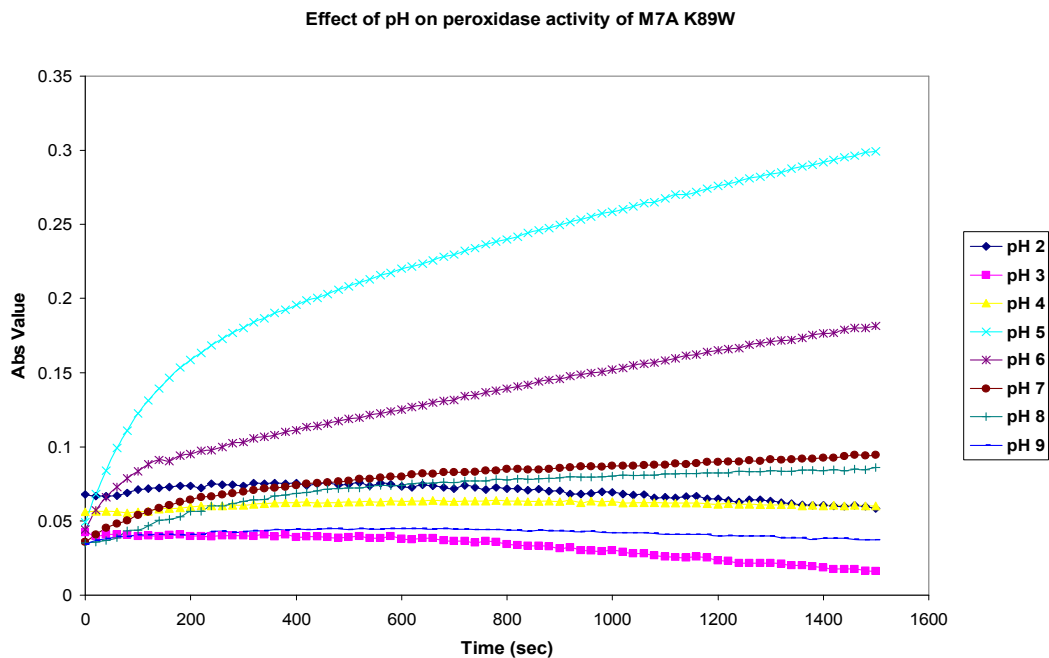


Figure 5.21: Effect of pH on peroxidase activity of M7A/K89W Cyt b_{562} . The enzyme displays optimum activity at pH 5.0.

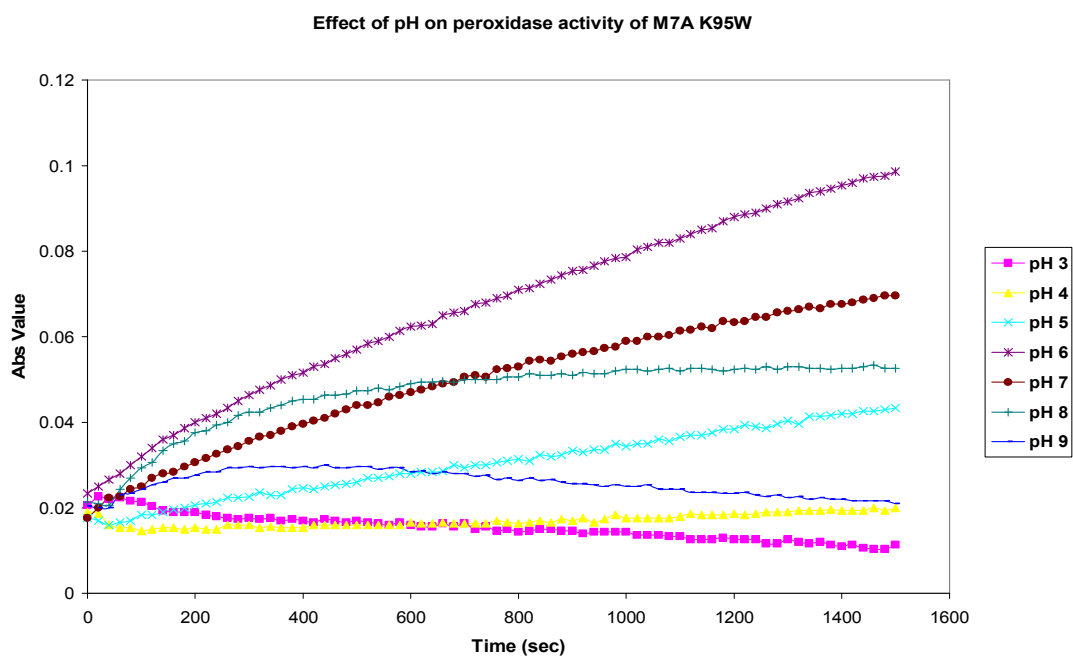


Figure 5.22: Effect of pH on peroxidase activity of M7A K95W Cyt b_{562} . The enzyme displays optimum activity at pH 6.0.

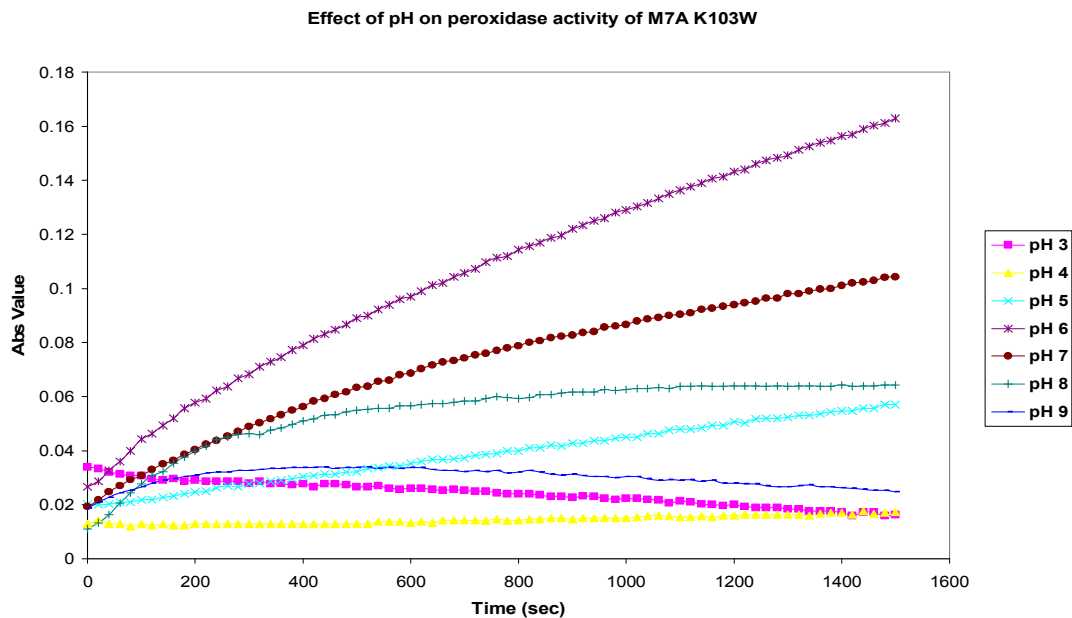


Figure 5.23: Effect of pH on peroxidase activity of M7A K103W Cyt b₅₆₂. The enzyme displays optimum activity at pH 6.0.

The higher pH maxima of M7A K95W and M7A K103W makes them more useful for potential bioremediation applications.

Effect of substrate concentration of peroxidase activity

The peroxidase assays performed to determine the effect of pH yielded an optimum pH for each of the active enzymes (M7A mutants of Cyt b₅₆₂). Because of time constraints, further kinetics experiments were conducted only with M7A Cyt b₅₆₂. Steady state kinetics were conducted with 1 μM enzyme concentration at pH 5.0 in 20 mM sodium citrate buffer. Initially the substrate concentration range of 0.1 to 20 mM ABTS was explored with 1 mM H₂O₂ concentration (Figure 5.24).

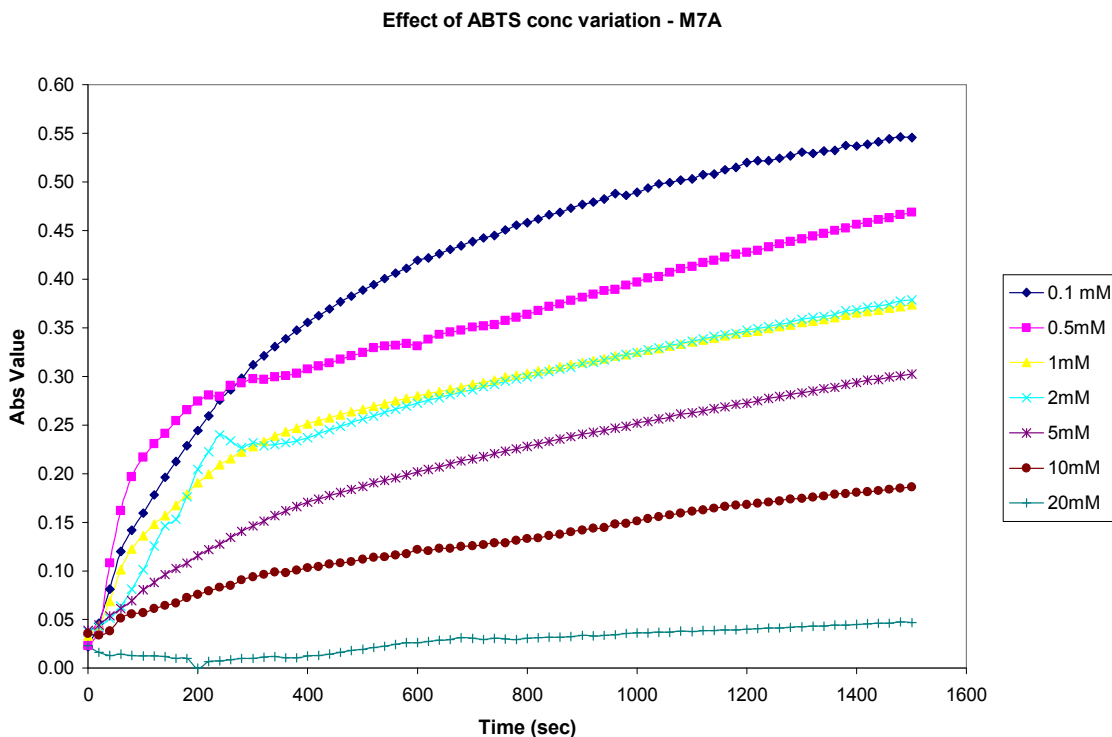


Figure 5.24: Effect of substrate (ABTS) concentration variation on peroxidase activity of M7A Cyt b₅₆₂.

It was found that the activity decreased as the concentration of ABTS was increased from 0.1 mM to 20 mM, which indicated that high concentration of ABTS inhibited the activity of enzyme. Hence a lower range (0.02 mM to 2 mM ABTS) was selected for the studies. Figure 5.25 shows the peroxidase activity data for various concentrations of ABTS at 1 μ M enzyme concentration and 1 mM H₂O₂ concentration. However, we were unable to fit any kinetic model to these experimental data by means of linear or non-linear regression. Since the activity profile as followed by hydrolysis of ABTS is not consistent with the increasing concentrations of ABTS, the data would not fit any kinetic models.

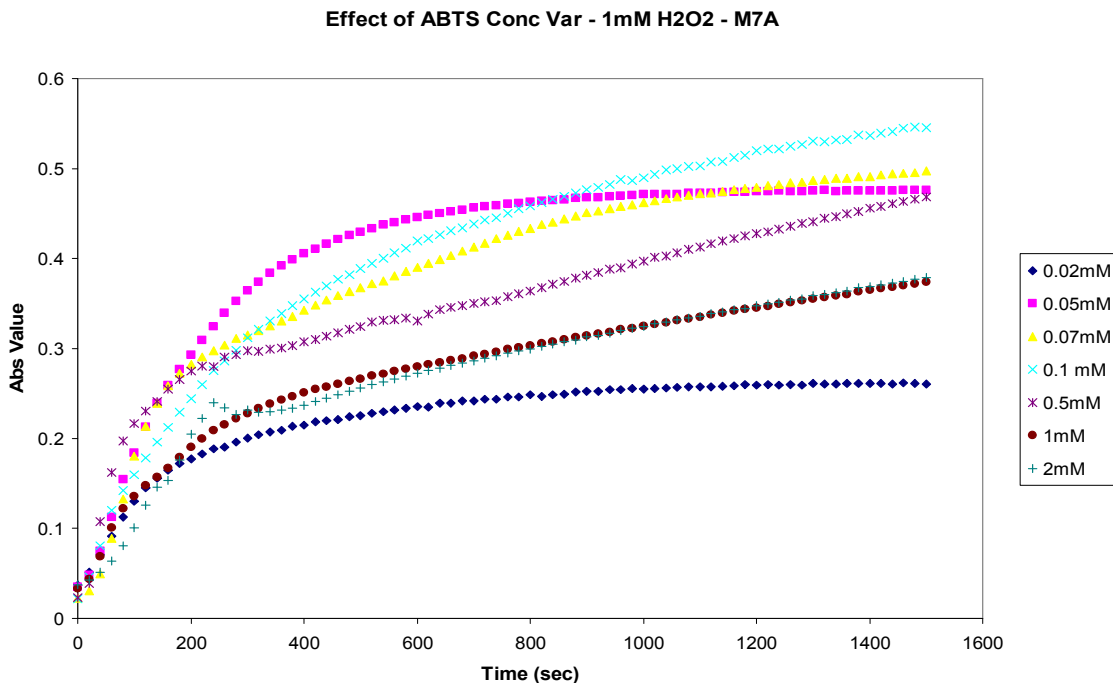


Figure 5.25: Peroxidase activity of M7A cyt b₅₆₂ at various concentrations of ABTS. The protein concentration was 1 μ M and H₂O₂ concentration was 1 mM.

Further experiments were done with the same with the same range of ABTS but over different concentrations of H₂O₂ (0.25 mM to 2 mM H₂O₂). We found that at 2 mM concentration of ABTS, the activity profile (Figure 5.26) was consistent with increasing concentrations of H₂O₂, thus we were able to fit the four parameter non-linear exponential model to this data. The rates obtained are plotted in Figure 5.27 with respect to varying concentrations of H₂O₂.

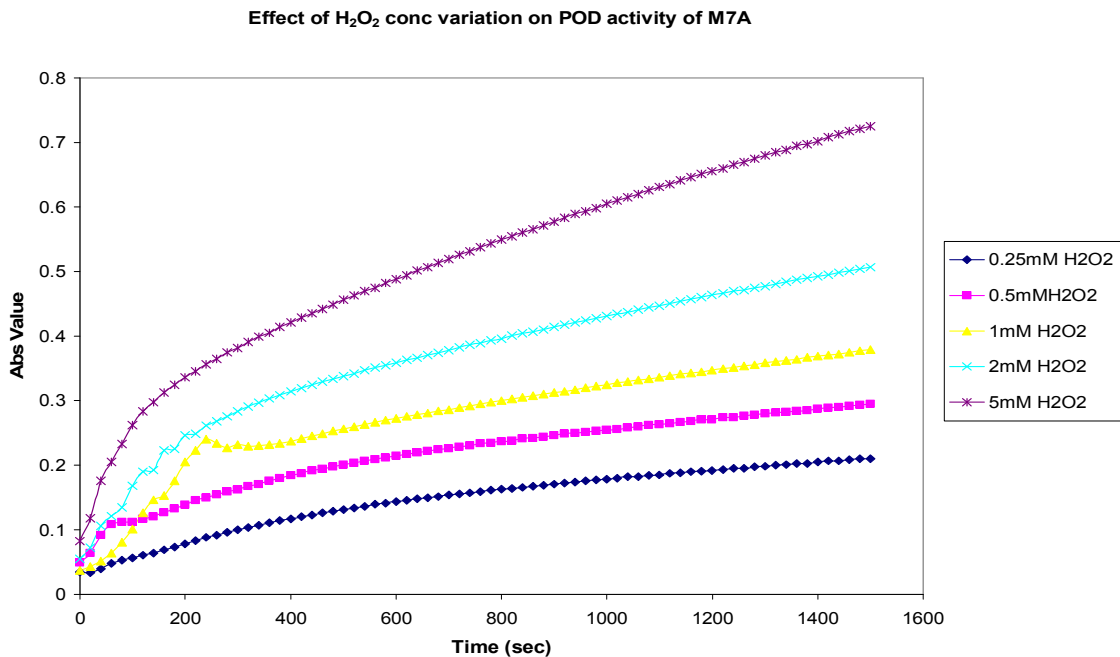


Figure 5.26: Effect of [H₂O₂] on the peroxidase activity of M7A Cyt b₅₆₂. The substrate concentration was constant at 2 mM.

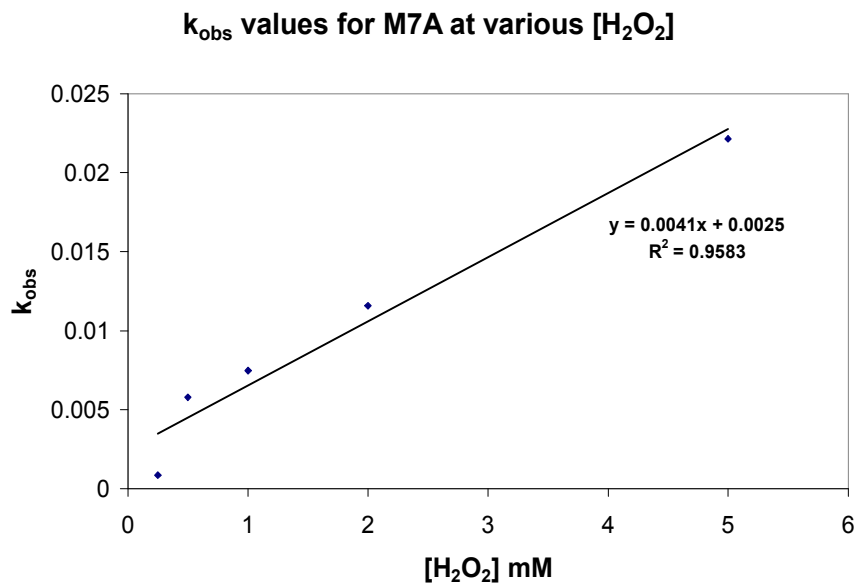


Figure 5.27: Dependence of the k_{obs} on [H₂O₂] for M7A Cyt b₅₆₂.

5.4 Conclusions

The *Y. enterocolitica* cyt b₅₆₂ gene was successfully cloned into *E. coli*. Nine different mutants were constructed in the gene of cyt b₅₆₂ and all the proteins were purified successfully. All these proteins were characterized using peroxidase assay and spectroscopic investigation. Only the proteins with methionine mutation (deletion of one axial ligand of heme) were observed to exhibit peroxidase activity. Introduction of tryptophan into these proteins altered the structure and heme binding ability. It was observed that the methionine single mutant possessed much higher activity than the methionine-tryptophan double mutants. The wild-type cyt b₅₆₂ and tryptophan single mutants did not show any peroxidase activity. The pH profiles showed that M7A mutant has pH optimum at 5.5 while M7A/K95W and M7A/K103W have pH optimum at 6 and show considerable activity up to pH 8.0, which may be very useful for bioremediation. However further experiments like EPR and NMR studies would be able to provide more useful information about the structure and function of these proteins.

5.5 Future work

This research effort creates several opportunities for further investigations. First it would be interesting to verify if the M7A mutants follow peroxidase like mechanism. These proteins can be redesigned using the cyt b₅₆₂ scaffold so that they closely approximate LiP activity. Using the directed evolution approach, random mutations can be generated in the vicinity of the active site of these proteins (surrounding the heme prosthetic group) and these mutants can be screened for peroxidase activity in an attempt

to produce enzymes possessing pH optima at 7.0 or above. Denaturation studies on these proteins will give an idea about the stability of these proteins.

The fluorescence experiments used to characterize the tryptophan residue and its radical cation form can be extended into some quantitative studies with EPR. With the use of EPR, it would be possible to actually detect the tryptophan radical cation and to get knowledge about the structure of the unstable reaction intermediates, from which the radical mechanism can be determined. Redox titrations can be used to obtain the values for heme reduction potential for these enzymes, which would give an idea about how effective they are over the naturally existing enzymes for the degradation of recalcitrant chemical contaminants.

GLOSSARY OF ACRONYMS

ABTS	2,2'-azino-di-(3-ethyl-benzthiazoline-6-sulphonic acid)
ACN	Acrylonitrile
APX	Ascorbate Peroxidase
ARP	<i>Arthromyces ramosus</i> Peroxidase
ATCC	American Type Culture Collection
BCA	Bicinchoninic Acid
BSA	Bovine Serum Albumin
CCP	Cytochrome <i>c</i> Peroxidase
CIP	Calf Intestine Alkaline Phosphatase
DIPEA	<i>N,N</i> -Diisopropylethylamine
DMF	<i>N,N</i> -dimethylformamide
DNA	Deoxynucleic Acid
dNTP	deoxynucleotide-triphosphate (containing all four nucleotides, A, T, C, G)
DOE	Department of Energy
DTT	Dithiothreitol
EDTA	Ethylenediaminetetraacetic Acid
EPO	Eosinophil Peroxidase
EPR	Electron Paramagnetic Resonance
ET	Electron Transfer
FPLC	Fast Performance Liquid Chromatography

HAc	Acetic Acid
HBTU	2-(1H-Benzotriazole-1-yl)-1,1,3,3-tetramethyluronium hexafluorophosphate
HCl	Hydrogen Chloride
HOBt	<i>N</i> -Hydroxybenzotriazole
HPLC	High-Performance Liquid Chromatography
HRP	Horseradish Peroxidase
IPTG	Isopropyl β -D-thiogalactopyranosidase
KCl	Potassium Chloride
LB	Luria Broth
LiP	Lignin Peroxidase
LPO	Lactoperoxidase
MALDI	Matrix Assisted Laser Desorption/Ionization
MeOH	Methanol
MnP	Manganese Peroxidase
MPO	Myeloperoxidase
NaCl	Sodium Chloride
NEB	New England Biolabs
NMP	1-methyl-2-pyrrolidone
NMR	Nuclear Magnetic Resonance
PAGE	Polyacrylamide Gel Electrophoresis
PCB	Polychlorinated Biphenyl
PCR	Polymerase Chain Reaction

PGHS	Prostaglandin H Synthase
PyBOP	Benzotriazole-1-yl-oxy-tris-pyrrolidino-phosphonium hexafluorophosphate
SDS	Sodium Dodecyl Sulfate
SPPS	Solid Phase Peptide Synthesis
TFA	Trifluoroacetic Acid
TPO	Thyroid Peroxidase
UV/VIS	Ultraviolet/Visible

APPENDICES

Appendix A

Preparation of competent *E. coli* cells and transformation

Competent *E. coli* BL21(DE)3 cells were prepared following the methods described by Sambrook et. al., 1989 using cold MgCl₂ and CaCl₂. For transformation, approximately 50 ml of competent cells were incubated with about 1 pmol of DNA for 30 min on ice. The cells were then heat-shocked at 42 °C for 90 seconds and 500 µl ml of LB media was added to the transformation mix. The cells were allowed to recover at 37 °C for 60 min. A 200 µL aliquot of the cell culture was spread onto LB plates with the appropriate antibiotic selection and incubated overnight at 37 °C.

Transformation of XL1-Blue supercompetent cells

The XL1-Blue supercompetent cells were gently thawed on ice. For each mutation reaction to be transformed, 50 µl of the supercompetent cells were aliquoted to a prechilled 1.5 ml eppendorf tube. From each mutation reaction, 1 µl of *Dpn* I treated DNA was transferred to separate aliquots of the supercompetent cells. The transformation reactions were swirled gently to mix and were then incubated on ice for 30 minutes. The cells were then heat pulsed for 45 seconds at 42 °C, incubated on ice for 2 minutes and then 500 µl of NZY⁺ broth (10 g NZ amine, 5 g yeast extract, 5 g NaCl, 12.5 ml of 1 M MgCl₂, 12.5 ml of 1 M MgSO₄ and 20 ml of 20% w/v glucose into a final volume of 1

liter) preheated to 42 °C was added to each transformation mix. The cells were allowed to recover at 37 °C for 1 hour with shaking at 250 rpm. Appropriate volume (250 µl) of each transformation reaction was plated on agar plates containing kanamycin. The transformation plates were incubated at 37 °C for >16 hours.

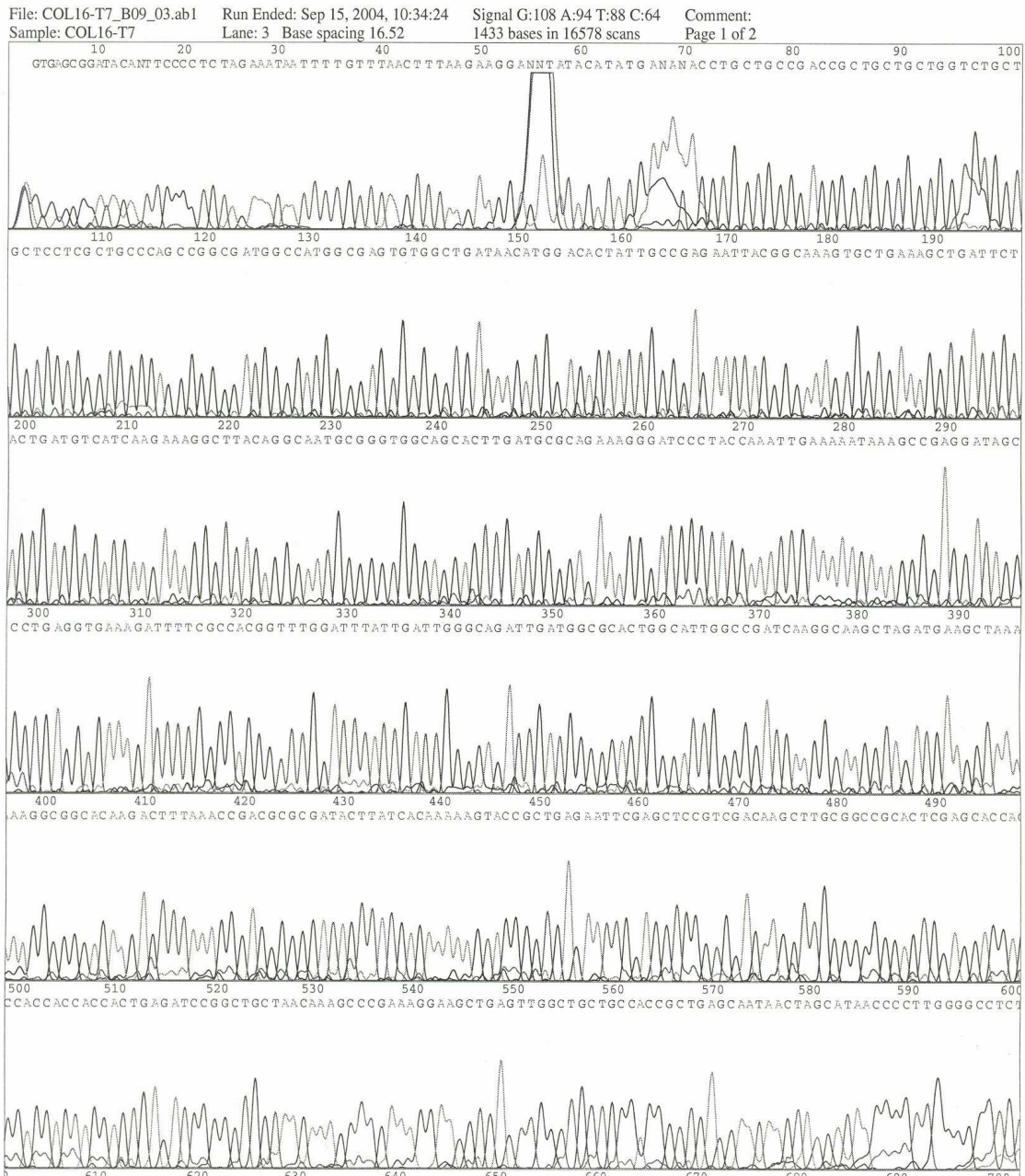
Calculation of transformation efficiency

The following formula was used to calculate the transformation efficiency as transformants (in cfu – colony forming units) per µg of plasmid DNA.

$$\frac{\text{\# of colonies}}{10 \text{ pg transformed DNA}} \times \frac{10^6 \text{ pg}}{\mu\text{g}} \times \frac{500 \text{ } \mu\text{l total transformation volume}}{X \text{ } \mu\text{l plated}} = \frac{\text{\# transformants}}{\mu\text{g plasmid DNA}}$$

According to the formula, for 128 transformants obtained using approximately 20 ng of the plasmid DNA, the transformation efficiency would be 2.56×10^5 cfu/µg of plasmid DNA.

Appendix B



Sequencing chromatogram for wild-type cytochrome b_{562} . The chromatogram was produced using the Chromas software Version 1.45 on a personal computer.

Appendix C

FPLC methods

Chromatography was performed on a Pharmacia Biotech FPLC. It was controlled using the FPLC director software version 1.30 from Pharmacia Biotech.

Method used for ion-exchange chromatography

Column: HiPrep™ 16/10 SP sepharose fast-flow (volume: 20 ml)

```
***** Main method SPFF *****
 0.00 FRACTION_COLLECTOR      START {}
 0.00 FLOW                    5.00 {}
 0.00 CONC_B                  0.00 {}
 5.00 CONC_B                  0.00 {}
75.00 CONC_B                  100.00 {}
78.00 CONC_B                  100.00 {}
78.10 CONC_B                  0.00 {}
80.00 FRACTION_COLLECTOR      Stop {}
80.00 FLOW                    0.00 {}
80.00 END_METHOD              {}
```

Method for size exclusion chromatography

Column: Superpose 6 HR 10/300 (volume: 24 ml)

```
***** Main method Sup6 *****
 0.00 FRACTION_COLLECTOR      START {}
 0.00 FLOW                    0.40 {}
 0.00 CONC_B                  0.00 {}
 1.00 INJ_VALVE               Inject{}
10.00 INJ_VALVE               Load {}
90.00 FRACTION_COLLECTOR      Stop {}
90.00 FLOW                    0.00 {}
90.00 END_METHOD              {}
```

Appendix D

Kaiser-ninhydrin test to assay for the presence of free amino group

A small aliquot of the resins was transferred from the synthesis vessel into a borosilicate glass tube. The resins were washed with 2 ml of absolute ethanol and resins were allowed to settle at the bottom of the tube and ethanol was removed carefully. This washing step was repeated three times. To this washed resin, two drops each of solution A (80% phenol+20% ethanol), solution B (5% ninhydrin in ethanol) and solution C (2 ml of 1 mM KCN in 98 ml pyridine) were added. The tube was placed in a heat block (set at 110 °C) for 3 minutes and color development was observed. If the solution remained pale yellow, it indicated that the amino groups on the resins were coupled and a blue color indicated the presence of free amino groups.

REFERENCES

- Barker P. D.; Nerou E. P.; Cheesman M. R.; Thomson A. J.; de Oliveira P.; Hill H. A.;
1996. Bis-methionine ligation to heme iron in mutants of cytochrome b_{562} .
Spectroscopic and electrochemical characterization of the electronic properties.
Biochemistry. 35: 13618-26.
- Bullock, P. A.; Myer, Y. P. 1978. Circular dichroism and resonance Raman studies of
cytochrome b_{562} from *Escherichia coli*. *Biochemistry*. 17: 3084-3091.
- Campa, A. 1991. Biological roles of plant peroxidases: known and potential function. *In*
Everse, J., Everse, K.E. and Grisham, M.B., Eds. *Peroxidases in Chemistry and*
Biology. CRC Press, Boca Raton, vol. II, pp. 25-50
- Chan, W. C.; White, P. D. 2000. Fmoc solid phase peptide synthesis: A practical
approach. Oxford university press, New York, New York.
- Childs, R. E.; Bardsley, W. G. 1975. The steady-state kinetics of peroxidase with 2,2'-
azino-di-(3-ethyl-benzthiazoline-6-sulphonic acid) as chromogen. *Biochem. J.*
145: 93-103.

- Choma, C. T.; Lear, J. T.; nelson, M. J.; Dutton, P. L.; Robertson, D. E.; DeGrado, W. F. **1994**. Design of heme-binding four-helix bundle. *J. Am. Chem. Soc.* 116: 856-865.
- Dahiyat, B. I.; Mayo S. L. **1997**. De novo protein design: Fully automated sequence selection. *Science*. 278: 82-87.
- DeGrado, W. F.; Summa, C. M.; Pavone, V.; Nastri, F.; Lombardi, A. **1999**. *De novo* design and structural characterization of proteins and metalloproteins. *Annu. Rev. Biochem.*, 68: 779-819.
- Dumont, M. E.; Corin, A. F.; Campbell, G. A. **1994**. Noncovalent binding of heme induces a compact apocytochrome *c* structure. *Biochemistry*. 33: 7368-7378.
- Dunford, H. B. **1991**. Peroxidases in chemistry and biology, in: Everse, J.; Everse, K.E.; Grishman M. B. (Eds.), *Horseradish Peroxidase: Structure and Kinetic Properties*, vol. 2, CRC Press, Boca Raton, FL, pp. 1-24.
- Dunford, H. B. **1999**. Heme peroxidases. John Wiley & Sons, Inc., NY. pp. 1-17.
- Englander, S. W.; Sosnick, T. R.; Mayne, L. C.; Shtilerman, M.; Qi, P. X.; Bai, Y.; **1998**. Fast and Slow Folding in Cytochrome *c*. *Acc. Chem. Res.* 31: 737-744.

- Feng, Y.Q.; Sligar, S.G. **1991**. Effect of heme binding on the structure and stability of *Escherichia coli* apocytochrome *b*₅₆₂. *Biochemistry* 30: 10150-10155
- Fezoui, Y.; Connolly, P. J.; Osterhout, J. J. **1997**. Solution structure of α -turn- α , a helical hairpin peptide of *de novo* design. *Protein Sci.* 6:1869-1877.
- Gebicka, L. **1999**. Kinetic studies on the oxidation of nitrite by horseradish peroxidase and lactoperoxidase. *Acta Biochim Pol.* 46: 919-927.
- Gibson, D. T.; Saylor G. S. **1992**. Scientific Foundations of Bioremediation: Current Status and Future Needs. Washington, D.C.: American Academy of Microbiology.
- Graupner, M.; Haalck, L.; Spener, F.; Lindner, H.; Glatter, O.; Paltauf, F.; Hermetter A. **1999**. Molecular dynamics of microbial lipases as determined from their intrinsic tryptophan fluorescence. *Biophys. J.* 77: 493-504.
- Hamada, K.; Bethge, P.H.; Mathews, F.S. **1995**. Refined structure of cytochrome *b*₅₆₂ from *Escherichia coli* at 1.4 Å resolution. *J. Mol. Biol.* 247: 947-962.
- Hargrove, M. S.; Barrick, D.; Olson, J. S. **1996**. The association rate constant for heme binding to globin is independent of protein structure. *Biochemistry.* 35: 11293-11299.

Hargrove, M. S.; Olson, J. S. **1996**. The stability of holomyoglobin is determined by heme affinity. *Biochemistry*. 35: 11310-11318.

Hargrove, M. S.; Wilkinson, A. J.; Olson, J. S. **1996**. Structural factors governing hemin dissociation from metmyoglobin. *Biochemistry*. 35: 11300-11309.

Hatefi, Y. **1985**. The mitochondrial electron transport and oxidative phosphorylation system. *Annu. Rev. Biochem.* 54: 1015-1069.

Hecht, M. H.; Richardson, J. S.; Richardson, D. C.; Ogden, R. C. **1990**. *De novo* design, expression, and characterization of felix: A four-helix bundle protein of native-like sequence. *Science*. 249: 884-891.

Hernandez M.E.; Newman D.K. **2001**. Extracellular electron transfer. *Cellular and Molecular Life Sciences*. 58:1562-1571

Hill, R. B.; DeGrado, W. F. **1998**. Solution Structure of α_2D , a Nativelike de Novo Designed Protein. *J. Am. Chem. Soc.* 120: 1138-1145.

Hiner, A. N .P.; Ruiz, J. H.; López, J. N. R.; Cánovas, F. G.; Brisset, N. C.; Smith, A. T.; Arnao, M. B.; Acosta, M. **2002**. Reactions of the Class II Peroxidases, Lignin

- Peroxidase and *Arthromyces ramosus* Peroxidase, with Hydrogen Peroxide. *J. Biol. Chem.* 277: 26879-26885.
- Ho, S. P.; DeGrado, W. F. **1987**. Design of a 4-helix bundle protein: synthesis of peptides which self-associate into a helical protein. *J. Am. Chem. Soc.* 109: 6751-6758.
- Huang, S. S.; Gibney B. R.; Stayrook, S. E.; Dutton P. L.; Lewis M. **2003**. X-ray structure of a maquette scaffold. *J. Mol. Biol.* 326: 1219-1225.
- Huffman D.L.; Rosenblatt M.M.; Suslick K.S. **1998**. Synthetic Heme-Peptide Complexes. *J. Am. Chem. Soc.* 120:6183-6184
- Janin J.; Wodak S.; Levitt M.; Maigret B. **1978**. Conformation of amino acid side-chains in proteins *J. Mol. Biol.* 125: 357 (1978).
- Kamiya, N.; Okimoto Y.; Ding Z.; Ohtomo H.; Shimizu M.; Kitayama A.; Morii H.; Nagamune T. **2001**. How does heme axial ligand deletion affect the structure and the function of cytochrome b_{562} ? *Protein Eng.* 14: 415-419.
- Karas M, Hillenkamp F. **1988**. Laser desorption ionization of proteins with molecular masses exceeding 10000 daltons. *Anal Chem* 60: 2299-2301.

- Kimura, S.; IkedaSaito, M. **1988**. Human myeloperoxidase and thyroid peroxidase, two enzymes with separate and distinct physiological functions, are evolutionarily related members of the same gene family. *Proteins*. 3: 113-120.
- Kumar, S.; Ma, B.; Tsai, T. J.; Sinha, N.; Nussinov, R. **2000**. Folding and binding cascades: Dynamic landscapes and population shifts. *Prot. Sci.* 9: 10-19.
- Laemmli, U. **1970**. Cleavage of structural proteins during the assembly of the head of bacteriophage T4. *Nature*. 227: 680-685.
- Landschulz W. H.; Johnson P. F.; McKnight S. L. **1988**. The leucine zipper: A hypothetical structure common to a new class of DNA binding proteins. *Science*. 240: 1759-1764.
- Lederer, F.; Glatigny, A.; Bethge, P.H.; Bellamy, H.D.; Mathews, F.S. **1981**. Improvement of the 2.5 Å resolution model of cytochrome *b*₅₆₂ by redetermining the primary structure and using molecular graphics. *J. Mol. Biol.* 148: 427-448.
- Lloyd, E.; King, B. C.; Hawkrige, F. M.; Mauk, A. G. **1998**. Electrostatic Modulation of Ligand Binding and Electrochemical Properties of Myoglobin: The Role of Charge Compensation. *Inorg. Chem.* 37: 2888-2892.

- Low, D. W.; Hill, M. G. **1998**. Rational Fine-Tuning of the Redox Potentials in Chemically Synthesized Rubredoxins. *J. Am. Chem. Soc.* 120: 11536-11537.
- Mathews, F.S.; Bethge, P.H.; Czerwinski, E.W. **1979** The structure of cytochrome *b*₅₆₂ from *Escherichia coli* at 2.5 Å resolution. *J. Biol. Chem.* 254: 1699-1706.
- Mazumdar, S.; Springs, S. L.; McLendon G. L. **2003**. Effect of redox potential of the heme on the peroxidase activity of cytochrome *b*₅₆₂. *Biophys. Chem.* 105: 263-268.
- Merrifield, R. B. **1963**. Solid phase peptide synthesis. I. The synthesis of a tetrapeptide. *J. Am. Chem. Soc.* 85: 2149-2154.
- Mester, T.; Ambert-Balay, K.; Ciofi-Baffoni, S.; Banci, L.; Jones, A. D.; Tien, M. **2001**. Oxidation of a tetrameric nonphenolic lignin model compound by lignin peroxidase. *J. Biol. Chem.* 276: 22985-22990.
- Myer, Y.P.; Bullock, P.A. **1978**. Cytochrome *b*₅₆₂ from *Escherichia coli*: conformational, configurational, and spinstate characterization. *Biochemistry* 17: 3723-3729.
- Narula, J.; Pandey, P.; Arbustini, E.; Haider, N.; Narula, N.; Kolodgie, F. D.; Dal Bello, B.; Semigran, M. J.; Bielsa-Masdeu, A.; Dec, G. W.; Israels, S.; Ballester, M.; Virmani, R.; Saxena, S; Kharbanda, S. **1999**. Apoptosis in heart failure: Release

- of cytochrome *c* from mitochondria and activation of caspase-3 in human cardiomyopathy. *Proc. Natl. Acad. Sci. USA*. 1999; 96: 8144-8149.
- Nelson, M.; McClelland, M. **1992**. Use of DNA methyltransferase/endonuclease enzyme combinations for megabase mapping of chromosomes. *Methods Enzymol* 216: 279-303.
- Nelson, R.E.; Fessler, L.I.; Takagi, Y.; Blumberg, B.; Keene, D.R.; Olson, P.F.; Parker, C. G.; Fessler, J. H. **1994**. Peroxidase: a novel enzyme-matrix protein of *Drosophila* development. *EMBO J*. 13: 3438-3447.
- Ohkuma, M.; Maeda, Y.; Johjima, T.; Kudo, T. 2001. Lignin degradation and roles of white rot fungi: Study on efficient symbiotic system in fungus-growing termites and its application to bioremediation. *Riken Reviews*. 42: 39-42.
- O' Neil, K.; DeGrado, W. F. **1990**. Thermodynamic Parameters for Helix Formation for the Twenty Commonly-Occurring Amino Acids. *Science*. 250: 246-250.
- Pikuleva, I.; Waterman, M. **1999**. Human cytochrome P450. *Mol Asp. Med*. 20: 43.
- Poulos, T. L.; Kraut, J. **1980**. The stereochemistry of peroxidase catalysis. *J. Biol. Chem*. 255: 8199-8205.

- Privett H. K.; Reedy C. J.; Kennedy M.L.; Gibney B. R. **2002**. Nonnatural Amino Acid Ligands in Heme Protein Design. *J. Am. Chem. Soc.* **124**:6828-6829.
- Reddy, C.A.; D'Souza, T.M. **1994**. Physiology and molecular biology of the lignin peroxidases of *Phanerochaete chrysosporium*. *FEMS Microbiol. Rev.* **13**: 137-152
- Richmond, T.J.; Richards, F.M. **1978**. Packing of α -helices: Geometrical constraints and contact areas. *J. Mol. Biol.* **119**: 537-555.
- Robertson, D. E.; Farid, R. S.; Moser, C. C.; Urbauer, J. L.; Mulholland, S. E.; Pidikiti, R.; Lear, J. D.; Wand, A. J.; DeGrado, W. F.; Dutton, P. L. **1994**. Design and synthesis of multi-haem proteins. *Nature.* **368**: 425-432.
- Sambrook, J.; Fritsch E. F.; Maniatis, T. **1989**. Molecular Cloning. A Laboratory Manual, p. A1-A2. Cold Spring Harbor Laboratory, Cold Spring Harbor, NY.
- Savenkova, M. I.; Kuo J. M.; Ortiz de Montellano P. R. **1998**. Improvement of peroxygenase activity by relocation of a catalytic histidine within the active site of horseradish peroxidase. *Biochemistry.* **37**: 10828–10836.
- Schafmeister, C. E.; Miercke, L. J. W.; Stroud, R. M. **1993**. Structure at 2.5 Å of designed peptide that maintains solubility of membrane proteins. *Science.* **262**: 734-738.

- Sharp, K. H.; Moody, P. C. E.; Raven E. L. **2003**. A new network for understanding substrate binding and functional diversity in heme peroxidases. *Dalton Trans.* 22: 4208-4215.
- Sheridan, R.P.; Levy, R. M.; Salemme, F. R. **1982**. α -helix Dipole Model and Electrostatic Stabilization of 4- α -helical Proteins. *Proc. Natl. Acad. Sci. USA.* 79: 4545-4549.
- Simmerman H. K.; Wang C. C.; Horwitz E. M.; Berzofsky J. A.; Gurd, F. R. 1982. Semisynthesis of sperm whale myoglobin by fragment condensation. *Proc. Natl. Acad. Sci.* 79: 7739-7743.
- Skalicky, J. J.; Gibney, B. R.; Rabanal, F.; Bieber Urbauer, R. J.; Dutton, P. L.; Wand, A. J. **1999**. Solution Structure of a Designed Four- α -Helix Bundle Maquette Scaffold. *J. Am. Chem. Soc.* 121: 4941-4951.
- Smith, P.K. *et al.* **1985**. Measurement of protein using bicinchoninic acid. *Anal. Biochem.* 150: 76-85.
- Springs S. L.; Bass S. E.; McLendon G. L. **2000**. Cytochrome b₅₆₂ variants: a library for examining redox potential evolution. *Biochemistry.* 39: 6075-82.

Struthers, M. D.; Cheng, R. P.; Imperiali, B. **1996**. Design of a monomeric 23 residue polypeptide with defined tertiary structure. *Science*. 271: 342-345.

Tanaka, M.; Nagano, S.; Ishimori, K.; Morishima, I. **1997**. Hydrogen bond network in the distal site of peroxidase: spectroscopic properties of Asn70→Asp horseradish peroxidase mutant. *Biochemistry*. 36: 9791-9798.

Wariishi H.; Gold, M. H. **1990**. Lignin peroxidase compound III. Mechanism of formation and decomposition. *J. Biol. Chem.* 265: 2070-2077.

Warshel, A.; Naray-Szabo, G.; Sussman, F.; Hwang, J. K. **1989**. How Do Serine Proteases Really Work? *Biochemistry* 28: 3629–3637.

Weber, P.C.; Salemme, F.R.; Mathews, F.S.; Bethge, P.H. **1981**. On the evolutionary relationship of the 4-alpha-helical heme proteins. The comparison of Cytochrome b₅₆₂ and Cytochrome c. *J. Biol. Chem.* 256: 7702-7704.

Welinder, K.G. **1985**. Plant peroxidases: Their primary, secondary and tertiary structures, and relation to cytochrome c peroxidase. *Eur J Biochem.* 151: 497-504.

Welinder, K.G. **1992**. Superfamily of plant, fungal and bacterial peroxidases. *Curr. Opin. Struct. Biol.* 2: 388-393.

Xavier, A.V.; Czerwinski, E.W.; Bethge, P.H.; Mathews, F.S. **1978** Identification of the heme ligands of cytochrome *b*₅₆₂ by X-ray and NMR methods. *Nature* 275: 245-247.

Yadav, J. S.; Quensen, 3rd, J. F.; Tiedje, J. M.; Reddy, C. A. **1995**. Degradation of polychlorinated biphenyl mixtures (Aroclors 1242, 1254, and 1260) by the white rot fungus *Phanerochaete chrysosporium* as evidenced by congener-specific analysis. *Appl. Environ. Microbiol.* 61: 2566-2571.

Yoshikawa, S. **2002**. Cytochrome *c* oxidase. *Adv. Protein Chem.* 60: 341-342.

VITAE

Kinjalkumar (Kinjal) Shah was born on May 18th, 1980 in Baroda, India. He obtained his Bachelor of Engineering from Maharaja Sayajirao University of Baroda, India, with Chemical Engineering as his major. He joined the Biological Systems Engineering department of Virginia Tech in August 2002 as a Master's student. In April 2003 he started working at the Virginia Bioinformatics Institute, under the guidance of Dr. Joel Gillespie as a Graduate Research Assistant. His research interests include protein design, protein expression and purification and development of enzymatic assays. He will join Siga Technologies, Inc., Corvallis, OR as Research Associate II after his graduation.